Doctoral Dissertation (Shinshu University)

# Study on nanocomposite hydrogel microspheres prepared by seeded emulsion polymerization in the presence of hydrogel microspheres

(ハイドロゲル微粒子存在下で実施するシード乳化重合による
ナノコンポジットゲル微粒子の創製と応用に関する研究)

**2020 年 3 月**

信州大学大学院総合工学系研究科 生命機能・ファイバー工学専攻

**Takumi Watanabe**

渡邊 拓巳

Table of Contents

## 3. Chapter II

**" Seeded Emulsion Polymerization of Styrene in the Presence of Water-swollen Hydrogel Microspheres"**

# 1. Introductory remarks

## 1.1. Background

The IUPAC defines colloids as molecules or polymolecular particles that show at least in one direction a dimension between approximately 1 nm and 1 μm when dispersed in a medium, or that are found at distances of that order when in a system of discontinuity.[1] Among the colloids, polymer colloids typically contain polymer nanoparticles with a size from ca. several nm to several μm. Due to the advantages associated with their concise synthesis, low cost, easy functionalization, and the possibility to up-scale the synthesis, synthetic polymer colloids have found wide-spread applications in e.g. cosmetics, food, latex products, coatings, and medicine. [2-5]

In order to improve the quality of those products, further functionalization of colloids are strongly desirable. For instance, the softness of polymer particles affects their adsorption kinetics on interfaces[6,7] and the robustness of particle assemblies.[8] Moreover, surface roughness, anisotropy, and size of colloid particles is strongly correlated to the interfacial activity[9-11] and particle interactions at fluid interface.[8, 12] Moreover, color and turbidity of dispersions and colloidal pastes can be tuned by optimizing the nanostructure of functionalized polymer colloids.[13-16] Furthermore, simulation studies have demonstrated that the surface roughness of soft particles is directly correlated to the concentration dependence of the system relaxation time (fragility) of glass behavior of colloids.[17] These examples demonstrate that understanding the relationship between the nanostructure of polymer colloids and their functionality is of great importance in order to develop advanced applications for polymer colloids. Thus, the development of both synthetic methods to design the structure of polymer colloids and characterization techniques to determine the particle morphology are required.

Colloid particles were initially discovered and used in form of natural latex. Advancements in the synthesis of polymer colloids have been intimately correlated to the developments in polymer chemistry. The first and arguably most representative synthetic route to polymer colloids is emulsion polymerization,[18-21] which has been used since the 1930s to synthesize latex, and the kinetic model were proposed in the 1940s.[20,21] Typically, emulsion polymerizations comprise a relatively hydrophobic monomer such as styrene, water, an appropriate amount of surfactant, and a water-soluble initiator. Above the critical micelle concentration, a hydrophobic monomer can be dissolved in the hydrophobic locations derived from the micelles to form spherical polymer particles via a free-radical polymerization of the vinyl monomer. Interestingly, in most cases, the surfactant serves as a polymerization site for the hydrophobic monomer and thus exerts a beneficial influence e.g. by increasing the monomer-conversion rate.[22-26] Moreover, the surfactant in the polymerization system affects not only the nucleation of the polymer particles, but also the colloidal stability; accordingly, the size and its uniformity can be tuned by the addition of surfactant.[26-28] Emulsion polymerization can also be applied to relatively hydrophilic monomers such as methyl methacrylate and vinyl acetate, albeit

that these monomers require careful attention as particle nucleation can occur inside the micelles and in the aqueous phase, which can lead to a non-uniform size of the colloidal particles.[29] Thus, emulsion polymerization is most efficient for solid particles composed of hydrophobic monomers. Even today, numerous functional polymer colloids are still prepared via emulsion polymerization techniques.[30-33]

Subsequently, seeded emulsion polymerization (SEP) has been developed[34,35] and used to prepare nanocomposite particles.[36-44] Initially, SEP was investigated in order to clarify the polymerization kinetics and mechanism of emulsion polymerization.[45,46] In some cases, this approach is employed to prepare sub-micron-sized solid microspheres by using the same type of monomer seeds for synthesis.[47] However, many researchers have recently employed SEP to construct nanocomposites and to control their particle morphology via phase-separation processes.[34-44] The particle properties, such as surface charge density and morphology, are essentially determined by the relationship between thermodynamic and kinetic aspects during SEP, and designing the particle morphology can be achieved by varying the polymerization conditions (e.g., temperature, stirring speed, pH conditions, and solvent) and particle characterization (e.g., size, charge density, charge distribution, and cross-linking density).[35-44] Therefore, SEP represents an efficient synthetic route to "non-spherical" hydrophobic particles and high-quality hydrophobic nanoparticles can be designed by combining more than one polymerization technique. However, in many cases, complicated and/or delicate processes such as prolonged monomer swelling are required, which is inferior in terms of particle yield relative to emulsion polymerization. Generally, emulsion droplets do not contribute to particle nucleation as the number of these droplets is significantly smaller than that of monomer-swollen micelles. However, by downsizing these emulsions, particle nucleation can occur efficiently, a process that is called mini-emulsion polymerization and that has been widely used as an efficient polymerization technique to obtain nanocomposite microgels with hydrophobic components that cannot be dissolved in water.[48-52]

The discovery of temperature-responsive polymers such as poly(*N*-isopropylacrylamide) (pNIPAm)[53] has made it possible to prepare novel types of polymer particles.[4,54] Such thermo-responsive polymer particles are usually synthesized by precipitation polymerization. At first, polymer chains are formed via free-radical polymerization in the aqueous phase. When the polymerization is conducted above the lower critical solubility temperature (LCST) of the polymers, these aggregate or self-assemble via a phase transition of the polymer during the polymerization.[4,54-56] Most importantly, microspheres that consist of water-hydrated polymer chains, which contain water similar to hydrogels, can be obtained by cooling colloidal dispersions after polymerization. It should be noted here that in this method, a chemically or physically cross-linked structure is necessary to obtain water-swollen microspheres.

Such water-swollen colloidal particles are called 'hydrogel particles' or 'microgels', and these have received much attention as a novel class of colloidal materials.[4, 54] Hydrogels typically consist of hydrophilic polymer materials that contain a three-dimensional network of hydrophilic (or amphiphilic) polymers and that can hold large amounts of water in a polymer network, which leads to excellent macroscopic properties such as softness, stimuli-responsivity, and

biocompatibility.[57-59] By downsizing the size of hydrogels to the colloid scale, these can be dispersed in water similar to colloidal particles, affording new fundamental insights and applications as polymer colloids. For example, given the unique properties of microgels, which include rapid stimuli-responsivity,[60-62] high colloidal stability and softness, [63-68] as well as high surface activity,[69-72] they have found a variety of applications, in e.g. sensors,[73-74] drug carrier systems,[75-80] reactors,[81-83] emulsion stabilizers,[70-72,84] autonomous oscillators,[85-88] and coating materials.[89-90] One particular aspect of microgels is that soft microgels, with a low cross-linking density, adsorb to the solid-liquid or liquid-air interface more quickly than hard microgels, and the surface of soft ellipsoidal hydrogels affords a robust particle assembly. In order to broaden the application range of microgels, several methods for the functionalization of water-swollen microgels are currently developed. One of the most advanced classes of microgels are thermo-responsive microgels such as pNIPAm microgels, which can be prepared by precipitation polymerization.[56]

Initially, radical copolymerization was used as an effective strategy for the functionalization of microgels. Since Kawaguchi *et al.* reported the first pH responsive poly[acrylamide-*co*-(methacrylic acid)](MAc) microgels prepared by precipitation polymerization,[91] the synthesis of various dual-functionality microgels that contain functional groups such as carboxy[92-95] or amino groups,[96] metallic complexes,[81-83] and pendant hydrophobic group[97] have been reported. In particular, the distribution of these functional groups inside the microgels can be controlled by adjusting the polymerization kinetics via the reactivity ratio, since the slower a comonomer reacts relative to NIPAm, the more likely the comonomer is localized on the microgel surface during precipitation polymerization. [93-95] Moreover, the size of the microgels can be controlled by modifying the precipitation polymerization conditions.[98-103] For example, the number of particle nuclei increases when a surfactant is added during the precipitation polymerization as the colloidal stability of precursor particles increases by adsorption of the surfactant, which leads to smaller microgels.[98,99] Conversely, when the precipitation polymerization is conducted at low temperature, the size of the microgels typically increases due to the decreased colloidal stability of the precursor particles.[100] Alternatively, the size of pNIPAm microgels can be increased by the monomer feed method, which is characterized by the fact that the monomer is fed into the reaction batch gradually.[101-103]

Moreover, the construction of core-shell structures by seeded precipitation polymerization (SPP) is important to improve microgel properties. Since Jones and Lyon proposed a synthetic strategy based on SPP in 2000,[104] a variety of hydrogel combinations comprising different types of cores and shells have been reported.[105-112] Typically, SPP comprises a relatively water-soluble monomer, pre-synthesized microgels, water, and a water-soluble initiator. After starting the polymerization, the formed polymers are deposited on the surface of the pre-synthesized microgels, which leads to a definite polymer distribution (e.g., core-shell and core-shell-shell structure) that exerts a significance influence on the macroscopic microgel properties. Therefore, well-defined core-shell structures in terms of e.g. charge density, cross-linking density, and thermo-responsivity can be constructed using SPP. One of the strong advantages of microgels

in applications in e.g. drug delivery systems and catalysts is the efficient use of their three-dimensional spatial structure,[113-115] which can be controlled effectively by SPP.

As mentioned above, various types of functionalized polymer colloids have been synthesized (**Table 1**). In contrast to solid polymer colloids, microgels also provide fascinating functionality derived from their softness and fuzzy surface. However, as hydrophobic treatments and fabricating non-spherical microgels are non-trivial, applications of microgels remain limited. For example, even though various nanocomposite structures, such core–shell microgels have been prepared systematically by SPP, such composite structures involve water-soluble polymers in most cases.[105-112] However, in the area of bulk-sized (~cm order) hydrogels, the synthesis of nanocomposite hydrogels with hydrophobic components including clay,[116] carbon materials,[117,118] and nanoparticles[119] has been realized as these hybrid materials can be prepared by solution polymerization in the presence of hydrophobic materials. It should be noted here that hydrophobic components in such composites provide excellent properties, e.g. high mechanical strength, that cannot be achieved with a single component.[117,118] Therefore, the importance of microgels in various applications may be enhanced once hydrophobic nanoparticles can be deposited inside microgels in a controlled fashion and if their structure can be controlled.

**Table 1-1**. Current State-of-the-art in Functional Polymer Colloids

| | Solid particles | Gel particles |
|---|---|---|
| Representative properties | ・Hydrophobicity<br>・Defined structure | ・Hydrophilicity (Amphiphilicity)<br>・Fuzzy structure |
| Morphology control | ・Seeded emulsion polymerization<br>(Control of thermodynamic balance) | |
| Size control | ・Seeded emulsion polymerization<br>・Emulsion polymerization<br>(Surfactant addition)<br>(Mini-emulsion polymerization) | ・Modified precipitation polymerization<br>(Temperature control, Surfactant addition, Feed method) |
| Fabricating composite structures | ・Seeded emulsion polymerization<br>・Mini-emulsion polymerization | ・Seeded precipitation polymerization |
| Softness | ・Optimizing glass-transition temperature | ・Optimizing cross-linked structure |

Against this background, this thesis focused on SEP in the presence of microgels. As summarized above, in most SEPs, solid microspheres, such as polystyrene and poly(methyl methacrylate) microspheres, have been used as seed microgels because of their compatibility with hydrophobic monomers.[35-44] In contrast, Suzuki *et al*., have recently prepared solid-hydrogel nanocomposite microgels by SEP of glycidyl methacrylate (GMA) and styrene in the presence of water-swellable pNIPAm microgels.[120-122] Surprisingly, in both cases, hydrophobic polyGMA[120]

and polystyrene (PS)[121,122] were formed only inside the pNIPAm microgels when the core microgels were highly dehydrated at elevated temperatures (70 °C, in water), leading to the generation of non-spherical nanocomposite structures that exhibit thermo-responsivity similar to the core pNIPAm microgels.[121,122] Unlike conventional microgels, composite microgels are non-spherical with hydrophobic domains. Therefore, nanocomposite microgels exhibit promising potential for next-generation stimuli-responsive nanomaterials. However, even though the effect of the styrene concentration[121,122] and the addition of sodium lauryl sulfate (SDS)[121] on the morphology of nanocomposite microgels have been examined, the relationship between the properties of the local micro-hydrogel environment, involving the charged state, the hydrated state, the inhomogeneous structures, and the capability to serve as a nucleation site for hydrophobic polymer nanoparticles remain unclear. In other words, the composite structure cannot yet be fully controlled.

In this thesis, the polymerization mechanism of SEP in the presence of microgels was examined and a new design concept for nanocomposite microgels was established. Moreover, the effects of the properties of the core microgels used for the SEP of styrene on the resulting composite structures and their properties were investigated. Especially, the impact of the charge group distribution in the core microgels and the hydrated state of the core microgels on the morphology of the obtained nanocomposite microgels was investigated. Finally, as an application of such nanocomposite microgels, the emulsification properties of the obtained nanocomposite microgels was demonstrated.

### 1.2. Outlines

This thesis covers three research topics. In **Chapter I**, the effect of the distribution of charge groups in the microgels on the morphology of the nanocomposite microgels is investigated. The obtained results revealed that polystyrene nanoparticles are formed inside deswollen microgels in order to avoid polyelectrolytes.[123] In **Chapter II**, the effect of the hydrated state of pNIPAm microgels on the morphology of the nanocomposite microgels prepared by SEP of styrene was examined. Nanocomposite microgels can be obtained by SEP with water-swollen hydrated microgels, which indicates that hydrated microgels may serve as polymerization sites for hydrophobic polystyrene during SEP and that the distribution of the charge groups inside of core microgels is a key factor for the design of the morphology of such nanocomposite microgels.[124] In **Chapter III**, the emulsification behavior of nanocomposite microgels was investigated in order to demonstrate the importance of nanocomposite microgels in colloidal applications. The results demonstrate that nanocomposite microgels can serve as emulsion stabilizers for water-in-oil emulsions with different types of oils, including non-polar ones, which usually do not form water in oil emulsions with conventional microgels.[125]

## 1.3. References


1. Everett, D. H. Manual of Symbols and Terminology for Physicochemical Quantities and Units, Appendix II: Definitions, Terminology and Symbols in Colloid and Surface Chemistry. *Pure and Applied Chemistry* **1972**, *31*, 577-638.
2. Zhang, J.; Grzybowski, B. A.; Granick, S. Janus Particle Synthesis, Assembly, and Application. *Langmuir* **2017**, *33*, 6964-6977.
3. Schulz, M.; Keddie, J. L. A Critical and Quantitative Review of the Stratification of Particles during the Drying of Colloidal Films. Soft Matter 2018, 14, 6181-6197.
4. Karg, M.; Pich, A.; Hellweg, T.; Hoare, T.; Lyon, L. A.; Crassous, J. J.; Suzuki, D.; Gumerov, R. A.; Schneider, S.; Potemkin, I. I.; Richtering, W. Nanogels and Microgels: From Model Colloids to Applications, Recent Developments, and Future Trends. *Langmuir* **2019**, *35*, 6231-6255.
5. Kim, Y. S.; Tamate, R.; Akimoto, A. M.; Yoshida, R. Recent Developments in Self-Oscillating Polymeric Systems as Smart Materials: from Polymers to bulk Hydrogels. *Mater. Horiz.*, **2017**, *4*, 38-54.
6. Takizawa, M.; Sazuka, Y,; Horigome, K.; Sakurai, Y.; Matsui, S.; Minato, H.; Kureha, T.; Suzuki, D. Self-organization of Soft Hydrogel Microspheres during the Evaporation of Aqueous Droplets. *Langmuir* **2018**, *34*, 15, 4515-4525
7. Matsui, S.; Kureha, T.; Hiroshige, S.; Shibata, M.; Takayuki, U.; Suzuki, D. Fast Adsorption of Soft Hydrogel Microspheres on Solid Surfaces in Aqueous Solution. *Angew. Chem. Int. Ed.* **2017**, *56*, 12146-12149.
8. Honda, K.; Sazuka, Y.; Iizuka, K.; Matsui, S.; Uchihashi, T.; Kureha, T.; Shibayama, M.; Watanabe, T.; Suzuki, D. Hydrogel Microellipsoids that Form Robust String-Like Assemblies at the Air/Water Interface. *Angew. Chem. Int. Ed.* **2019**, *58*, 7294-7298.
9. San-Miguel, A.; Behrens, S. H. Influence of Nanoscale Particle Roughness on the Stability of Pickering Emulsions. *Langmuir* **2012**, *28*, 12038-12043.
10. Dugyala, V. R.; Daware, S. V.; Basavaraj, M. G. Shape anisotropic colloids: synthesis, packing behavior, evaporation driven assembly, and their application in emulsion stabilization. *Soft Matter* **2013**, *9*, 6711-6725.
11. Zanini, M.; Marschelke, C.; Anachkov, S. E.; Marini, E.; Synytska, A.; Isa, L. Universal emulsion stabilization from the arrested adsorption of rough particles at liquid-liquid interfaces. *Nature Communications* **2017**, *8*, 15701.
12. Yunker, P. J.; Still, T.; Lohr, M. A.; Yodh, A. G. Suppression of the coffee-ring effect by shape-dependent capillary interactions. *Nature* **2011**, *476*, 308-311.
13. Suzuki, D.; Kawaguchi, H. Hybrid Microgels with Reversibly Changeable Multiple Brilliant Color. *Langmuir* **2006**, *22*, 3818-3822.
14. Choe, A.; Yeom, J.; Shanker, R.; Kim, M. P.; Kang, S.; Ko, H. Stretchable and wearable colorimetric patches based on thermoresponsive plasmonic microgels embedded in a hydrogel film. *NPG Asia Materials* **2018**, *10*, 912-922.

15. Acciaro, R.; Gilanyi, T.; Varga, I. Preparation of Monodisperse Poly(*N*-isopropylacrylamide) Microgel Particles with Homogeneous Cross-Link Density Distribution. *Langmuir* **2011**, *27*, 7917-7925.
16. Kawamura, A.; Kohri, M.; Morimoto, G.; Nannichi, Y.; Taniguchi, T.; Kishikawa, K. Full-Color Biomimetic Photonic Materials with Iridescent and Non-Iridescent Structural Colors. *Scientific Reports* **2016**, *6*, 33984.
17. Asai, M.; Cacciuto, A.; Kumar, S. K. Surface Fluctuations Dominate the Slow Glassy Dynamics of Polymer-Grafted Colloid Assemblies. *ACS Cent. Sci.* **2018**, *4*, 1179-1184.
18. Thickett, S. C.; Gilbert, R. G. Emulsion Polymerization: State of the art in kinetics and mechanisms. *Polymer* **2007**, *48*, 6965-6991.
19. Chern, C. S. Emulsion Polymerization mechanisms and kinetics. *Progress in Polymer Science* **2006**, *31*, 443-486.
20. Harkins, W. D. A general theory of the mechanism of emulsion polymerization. *J. Am. Chem. Soc.* **1947**, *69*, 1428-1444.
21. Smith, W. V.; Ewart, R. H. Kinetics of Emulsion Polymerization. *J. Chem. Phys.* **1948**, *16*, 592-599.
22. Roe, C. P. Surface Chemistry Aspects of Emulsion Polymerization. *Ind. Eng. Chem.* **1968**, *60*, 20-33.
23. Priest, W. J. Particle Growth in the Aqueous Polymerization of Vinyl Acetate. *J. Phys. Chem.* **1952**, *56*, 1077-1082.
24. Feeney, P. J.; Napper, D. H.; Gilbert, R. G. Surfactant-Free Emulsion Polymerizations: Predictions of the Coagulative Nucleation Theory. *Macromolecules* **1987**, *20*, 2922-2930.
25. Lichti, G.; Gilbert, R. G.; Napper, D. H. The Mechanisms of Latex Particle Formation and Growth in the Emulsion Polymerization of Styrene using the Surfactant Sodium Dodecyl Sulfate. *J. Polym. Sci. Polym. Chem. Ed.* **1983**, *21*, 269-291.
26. Chern, C. S.; Lin, C. H. Using a Water-insoluble Dye to Probe the Particle Nucleation Loci in Styrene Emulsion Polymerization. *Polymer* **1998**, *40*, 139-147.
27. Nagao, D.; Sakamoto, T.; Konno, H.; Gu, S.; Konno, M. Preparation of Micrometer-Sized Polymer Particles with Control of Initiator Dissociation during Soap-Free Emulsion Polymerization.
28. Sajjadi, S. Extending the limits of Emulsifier-free Emulsion Polymerization to Achieve Small Uniform Particles. *RSC Adv.* **2015**, *5*, 58549-58560.
29. Chern, C. S.; Lin, C. H. Particle Nucleation Loci in Emulsion Polymerization of Methyl Methacrylate. *Polymer* **2000**, *41*, 4473-4481.
30. Kurozuka, A.; Onishi, S.; Nagao, T.; Yamaguchi, K.; Suzuki, T.; Minami, H. Emulsion Polymerization with a Biosurfactant. *Langmuir* **2017**, *33*, 5814-5818.
31. Lutierzo, A.; Longbottom, B. W.; Lee, W. H.; Bon, S. A. F. Synthesis of Janus and Patchy Particles Using Nanogels as Stabilizers in Emulsion Polymerization. *ACS Nano* **2019,** *13*, 399-407.
32. Cater, M. C. D. Chen, L.; Moglia, R. S.; Luo, P.; Ratani, T. S.; Janco, M.; Gu, J.; Ngunjiri, J. N.; Gao, W.; Jackson, C. J.; Even, R. C. Design and Fabrication of Polyolefin–Acrylic Hybrid Latex Particles. *ACS Appl. Polym. Mater*. **2019**, *1*, 3185-3195.

33. Dai, X.; Yu, L.; Zhang, Y.; Zhang, Y.; Zhang, L.; Tan, J.; Polymerization-Induced Self-Assembly via RAFT-Mediated Emulsion Polymerization of Methacrylic Monomers. *Macromolecules* **2019**, *52*, 7468-7476.
34. Okubo M.; Yoshida, A.; Matsumoto, T. Estimation of Morphology of Composite Polymer Emulsion Particles by the Soap Titration Method. *J. Polym. Sci.: Polym. Chem. Ed*. **1980**, *16*, 3219-3228.
35. Sheu, H. R.; El-Aasser, M. S.; Vanderhoff, J. W. Phase Separation in Polystyrene Latex Interpenetrating Polymer Networks. *J. Polym. Sci.: Part A: Polym. Chem*. **1990**, *28*, 629-651.
36. Mock, E. B.; De Bruyn, H.; Hawkett, B. S.; Gilbert, R. G.; Zukoski, C. F. Synthesis of Anisotropic Nanoparticles by Seeded Emulsion Polymerization. *Langmuir* **2006**, *22*, 4037-4043.
37. Liu, Y.; Ma, Y.; Liu, L.; Yang, W. Facile Synthesis of Core-Shell/Hollow Anisotropic Particles via Control of Cross-Linking during One-pot Dispersion Polymerization. *J. Coll. Int. Sci.* **2015**, *445*, 268-276.
38. Minami, H.; Wang, Z.; Yamashita, T.; Okubo, M. Thermodynamic Analysis of the Morphology of Monomer-adsorbed, Cross-linked Polymer Particles Prepared by the Dynamic Swelling Method and Seeded Polymerization. *Colloid Polym. Sci.* **2003**, *281*, 246-252.
39. Tu, F.; Lee, D. Shape-Charging and Amphiphilicity-Reversing Janus Particles with pH-Responsive Surfactant Properties. *J. Am. Chem. Soc*. **2014**, *136*, 9999-10006.
40. Okubo, M.; Kanaida, K.; Matsumoto, T. Production of Anomalously Shaped Carboxylated Polymer Particles by Seeded Emulsion Polymerization. *Colloid and Polym. Sci*. **1987**, *265*, 876-881.
41. Okubo, M. and Minami, H. Control of Hollow Size of Micron-sized Monodispersed Polymer Particles Having a Hollow Structure. *Colloid Polym. Sci*. **1996**, *274*, 433-438.
42. Li, B.; Xu, Y.; Wang, M.; Ge, X. Morphological Control of Multihollow Polymer Latex Particles through Controlled Phase Separation in the Seeded Emulsion Polymerization. *Langmuir* **2013**, *29*, 14787-14794.
43. Duracher, D.; Sauzedde, F.; Elaissari, A.; Perrin, A.; Pichot, C. Cationic Amino-Containing *N*-isopropyl-acrylamide-Styrene Copolymer Latex Particles: 1-Particle Size and Morphology vs. Polymerization Process. *Colloid Polym. Sci*. **1998**, *276*, 219-231.
44. Ravensteijn, B. G. P.; Kegel, W. K. Tuning Particle Geometry of Chemically Anisotropic Dumbbell-Shaped Colloids. *J. Coll. Int. Sci.* **2017**, *490*, 462-477.
45. Smith, W. V.; Ewart, R. H. Kinetics of Emulsion Polymerization. *J. Chem. Phys.* **1948**, *16*, 592-599.
46. Thickett, S. C.; Gilbert, R. G., Emulsion Polymerization: State of the Art in Kinetics and Mechanisms. *Polymer* **2007**, *48*, 6965-6991.
47. Okubo, M.; Shiozaki, M.; Tsujihiro, M.; Tsukuda, Y. Preparation of micron-size monodisperse polymer particles by seeded polymerization utilizing the dynamic monomer swelling method. *Colloid and Polym. Sci*. **1991**, *269*, 222-226.
48. Asua, J. M. Miniemulsion Polymerization. *Prog. Polym. Sci.* **2002**, *27*, 1283-1346.
49. Aninietti, M.; Landfester, K. Polyreactions in Miniemulsions. *Prog. Polym. Sci*. **2002**, *27*, 689-757.

50. Meng, X.; Wen, T.; Qiang, L.; Ren, J.; Tang, F. Luminescent Electrophoretic Particles via Miniemulsion Polymerization for Night-Vision Electrophoretic Displays. *ACS Appl. Mater. Inter.* **2013**, *5*, 3638-3642.
51. Hiroshige, S.; Kureha, T.; Aoki, D.; Sawada, J.; Aoi, D.; Takata, T. Formation of Tough Films by Evaporation of Water from Dispersions of Elastomer Microspheres Crosslinked with Rotaxane Supramolecules. *Chem. Euro. J.* **2017**, *23*, 8405-8408.
52. Zhang, S. W.; Zhou, S. X.; Weng, Y. M.; Wu, L. M. Synthesis of SIO2/Polystyrene Nanocomposite Particles via Miniemulsion Polymerizaion. *Langmuir* **2005**, *21*, 2124-2128.
53. Heskins, M.; Guillet, J. E. Solution Properties of Poly(N-isopropylacrylamide). *J. Macromol. Sci.* **1968**, *2*, 1441-1455.
54. Suzuki, D.; Horigome, K.; Kureha, T.; Matsui, S.; Watanabe, T. Polymeric hydrogel microspheres: design, synthesis, characterization, assembly and applications. *Polym. J.* **2017**, *49*, 695–702.
55. Pelton, R. Temperature-Sensitive Aqueous Microgels. *Advances in Colloid and Interface Science* **2000**, *85*, 1-33
56. Pelton, R.H.; Chibante, P. Preparation of aqueous latices with N-isopropylacrylamide. *Colloids and Surfaces* **1986**, *20*, 247-256.
57. Tanaka, T.; Fillmore, D. J. Kinetics of swelling of gels. *J. Chem. Phys.* **1979**, *70*, 1214−1218.
58. Matsuda, T.; Kawakami, R.; Namda, R.; Nakajima, T.; Gong, J. P. Mechanoresponsive self-growing hydrogels inspired by muscle training. Science 2019, 363, 504-508.
59. Kamata, H.; Akagi, Y.; Kariya, Y. K.; Chung, U. I.; Sakai, T. "Nonswellable" Hydrogel Without Mechanical Hysteresis. Science 2014, 343, 873-875.
60. Hirai, T.; Maruyama, H.; Suzuki, T.; Hayashi, S.; Shape Memorizing Properties of a Hydrogel of Poly(Vinyl Alcohol). Pplied Polymer Science 1992, 45, 1849-1855.
61. Keidel, R.; Ghavami, A.; Lugo, D. M.; Lotze, G.; Virtanen, O.; Beumers, P.; Pedersen, J. S.; Bardow, A.; Winkler, R. G.; Richtering, W. Time-resolved structural evolution during the collapse of responsive hydrogels: The microgel-to-particle transition. *Sci. Adv.* **2018**, *4*, eaao7086.
62. Nishizawa, Y.; Matsui, S.; Urayama, K.; Kureha, T.; Shibayama, M.; Uchihashi, T.; Suzuki, D. Non-Thermoresponsive Decanano-sized Domains in Thermoresponsive Hydrogel Microspheres Revealed by Temperature-Controlled High-Speed Atomic Force Microscopy. *Angew. Chem. Int. Ed.* **2019**, *58*, 8809-8813.
63. Suzuki, D.; Kobayashi, T.; Yoshida, R.; Hirai, T. Soft Actuators of Organized Self-Oscillating Microgels. *Soft Matter* **2012**, 8, 11447-11449
64. Minami, S.; Watanabe, T.; Suzuki, D.; Urayama, K. Rheological Properties of Suspensions of Thermo-responsive Poly(*N*-isopropylacrylamide) Microgels Undergoing Volume Phase Transition. *Polymer Journal* **2016**, *48*, 1079-1086.
65. Minami, S.; Watanabe, T.; Suzuki, D.; Urayama, K. Viscoelasticity of Dense Suspensions of Thermosensitive Microgel Mixtures Undergoing Colloidal Gelation. *Soft Matter* **2018**, *14*, 1596-1607.

66. Nakaishi, A.; Minami, S.; Oura, S.; Watanabe, T.; Suzuki, D.; Urayama, K. Elastic and Flow Properties of Densely Packed Microgel Mixtures with Size- and Stiffness Disparitiess. *Macromolecules* **2018**, *51*, 9901-9914.
67. Minato, M.;Murai, M.; Watanabe, T.; Matsui, S.; Takizawa, M.; Kureha, T.; Suzuki, D. The Deformation of Hydrogel Microspheres at the Air/Water Interface. *Chem. Commun*. **2018**, *54*, 932-935.
68. Conley, G. M.; Aebischer, P.; Noid, S.; Schurtenberger, P.; Scheffold, F. Jamming and Overpacking Fuzzy Microgels: Deformation, Interpenetration, and Compression. *Science Adv.* **2017**, *3*, e1700969.
69. Suzuki, D.; Horigome, K. Binary Mixtures of Cationic and Anionic Microgels. *Langmuir* **2011**, *27*, 20, 12368-12374.
70. Richtering, W. Responsive Emulsions Stabilized by Stimuli-Sensitive Microgels: Emulsions with Special Non-Pickering Properties. *Langmuir* **2012**, *28*, 17218-27229.
71. Ngai, T.; Behrens, S. H.; Auweter, H. Novel emulsions stabilized by pH and temperature sensitive microgels. *Chem. Commin.* **2005**, *3*, 331-333.
72. Tsuji, S.; Kawaguchi, H. Thermosensitive Pickering Emulsion Stabilized by Poly(*N*-isopropylacrylamide)-Carrying Particles. *Langmuir* **2008**, *24*, 3300-3305.
73. Holtz, J. H.; Asher, S. A. Polymerized Colloidal Crystal Hydrogel Films as Intelligent Chemical Sensing Materials. *Nature* **1997**, *389*, 829-832.
74. Li, X.; Gao, Y.; Serpe, M. J. Responsive Polymer-Based Assemblies for Sensing Applications. *Macromol. Rapid Commun*. **2015**, *36*, 1382-1392.
75. Nayak, S.; Lee, H.; Chmielewski, J.; Lyon, L. A. Folate-Mediated Cell Targeting and Cytotoxicity Using Thermoresponsive Microgels. *J. Am. Chem. Soc*. **2004**, *126*, 10258-10259.
76. Kataoka, K.; Harada, A.; Nagasaki, Y. Block Copolymer Micelles for Drug Delivery: Design, Characterization and Biological Significance. *Advanced Drug Delivery Reviews* **2001**, *47*, 113-131.
77. Deshayes, S.; Kasko, A. M. Polymeric Biomaterials with Engineered Degradation. *J. Polym. Sci., Part A: Polym. Chem.* **2013**, *51*, 3531-3566.
78. Cinay, G. E.; Erkoc, P.; Alipour, M.; Hashimoto, Y.; Sasaki, Y.; Akiyoshi, K.; Kizilel, S. Nanogel-Intergrated pH-Responsive Composite Hydrogels for Controlled Drug Delivery. *ACS Biomater. Sci. Eng.* **2017**, *3*, 370-380.
79. Tahara, Y.; Sakiyama, M.; Takeda, S.; Nishimura, T.; Mukai, S.; Sasaki, Y.; Akiyoshi, K. Self-Assembled Nanogels of Cholesterol-Bearing Hydroxypropyl Cellulose: A Thermoresponsive Building Block for Nanogel Tectonic Materials. *Langmuir* **2016**, *32*, 12283-12289.
80. Chuah, J. A.; Matsugami, A.; Hayashi, F.; Numata, K. Self-Assembled Peptide-Based System for Mitochondrial-Targeted Gene Delivery: Functional and Structural Insights. *Biomacromolecules* **2016**, *17*, 3547-3557.
81. Zhang, J.; Xu, S.; Kumacheva, E. Polymer Microgels: Reactors for Semiconductor, Metal, and Magnetic Nanoparticles. *J. Am. Chem. Soc.* **2004**, *126*, 7908-7914.
82. Suzuki, D.; Kawaguchi, H. Modification of Gold Nanoparticle Composite Nanostructures Using Thermosensitive Core-Shell Particles as a Template. *Langmuir* **2005**, *21*, 8175-8179.

83. Lu, Y.; Mei, Y.; Drechsler, M.; Ballauff, M. Thermosensitive Core-Shell Particles as Carriers for Ag Nanoparticles: Modulating the Catalytic Activity by a Phase Transition in Networks. *Angew. Chem. Int. Ed*. **2006**, *45*, 813-816.
84. Richtering, W. Responsive Emulsions Stabilized by Stimuli-Sensitive Microgels: Emulsions with Special Non-Pickering Properties. *Langmuir* **2012**, *28*, 17218-17229.
85. Suzuki, D.; Sakai, T.; Yoshida, R. Self-Flocculating/self-Dispersing Oscillation of Microgels. *Angew. Chem. Int. Ed*. **2008**, *47*, 917-920.
86. Suzuki, D.; Taniguchi, H.; Yoshida, R. Autonomously Oscillating Viscosity in Microgel Dispersions. *J. Am. Chem. Soc*. **2009**, *131*, 12058-12059.
87. Suzuki, D.; Kobayashi, T.; Yoshida, R.; Hirai, T. Soft Actuators of Organized Self-Oscillating Microgels. *Soft matter* **2012**, *8*, 11447-11449.
88. Matsui, S.; Kureha, T.; Nagase, Y.; Okeyoshi, K.; Yoshida, R.; Sato, T.; Suzuki, D. Small-Angle X-ray Scattering Study on Internal Microscopic Structures of Poly(*N*-isopropylacrylamide-*co*-tris(2,2'-bipyridyl))ruthenium( II ) Complex Microgels. *Langmuir* **2015**, *31*, 7228-7237.
89. Cors, M. Wrede, O.; Genix, A. C.; Anselmetti, D.; Oberdisse, J.; Hellweg, T. Core-Shell Microgel-Based Surface Coatings with Linear Thermoresponse. *Langmuir* **2017**, *33*, 6804-6811.
90. Horigome, K.; Suzuki, D. Drying Mechanism of Poly(*N*-isopropylacrylamide) Microgel Dispersions. *Langmuir* **2012**, *28*, 12962−12970.
91. Kawaguchi, H,; Fujimoto, K.; Saito, M.; Kawasaki, T.; Yujiro Urakami, Y. Preparation and modification of monodisperse hydrogel microspheres. *Polymer Int*. **1993**, *30*, 225-231.
92. Hoare, T. and McLean, D. Kinetic Prediction of Functional Group Distributions in Thermosensitive Microgels. *J. Phys. Chem. B.* **2006**, *110*, 20327-20336.
93. Hoare, T.; Pelton, R. Highly pH and Temperature Responsive Microgels Functionalized with Vinylacetic Acid. *Macromolecules* **2004**, *37*, 2544-2550.
94. Hoare, T.; Pelton, R. Titrametric Characterization of pH-Induced Phase Transitions in Functionalized Microgels. *Langmuir* **2006**, *22*, 7342-7350.
95. Hoare, T.; Pelton, R. Characterizing Charge and Crosslinker Distributions in Polyelectrolyte Microgels. *Current Opinion in Colloid & Interface Science* **2008**, *13*, 413-428.
96. Guo, Z.; Chen, Q.; Gu, H.; He, Z.; Xu, W.; Zhang, J.; Liu, Y.; Xiong, L.; Zheng, L.; Feng, Y. Giant Microgels with CO2-Induced On–Off, Selective, and Recyclable Adsorption for Anionic Dyes. *ACS Appl. Mater. Interfaces* **2018**, *10*, 38073-38083.
97. Zhang, Q.; Zha, L.; Ma, J.; Liang, B. Synthesis and characterization of novel, temperature-sensitive microgels based on *N*-isopropylacrylamide and tert-butyl acrylate. *Journal of Applied Polymer Science* **2007**, *103*, 2962-2967.
98. McPhee, W. M.; Tam, K. C.; Pelton, R. Poly(*N*-isopropylacrylamide) Latices Prepared with Sodium Dodecyl Sulfate. *J. Coll. Int. Sci.* **1993**, *156*, 24-30.
99. Tam, K. C.; Ragaram, S.; Pelton, R. H. Interaction of Surfactants woth Poly(N-isopropylacrylamide) Microgel Latexes. *Langmuir* **1994**, *10*, 418-422.
100. Meng, Z.; Smith, M. H.; Lyon, L. A. Temperature-programmed Synthesis of Micron-Sized Multi-responsive Microgels. *Colloid Polym. Sci*. **2009**, *287*, 277-285.

101. Li, Z.; Kwok, M. H.; Ngai, T. Preparation of Responsive Micrometer-Sized Microgel Particles with a Highly Functionalized Shell. Macromol. *Rapid Commun.* **2012**, *33*, 419-425.
102. Kwok, M. H.; Li, Z.; Ngai, T. Controlling the Synthesis and Characterization of Macrometer-Sized PNIPAM Microgels with Tailored Morphologies. *Langmuir* **2013**, *29*, 9581-9591.
103. Minato, H.; Murai, M.; Watanabe, T.; Matsui, S.; Takizawa, M.; Kureha, T.; Suzuki, D. The Deformation of Hydrogel Microspheres at the Air/Water Interface. *Chemical Communications* **2018**, *54*, 942-935.
104. Jones, C. D.; Lyon, L. A. Synthesis and Characterization of Multiresponsive Core−Shell Microgels. *Macromolecules* **2000,** *33,* 8301-8306.
105. Jones, C. D.; Lyon, L A. Dependence of Shell Thickness on Core Compression in Acrylic Acid Modified Poly(N-isopropylacrylamide) Core/Shell Microgels. *Langmuir* **2003,** *19,* 4544-4547.
106. Keerl, M.; Pedersen, J. S.; Richtering, W. Temperature Sensitive Copolymer Microgels with Nanophase Separated Structure. *J. Am. Chem. Soc*. **2009**, *131*, 3093–3097.
107. Bradley, M.; Vincent, B.; Burnett, G. Uptake and Release of Anionic Surfactant into and from Cationic Core-Shell Microgel Particles. *Langmuir* **2007***, 23,* 9237-9241.
108. Hu, X.; Tong, Z.; Lyon, L. A. One-Pot Synthesis of Microcapsules with Nanoscale Inclusions. *Macromol. Rapid Commun*. **2011**, *32*, 1461-1466.
109. Smith, M. H.; Lyon, L. A. Multifunctional Nanogels for siRNA Delivery. *Accounts of Chemical Research* **2012**, *45*, 985-993.
110. Hellweg, T. Responsive Core-Shell Microgels: Synthesis, Characterization, and Possible Applications. *J. Polym. Sci., Part B: Polym. Phys.* **2013**, *51*, 1073-1083.
111. Saxena, S.; Hansen, C. E.; Lyon, L. A. Microgel Mechanics in Biomaterial Design. *Acc.Chem. Res*. **2014**, *47*, 2426-2434.
112. Dubbert, J.; Nothdurft, K.; Karg, M.; Richtering, W. Core-Shell-Shell and Hollow Double-Shell Microgels with Advanced Temperature Responsiveness. *Macromol. Rapid Commun*. **2015**, *36*, 159-164
113. Wu, S.; Dzubiella, J.; Kaiser, J.; Drechser, M.; Guo, X.; Ballauff, M.; Lu, Y. Thermosensitive Au-PNIPA Yolk-Shell Nanoparticles with Tunable Selectivity for Catalysis. *Angew. Chem. Int. Ed.* **2012**, *51*, 2229-2233.
114. Romero, S. C.; Buurma, N. J.; Juste, J. P.; Marzan, L. M. L.; Herves, P. Catalysis by Au@pNIPAM Nanocomposites: Effect of the Cross-Linking Density. *Chem. Mater.* **2010**, *22*, 3051-3059.
115. Kureha, T.; Nagase, Y.; Suzuki, D. High Reusability of Catalytically Active Gold Nanoparticles Immobilized in Core-Shell Hydrogel Microspheres. *ACS Omega* **2018**, *3*, 6158-6165.
116. Haraguchi, K.; Takehisa, T. Nanocomposite Hydrogels: A Unique Organic-Inorganic Network Structure with Extraordicary Mechanical, Optical, and Swelling/De-swelling Properties. *Advanced Materials* **2002**, *14*, 1120-1124.
117. Cha, C.; Shin, S. R.; Annabi, N.; Dokmeci, M. R.; Khademhosseini, A. Carbon-Based Nanomaterials: Multifunctional Materials for Biomedical Engineering. *ACS Nano* **2013**, *7*, 2891-2897.

118. Shin, S. R.; Jung, S. M.; Zalabany, M.; Kim, K.; Zorlutuna, P.; Kim, S. B.; Nikkhan, M.; Khabiry, M.; Azize, M.; Kong, J.; Wan, K. T.; Palacios, T.; Dokmeci, M. R.; Bae, H.; Tang, X. S.; Khademhosseini, A. Carbon-Nanotube-Embedded Hydrogel Sheets for Engineering Cardiac Constructs and Bioactuators. *ACS Nano* **2013**, *7*, 2369-2380.
119. Liu, K.; Pan, X.; Chen, L.; Huang, L.; Ni, Y.; Liu, J.; Cao, S.; Wang, H. Ultrasoft Self-Healing Nanoparticle-Hydrogel Composites with Conductive and Magnetic Properties. *ACS Sustainable Chemistry & Engineering* **2018**, *6*, 6395-6403.
120. Suzuki, D.; Yamagata, T.; Murai, M. Multilayered Composite Microgels Synthesized by Surfactant-Free Seeded Polymerization. *Langmuir* **2013**, *29*, 10579-10585.
121. Suzuki, D.; Kobayashi, C. Raspberry-Shaped Composite Microgel Synthesis by Seeded Emulsion Polymerization with Hydrogel Particles. *Langmuir* **2014**, *30*, 7085-7092.
122. Kobayashi, C.; Watanabe, T.; Murata, K.; Kureha, T.; Suzuki, D. Localization of Polystyrene Particles on the Surface of Poly(*N*-isopropylacrylamide-*co*-methacrylic acid) Microgels Prepared by Seeded Emulsion Polymerization of Styrene, *Langmuir* **2016**, *32*, 1429-1439.
123. Watanabe, T.; Kobayashi, C.; Song, C.; Murata, K.; Kureha, T.; Suzuki, D. Impact of Spatial Distribution of Charged Groups in Core Poly(N-isopropylacrylamide)-Based Microgels on the Resultant Composite Structures Prepared by Seeded Emulsion Polymerization of Styrene. *Langmuir* **2016**, *32*, 12760-12773.
124. Watanabe, T.; Song, C.; Murata, K.; Kureha, T.; Suzuki, D. Seeded Emulsion Polymerization of Styrene in the Presence of Water-Swollen Hydrogel Microspheres. *Langmuir* **2018**, *34*, 8571-8580.
125. Watanabe, T.; Takizawa, M.; Jiang, H.; Ngai, T.; Suzuki, D.; Hydrophobized Nanocomposite Hydrogel Microspheres as Particulate Stabilizers for Water-in-Oil Emulsions. *Chemical Communications* **2019**, *55*, 5990-5993.

# 2. Chapter I

# " Impact of Spatial Distribution of Charged Groups in Core Poly(*N*-isopropyl acrylamide)-Based Microgels on the Resultant Composite Structures Prepared by Seeded Emulsion Polymerization of Styrene "

*Part of this work was published in "Takumi Watanabe, Chiaki Kobayashi, Song, Chihong, Kazuyoshi Murata, Takuma Kureha, and Daisuke Suzuki *Langmuir*, **2016**, *32*, 12760-12773." Reprinted with permission from Copyright (2016), American Chemical Society.

## 2.1. Introduction

To broaden the application range of microgels, the construction of well-defined microgel architectures is important. As mentioned in introductory remarks, since Jones and Lyon first reported core–shell microgels whose core and shell are both hydrogels,[1] the synthesis, characterization, and application of these core–shell microgels have been systematically studied.[2-10] Such core–shell microgels have typically been synthesized by seeded "precipitation" polymerization, where water-soluble monomers used for shell synthesis become water-insoluble polymer chains during the polymerization and the polymer chains attach to the pre-existing core microgels. Recently, Suzuki et al., reported the seeded emulsion polymerization of glycidyl methacrylate, which is a relatively water-soluble oil monomer (GMA, solubility 120 mM at 25 °C)[11,12], or styrene (solubility 2.9 mM at 25 °C).[11, 13,14] In the course of this previous work, they observed that composite microgels could be obtained without forming secondary (or individual) polyGMA or polystyrene particles when core microgels were highly dehydrated at elevated temperatures (70 °C, in water). In particular, raspberry-shaped composite microgels were formed when styrene monomer was used for seeded emulsion polymerization.[13,14] They prepared three types of raspberry-shaped microgels: non uniform-sized polystyrene particles covering pNIPAm microgels,[13] uniform-sized polystyrene nanoparticles bound to core microgels not only on their surface but also inside,[13] and a monolayer of polystyrene nanoparticles bound to core microgels.[14] To control these non-spherical shapes of composite microgels, the structural design of the core microgels appears to be important; hydrophobic domains formed by association of isopropyl groups of NIPAm or anionic surfactant (sodium dodecyl sulfate (SDS)) in seed microgels attracted styrene monomer, and polystyrene was formed in situ.[13] By contrast, polystyrene nanoparticles did not form in the polyelectrolyte network of crosslinked poly(NIPAm-*co*-methacrylic acid).[14] It is believed that raspberry-shaped particles are important in applications such as super hydrophobic-coatings,[15-17] high-performance catalysts,[18,19] and antibacterial agents[20] because of their high surface area and roughness. Therefore, clarifying the details of seeded emulsion polymerization in

the presence of microgels and controlling the morphology (i.e., surface roughness, internal structure, softness) of stimuli-responsive raspberry-shaped composite microgels are important research topics.

Different from the seeded emulsion polymerization using micro-hydrogels as cores, the polymerization system using solid cores, such as polystyrene and poly(methyl methacrylate) particles, in aqueous solution have been systematically studied, and various functional particles,[21-24] such as snowman-shaped particles,[25-27] hollow particles,[28,29] octopus ocellatus-like particles[30] were developed. However, relationship between the properties of the local micro-hydrogel environment, such as polarity and hydrophobicity, and the capability to serve as a nucleation site for hydrophobic polystyrene particles remained unclear. Understanding the relationship will help to design and synthesize of novel shape-anisotropic composite micro-hydrogels for potential applications in the fields of surface coatings, catalysis, and molecular separation carriers.

In this study, building upon our previous works, the author investigate the effects of charge group distribution in core microgels used for the seeded emulsion polymerization of styrene on the resulting composite structures and properties. To this end, the author focused on pNIPAm-based microgels with carboxyl groups localized on their surfaces, in contrast to poly(NIPAm-*co*-MAA) microgels, in which the carboxyl groups are localized at the center of the microgels, as studied in SEP in the presence of microgels.[14] Through careful evaluation of the resultant composite microgels, the author investigate important factors affecting the composite structures synthesized by seeded emulsion polymerization.

## 2.2. Experimental Section

**Materials.** *N*-Isopropylacrylamide (NIPAm, purity 98 %), *N*,*N*′-methylenebis(acrylamide) (BIS, 97%), styrene (99%), potassium peroxodisulfate (KPS, 95%), methacrylic acid (MAc, 99%), SDS (95%), and fumaric acid (FAc, 98%) were purchased from Wako Pure Chemical Industries, Ltd. and were used as received. Acrylic acid (AAc, 99 %) was purchased from Sigma-Aldrich and was used as received. A 0.5 % ruthenium tetroxide ($RuO_4$) stabilized aqueous solution was purchased from Electron Microscopy Sciences and was also used as received. For all experiments, water was distilled and then ion-exchanged (EYELA, SA-2100E1) before use.

**Microgel synthesis.** pNIPAm-based core microgels were synthesized by precipitation polymerization in water according to the recipes outlined in **Table 2-1**. A mixture of NIPAm, BIS, carboxyl-group-containing comonomer, and water was poured into a 1 L three-neck round-bottom flask equipped with a mechanical stirrer, a condenser, and nitrogen gas inlet. The monomer solutions were heated at 70 °C under stirring at 250 rpm and then bubbled with nitrogen gas for 30 min to purge oxygen. KPS dissolved in 5 mL of water was injected into the flask to start the free-radical polymerization. The reactions were allowed to proceed for 4 h, and the microgel

dispersions were then allowed to cool to room temperature. The microgels were purified twice by centrifugation/redispersion with water using a relative centrifugal force of 70,000×*g*. In this manuscript, each microgel is denoted as **NX*Y***, where **N** indicates pNIPAm, **X** indicates kinds of comonomer introduced in the microgels, and ***Y*** indicates mole percentage of comonomers in the feed.

**Table 2-1.** Chemical Composition of Core Microgels

| code | monomer | | | | comonomer | | | Initiator | | | water /ml | colloidal stability |
|---|---|---|---|---|---|---|---|---|---|---|---|---|
| | NIPAm | | BIS | | | | | | | | | |
| | mol.% | g | mol.% | g | type | mol.% | g | type | mM | g | | |
| NM5 | 90 | 7.6383 | 5 | 0.5781 | MAc | 5 | 0.1291 | KPS | 2 | 0.2703 | 500 | good |
| NA5 | 90 | 7.6383 | 5 | 0.5781 | AAc | 5 | 0.2702 | KPS | 2 | 0.2703 | 500 | good |
| NA40 | 55 | 4.6679 | 5 | 0.5781 | AAc | 40 | 2.1618 | KPS | 2 | 0.2703 | 500 | good |
| NA50 | 45 | 0.2291 | 5 | 0.0347 | AAc | 50 | 0.3243 | KPS | 2 | 0.0162 | 50 | aggregated |
| NF5 | 90 | 7.6383 | 5 | 0.5781 | FAc | 5 | 0.4353 | KPS | 2 | 0.2703 | 500 | good |
| NF20 | 75 | 6.3653 | 5 | 0.5781 | FAc | 20 | 1.7411 | KPS | 2 | 0.2703 | 500 | good |
| NF40 | 55 | 7.4686 | 5 | 0.925 | FAc | 40 | 5.5714 | KPS | 2 | 0.4325 | 800 | good |
| NF50 | 45 | 6.1106 | 5 | 0.925 | FAc | 50 | 6.9642 | KPS | 2 | 0.4325 | 800 | good |
| NF60 | 35 | 0.5941 | 5 | 0.1156 | FAc | 60 | 1.0446 | KPS | 2 | 0.0541 | 100 | aggregated |

**Synthesis of Core–Shell Microgels.** Core–shell microgels were prepared by semi-batch seeded precipitation polymerization. A mixture containing NIPAm (0.7638 g, 90 mol.%), BIS (0.0578 g, 5 mol.%), FAc (0.0435 g, 5 mol.%), and water (45 mL) was poured into a 200 mL three-neck round-bottom flask equipped with a mechanical stirrer, a condenser, and nitrogen gas inlet. The monomer solution was heated to 70 °C under stirring at 250 rpm, and bubbled for 30 min to purge oxygen. KPS (0.0270 g, 2 mM) dissolved in 5 mL of water was injected into the flask to start the polymerization. The reaction was allowed to proceed for 4 h, and then the monomer solution of NIPAm (0.7469 g, 55 mol.%), BIS (0.0925 g, 5 mol.%), AAc (0.5571 g, 40 mol.%), and water (50 mL) was added into the flask for the shell synthesis. The reaction was allowed to proceed for 4 h; the microgel dispersion was then cooled to room temperature. The microgel was purified twice by centrifugation/redispersion with water using a relative centrifugal force of 70,000×*g*. The resulting microgel is denoted hereafter as **NF5-NA40**.

**Synthesis of Core–Shell Microgels.** Core–shell microgels were prepared by semi-batch seeded precipitation polymerization. A mixture containing NIPAm (0.7638 g, 90 mol.%), BIS (0.0578 g,

5 mol.%), FAc (0.0435 g, 5 mol.%), and water (45 mL) was poured into a 200 mL three-neck round-bottom flask equipped with a mechanical stirrer, a condenser, and nitrogen gas inlet. The monomer solution was heated to 70 °C under stirring at 250 rpm, and bubbled for 30 min to purge oxygen. KPS (0.0270 g, 2 mM) dissolved in 5 mL of water was injected into the flask to start the polymerization. The reaction was allowed to proceed for 4 h, and then the monomer solution of NIPAm (0.7469 g, 55 mol.%), BIS (0.0925 g, 5 mol.%), AAc (0.5571 g, 40 mol.%), and water (50 mL) was added into the flask for the shell synthesis. The reaction was allowed to proceed for 4 h; the microgel dispersion was then cooled to room temperature. The microgel was purified twice by centrifugation/redispersion with water using a relative centrifugal force of 70,000×*g*. The resulting microgel is denoted hereafter as **NF5-NA40**.

**Composite Microgels Synthesized by Seeded Emulsion Polymerization of Styrene.** The core microgel dispersion (100 mL, solid content: 0.17 g) was poured into a 200 mL three-neck round-bottom flask equipped with a mechanical stirrer, a condenser, and a nitrogen gas inlet and was heated at 70 °C with constant stirring at 250 rpm. Sufficient 1 M NaOH was added to the flask to adjust the pH of the system to ~10. As a control experiment, where appropriate, SDS (0.4614 g, final concentration: 16 mM) was added to the monomer solution. KPS (0.0271 g, 1 mM) dissolved in 5 mL of water was injected into the flask. Next, styrene monomer was added to start the polymerization. The polymerization was allowed to proceed for 24 h, and the resultant microgel dispersion was cooled to room temperature. The composite microgels were purified twice by centrifugation/redispersion in water using a relative force of 20,000×*g*. In this manuscript, the composite microgels are denoted as **NX*Y*-S*Z***, where **NX*Y*** denotes the core microgel, **S** indicates polystyrene, and ***Z*** indicates the styrene concentration during seeded emulsion polymerization.

**Characterization.** The hydrodynamic diameters of individual microgels were determined by dynamic light scattering (DLS) using a Zetasizer Nano S (Malvern Instruments Ltd., UK). The DLS data correspond to an average of 15 independent measurements of the intensity autocorrelation acquired over 30 s and the average of the results for three replicate measurements. The scattering intensity was detected at a total scattering angle of 173°. For the sample preparation, the particle concentration was adjusted to ~0.005 wt.% and the ionic strength was adjusted to 1 mM using NaOH, HCl, and NaCl solutions. Hydrodynamic diameters were calculated from the measured diffusion coefficients using the Stokes–Einstein equation (Malvern, Zetasizer software v. 6.12).

Electrophoretic mobility (EPM) was measured using a Zetasizer NanoZS (Malvern, Zetasizer software v. 4.20). For the sample preparation, the particle concentration was adjusted to ~0.005 wt.% and the ionic strength was adjusted to 1 mM with NaOH, HCl, and NaCl solutions. The EPM data correspond to an average of 20 independent measurements, and the average of the results for three replicate measurements. For all measurements, the sample was equilibrated for 5 min at a set temperature before the measurements. The amount of carboxyl-group-containing-monomer copolymerized in the core microgels was determined by conductometric titration. The

microgel dispersion was adjusted to ~pH 11 with 1 M NaOH solution, and the microgel concentration was adjusted to ~0.08 wt.%. The titration was performed using standardized 0.01 M HCl solution.

Particle morphologies in the dried state were visualized by scanning electron microscopy (FE-SEM, Hitachi Ltd., S-5000) and transmission electron microscopy (TEM, JEOL2010, operated at 200 kV). For FE-SEM observations, the microgels were dried on a polystyrene substrate at room temperature, after which they were washed with pure water. The sample substrates were sputtered with Pt/Pd before observations (15 mA, 6 Pa, 80 s). For TEM observations, the microgel dispersions were purified by centrifugation to remove secondary (or individual) polystyrene nanoparticles formed during seeded emulsion polymerization, and the purified dispersions were dried on a carbon-coated copper grid (Okenshoji Co., Ltd).

Lyophilized composite microgels were stained for 30 min with $RuO_4$ vapor and were dispersed in epoxy matrices (EPON812, TAAB Laboratories Equipment). The matrices were heated at 40 °C for 6 h and at 60 °C for 24 h. They were then microtomed into ultrathin cross sections and observed by TEM (JEOL JEM-2100, operated at 200 kV). Polystyrene occupied areas were calculated by ImageJ (ver.1.50) from images of ultra-thin cross section images. Note that the calculated polystyrene areas were used as reference because these ultra-thin cross section images were 2D images of 3D particles.

Hydrated composite microgels were observed by cryo-TEM. 2.5 μL of the aqueous samples were applied onto R 3.5/1 Quantifoil grids (Quantifoil Micro Tools) glow-discharged beforehand. The grids were then blotted and plunge-frozen using a Vitrobot, Mark III (FEI Company) with the setting of 95 % humidity, 4 °C, and 4 sec blotting time. The frozen hydrated grids were individually mounted onto a cryo-specimen holder (Gatan model 914) at liquid-nitrogen specimen temperature, and were imaged using a JEM2200FS electron microscope (JEOL Inc.) equipped with a field-emission electron source operated at 200 kV and an in-column (omega-type) energy filter operated in zero-energy-loss mode with a slit width of approximately 20 eV. Images of the frozen hydrated microgels were recorded using a 4k×4k CCD camera (F415, TVIPS, Germany) with low electron dose of approximately ~20 $e^-/Å^2$ at a nominal magnification of 1,6026, corresponding to 9.36 Å per pixel.

Monodispersities of each microgel were checked by making colloidal crystals in Vitrotube borosilicate rectangular capillaries ($0.1 \times 2.0$ $mm^2$). Microgel dispersions were inserted into the vitro tube by capillary action and were treated by thermal annealing to form colloidal crystals.[31,32]

## 2.3. Results and discussion

### 2.3.1. Synthesis and Characterization of Core Microgels

Control of the spatial distributions of functional groups in microgels can be achieved by (i) choosing an appropriate comonomer in terms of reactivity ratio[33-35] or (ii) conducting two step, seeded precipitation polymerization.[1,2] Here, to confirm how the carboxyl-group distribution in pNIPAm microgels affects the resulting composite microgels, three different carboxyl-group-containing monomers, FAc, AAc, and MAc, were chosen for aqueous free-radical precipitation polymerization (**Scheme 2-1**). The slower a comonomer reacts relative to NIPAm, the more the comonomer is localized on the surface of microgels synthesized by precipitation polymerization (however, the faster the comonomer relative to NIPAm, the more the comonomer is localized at the center of core microgels). [33-35] Therefore, carboxyl-group distribution within core microgels can be controlled by changing the types of comonomer. According to the copolymer–monomer copolymerization curves for the radical copolymerization of NIPAm and the three carboxyl-group-containing monomers (**Scheme 2-1(A)**), MAc is localized at the center of core microgels ($r_1$ = 2.8, $r_2$ = 0.2, MAc ($r_1$) and NIPAm ($r_2$), respectively), [35] AAc is nearly homogeneously distributed in microgels ($r_1$ = 0.32, $r_2$ = 0.57, AAc ($r_1$) and NIPAm ($r_2$), respectively), [35] and FAc is localized on the surface of core microgels ($r_1$ = 0.09, $r_2$ = 7.0, FAc ($r_1$) and NIPAm ($r_2$), respectively). [35] **Scheme 2-1(B)** shows the expected carboxyl-group distribution in the resultant microgels.

Here, for the convenience of comparison among these three microgels, the amount of comonomer fed during precipitation polymerization was fixed at 5 mol.%. **Figure 2-1** shows the electron microscope images of dried **NM5**, **NA5**, and **NF5** microgels. From these FE-SEM images (a)–(c), the diameters of these microgels were measured to be 472 ± 18 nm (**NM5**, CV = 4.1 %, $N$ = 50), 523 ± 19 nm (**NA5**, CV = 3.5 %, $N$ = 50), and 723 ± 35 nm (**NF5**, CV = 4.8 %, $N$ = 50), indicating that they are uniform and submicron-sized microgels. Moreover, the monodispersities of these microgels in aqueous solution were confirmed by colloidal crystal formation in water (**Figure 2-1(a)–(c)** ). [32,38]

The author subsequently evaluated the multiresponsive properties (i.e., temperature- and pH-responsive properties) of these microgels to demonstrate that the expected structures were indeed constructed. Here in each case, approximately the same amount of carboxyl-group-containing monomer was incorporated into the core microgels, as confirmed by conductometric titration (**Table 2-2**). As evident from the results in **Table 2-2**, all of the microgels exhibit temperature- and pH-responsive changes in hydrodynamic diameters. In particular, the hydrodynamic diameter of the **NF5** microgels dramatically increased (approximately fivefold) with increasing pH at 25 °C (compared to approximately twofold and threefold increases for **NM5** and **NA5** microgels, respectively). The difference between the three microgels is consistent with the previous report by Hoare and Pelton that pNIPAm-based microgels with shell-localized carboxyl groups swell dramatically. [33] In addition, differences in the carboxyl-group distributions in these microgels are evident from their EPM values (**Table 2-2**). First, all of the EPM values are

negative, indicating that the microgels are negatively charged. At 25 °C, where these microgels are highly swollen, the EPM measured at pH 10 exhibits a larger absolute value than that measured at pH 3, indicating the deprotonation of carboxyl groups located at the surface of the microgels. In particular, the absolute value of the EPM for **NF5** microgels is larger than that for the **NM5** and **NA5** microgels at both pH 10 and pH 3. At 70 °C, the absolute values of the EPMs became larger than those measured at 25 °C in all cases because the surface charge densities of these deswollen microgels increased.[27] Notably, the absolute value of the EPM for **NF5** microgels measured at pH 10 was the largest even though these microgels did not deswell completely (**Table 2-2**), indicating that the **NF5** microgels possess the expected structures, that is, carboxyl groups localized on the surface of the microgels.

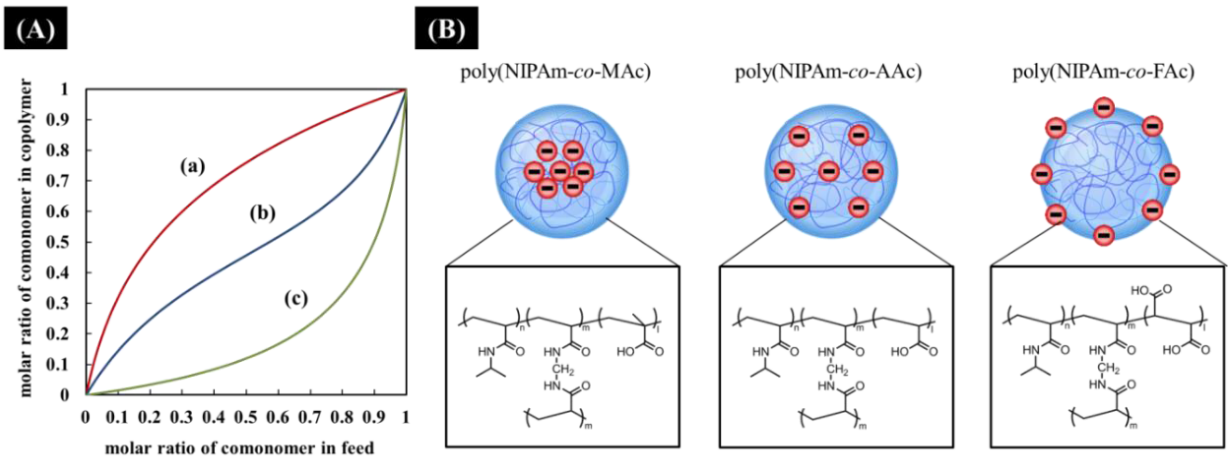


**Scheme 2-1**. (A) Copolymer-monomer copolymerization curves for the radical copolymerization of NIPAm and the three carboxyl group-containing monomers ((a) MAc, (b) AAc, (c) FAc), and (B) expected carboxyl group distribution in pNIPAm-based microgels. The copolymerization curves were calculated with the reactivity ratio of MAc ($r_1$ = 2.8, $r_2$ = 0.2, MAc ($r_1$) and NIPAm ($r_2$), respectively),[36] AAc ($r_1$ = 0.32, $r_2$ = 0.57, AAc ($r_1$) and NIPAm ($r_2$), respectively) and FAc ($r_1$ = 0.09, $r_2$ = 7.0, FAc ($r_1$) and NIPAm ($r_2$)) respectively.

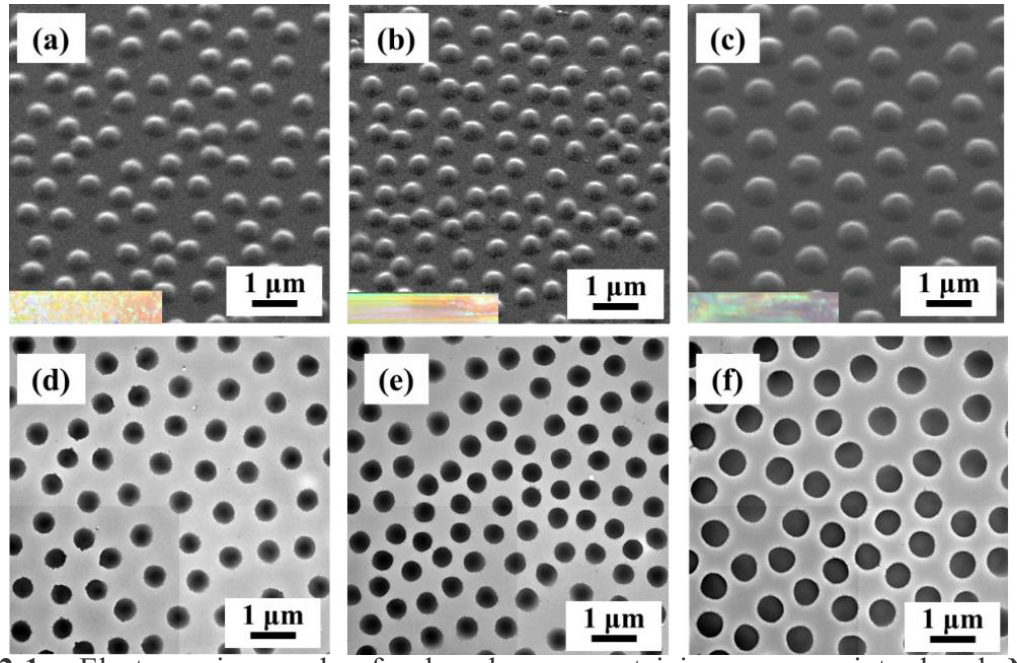


**Figure 2-1.** Electron micrographs of carboxyl group-containing monomer introduced pNIPAm-based microgels dried at room temperature. (a, d) **NM5**, (b, e) **NA5**, (c, f) and **NF5** microgels. (a-c) FE-SEM images. (d-f) TEM images. Insets were photographs of colloidal crystals composed of each microgel.

**Table 2-2**. Hydrodynamic Diameters and Electrophoretic Mobilities of **NM5**, **NA5**, and **NF5** Microgels

| Code | pH | Hydrodynamic diameter / nm | | electrophoretic mobility / × $10^{-8}$ $m^2$/Vs | | content of –COOH in microgels mmol/g |
|---|---|---|---|---|---|---|
| | | 25 °C | 70 °C | 25 °C | 70 °C | |
| NM5 | 3 | 566 ±3.8 | 292 ± 21 | -0.30 ± 0.004 | -2.67 ± 0.008 | 0.40 |
| | 10 | 995 ±41 | 363 ± 3.4 | -0.82 ± 0.02 | -2.79 ± 0.09 | |
| NA5 | 3 | 623 ±5.3 | 360 ± 6.6 | -0.34 ± 0.003 | -3.18 ± 0.08 | 0.40 |
| | 10 | 1881 ±38 | 582 ± 3.4 | -1.68 ± 0.01 | -3.08 ± 0.04 | |
| NF5 | 3 | 570 ±3.8 | 479 ± 7.2 | -0.70 ± 0.01 | -3.31 ± 0.06 | 0.44 |
| | 10 | 2605 ±38 | 946 ± 13 | -2.08 ± 0.01 | -3.66 ± 0.09 | |

### 2.3.2. Effect of the Charged Group Distribution of Core Microgels on the Morphologies of Resultant Composite Microgels

Next, composite microgels with polystyrene were synthesized by surfactant-free seeded emulsion polymerization in the presence of carboxyl-group-containing pNIPAm microgels. In all cases, the pH of the reaction solutions was adjusted to ~10 by the addition of 1 M NaOH solution to keep the carboxyl groups deprotonated. **Figure 2-2** shows electron microscopy images of the three composite microgels prepared with the styrene concentration during seeded emulsion polymerization fixed at 100 mM. As evident in the FE-SEM images (**Figure 2-2(a)–(c)**), all of these composite microgels possess polystyrene nanoparticles attached to the core microgels, resulting in raspberry-shaped composite structures. The diameters of these composite microgels and polystyrene nanoparticles attached on the core microgels were listed in **Table 2-3**. Here, polystyrene nanoparticles were not removed from core microgels via centrifugal purification, as verified by TEM observations (**Figure 2-3(d)–(f)**), indicating that the nanoparticles were strongly bound to each core microgel. [13,14] Notably, secondary (or individual) polystyrene nanoparticles were observed in the cases of **NA5-S100** and **NF5-S100** composite microgels (**Figure 2-4**); however, these secondary polystyrene nanoparticles were removed by centrifugal purification (TEM observation, **Figure 2-2(d)–(f)**). **Figure 2-2(g)–(i)** shows TEM images of ultra-thin cross sections of each composite microgel (polystyrene domains were stained black with $RuO_4$). In the cases of the **NM5-S100** and **NA5-S100** microgels (**Figure 2-2(g),(h)**), polystyrene nanoparticles appear to be located (or richer) on the surface of the core microgels. By contrast, the black region (i.e., polystyrene domains) was dominant not only on the surface but also in the interior of the core microgels when **NF5** microgels were used as cores (**Figure 2-2(i)**). On the basis of these images, the number of polystyrene nanoparticles was calculated to be ~10 (for **NM5-S100**), ~16 (for **NA5-S100**), and ~25 (for **NF5-S100**), and their sizes were roughly estimated to be 24 ± 5 nm (CV = 20 %, $N$ = 50), 37 ± 6 nm (CV = 17 %, $N$ = 50), and 48 ± 9 nm (CV = 18 %, $N$ = 50), and polystyrene occupied area in core microgels were 50 ± 8 % (CV = 16 %), 57 ± 9 % (CV = 17 %), and 71 ± 6 % (CV = 9 %), respectively. Note that the accurate size of polystyrene nanodomain formed inside of microgels is difficult to be evaluated by these ultra-thin cross sections. However, these results are still efficient to estimate how the composite is formed and developed during seeded emulsion polymerization. Detail analysis will be conducted by cryo-tomography technique, and will be reported elsewhere. The author have already reported that polystyrene nanoparticles do not form in core **NM** microgels when the core microgel contains a certain amount of methacrylic acid (more than 10 mol.% in the feed during precipitation polymerization). [14] Given these results, polystyrene nanoparticles (or domains) clearly do not form where polyelectrolytes, such as poly(NIPAm-*co*-MAc), exist; furthermore, the formation of polystyrene nanoparticles (or domains) within core microgels is favored even though the surface charge density of core microgels is high (i.e., for **NF5** microgels).

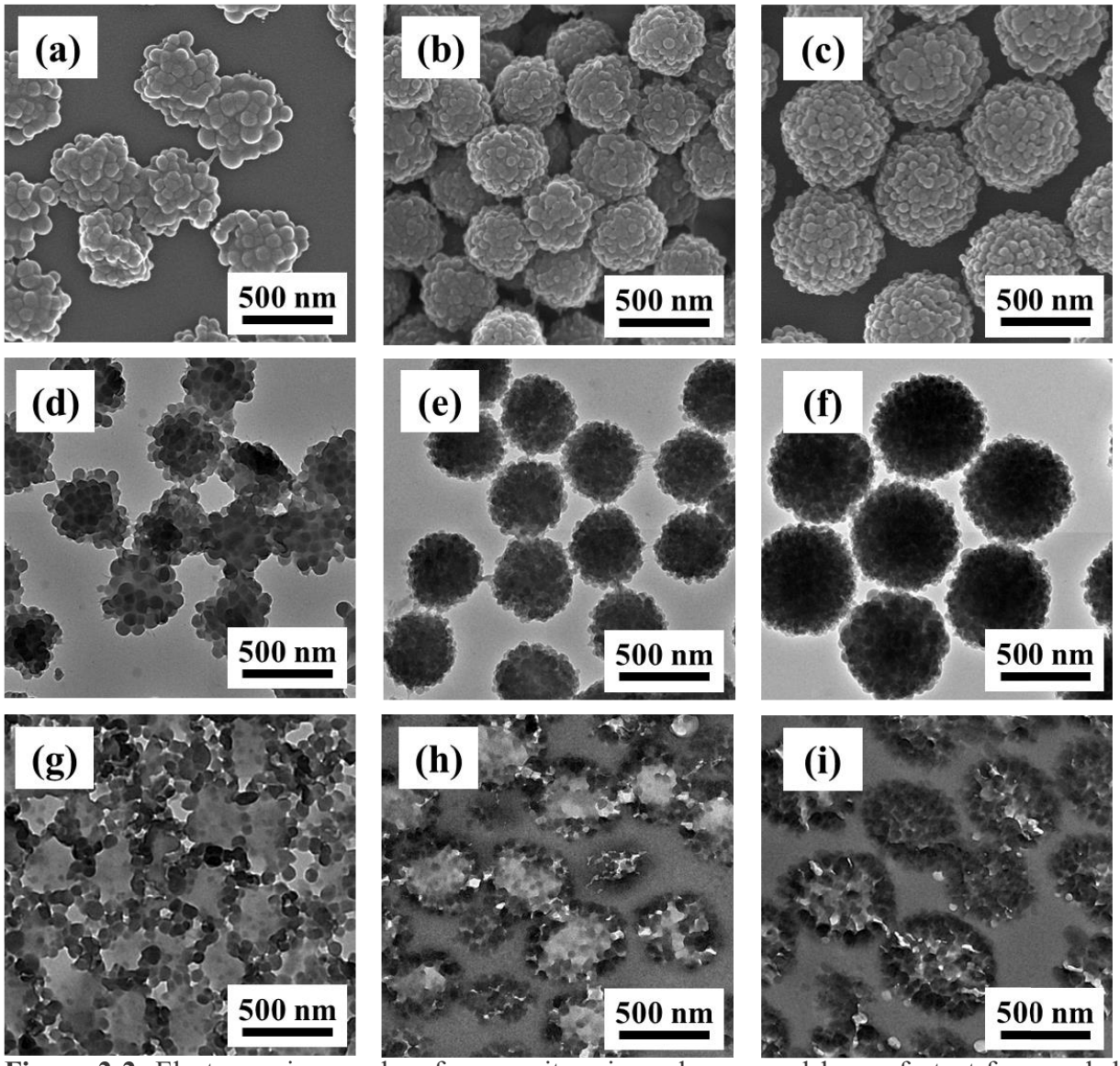


**Figure 2-2**. Electron micrographs of composite microgels prepared by surfactant-free seeded emulsion polymerization under pH 10 using (a, d, g) **NM5**, (b, e, h) **NA5**, and (c, f, i) **NF5** microgels as seeds. (a, b, c) FE-SEM images. (d, e, f) TEM images. (g, h, i) TEM images of ultra-thin sections of the composite microgels. The styrene concentration was fixed at 100 mM during seeded emulsion polymerization.

**Table 2-3.** The Mean Diameters of Composite Microgels and Polystyrene Nanoparticles Attached on the Core Microgels.

| Code | Diameter of composite microgels | | Diameter of polystyrene nanoparticles | |
|---|---|---|---|---|
| | nm | CV / % | nm | CV / % |
| NM5-S100 | 496 ± 24 | 4.8 | 80 ± 12 | 15 |
| MA5-S100 | 439 ± 22 | 5.0 | 45 ± 9 | 19 |
| NF5-S50 | 643 ± 43 | 6.7 | 23 ± 5 | 20 |
| NF5-S100 | 654 ± 27 | 4.2 | 48± 7 | 15 |
| NF5-S200 | 805 ± 33 | 4.1 | 100 ± 29 | 29 |
| NF5-S300 | 1033 ± 41 | 4.0 | 205 ± 35 | 17 |
| NF20-S100 | 810 ± 38 | 4.7 | 59 ± 6 | 10 |
| NF40-S100 | 869 ± 61 | 7.0 | 70 ± 8 | 11 |
| NF50-S100 | 1163 ± 80 | 6.8 | 82 ± 9 | 12 |

※The mean diameters were measured from FE-SEM images (**Figures 1-3**, $N = 50$)

### 2.3.3. Effect of Styrene Concentration on the Seeded Emulsion Polymerization in the Presence of Carboxyl Group Containing Microgels

Subsequently, the author examined the effect of styrene concentration during seeded emulsion polymerization on the structure of the resultant composite microgels. In the case of **NM5** core microgels, composite microgels were aggregated during the polymerization when the styrene concentration was increased to 200 mM, consistent with our previous work on seeded emulsion polymerization of styrene in the presence of **NM*X*** microgels (***X*** = 1, 10, 30, 50 mol.%). [14] By contrast, in the cases of the **NA5** and **NF5** systems, the resultant composite microgels were stable even though the concentration of styrene monomer was increased to 300 mM; however, the composites aggregated when the concentration was 400 mM in both cases. The difference in colloidal stability for each composite microgel will be discussed later. **Figure 2-3** shows electron micrographs of the dried composite microgels prepared with **NF5** microgels under different styrene concentrations. The diameters of these composite microgels and polystyrene nanoparticles attached on the core microgels were listed in **Table 3** Additionally, polystyrene occupied areas in microgels were 37 ± 9 % (**NF5-S50,** CV = 15 %, *N* = 50, **Figure 2-3(g)**), 71 ± 6 % (**NF5-S100,** CV = 9 %, *N* = 50, **Figure 2-2(i)**), 85 ± 6 % (**NF5-S200,** CV = 6 %, *N* = 50, **Figure 2-3(h)**), and 97 ± 2 % (**NF5-S300,** CV = 2 %, *N* = 50, **Figure 2-3(i)**), respectively. The diameters of both composite microgels and polystyrene nanoparticles increased with increasing styrene concentration during seeded emulsion polymerization. Moreover, a higher styrene monomer concentration resulted in more polystyrene nanoparticles fusing with each other, which, in turn, resulted in a smoother surface of the composite microgels because of the minimization of interfacial free energy between the polystyrene and the aqueous phase. As evident in **Figure 2-3(g)–(i)**, polystyrene nanoparticles were formed inside the core **NF5** microgels. The diameters of these polystyrene nanoparticles formed inside of the cores were measured to be 23 ± 4 nm (CV = 17 %, *N* = 50, **NF5-S50, Figure 2-3(g)**), 48 ± 9 nm (CV = 18 %, *N* = 50, **NF5-S100, Figure 2-2(i)**), 55 ± 13 nm (CV = 24 %, *N* = 50, **NF5-S200, Figure 2-3(h)**).These results indicate that the size of polystyrene nanoparticles formed inside the core microgels increased with increasing styrene monomer concentration during seeded emulsion polymerization. In the case of **NF5-S50** microgels and **NF5-S100** microgels, the diameters of the polystyrene nanoparticles formed inside the microgels were nearly as large as those attached to the surface of the core microgels (23 ± 5 nm, **NF5-S50**, **Figure 2-3(a)** and 48 ± 7 nm for **NF5-S100**, **Figure 2-2(c))**. Conversely, in the case of **NF5-S200** composite microgels, the sizes of polystyrene nanoparticles formed inside the microgels were smaller than those attached to the surfaces of the microgels (100 ± 29 nm for **NF5-S200**, **Figure 2-3(b)**), indicating that diffusion of styrene monomer inside the microgels was limited to some extent in this method. In light of the importance of the styrene addition mode on seeded emulsion polymerization,[36] the effect of the styrene addition mode on the structure of resultant composite microgels in this case will be reported in near future.

Interestingly, in the case of the **NF5-S300** composite microgels (**Figure 2-3(i)**), the shape of polystyrene was no longer spherical and the core **NF5** microgels were occupied almost entirely by polystyrene. As a control experiment, the seeded emulsion polymerization of styrene was also performed in the presence of **NA5** microgels; however, the core microgels were not entirely occupied with polystyrene compared to **NF5-S300** microgels even though the styrene concentration was increased to 300 mM; in addition, spaces (i.e., white regions) were present, where polystyrene domains did not exist (**Figure 2-5 (b),(d)**). The difference in the composite structures between **NF-S** and **NA-S** composite microgels is explained by the amount of carboxyl groups inside **NA5** microgels being substantially greater than the amount in **NF5** microgels, as previously described. Because **NM*X*** (***X*** = 5, 10, 30, 50 mol.%), in which carboxyl groups are localized at the center of cores, did not form polystyrene nanoparticles inside the microgels, [29] the polyelectrolyte networks of **NA5** microgels suppressed the formation of polystyrene inside the microgels. However, a comparison between **NM*X*** microgel systems and the other systems (i.e., **NA5** and **NF5** microgels) reveals that carboxyl groups located on seed microgels play an important role in stabilizing the composite microgels during seeded emulsion polymerization and in determining the sites where hydrophobic polystyrene nanoparticles are bound.

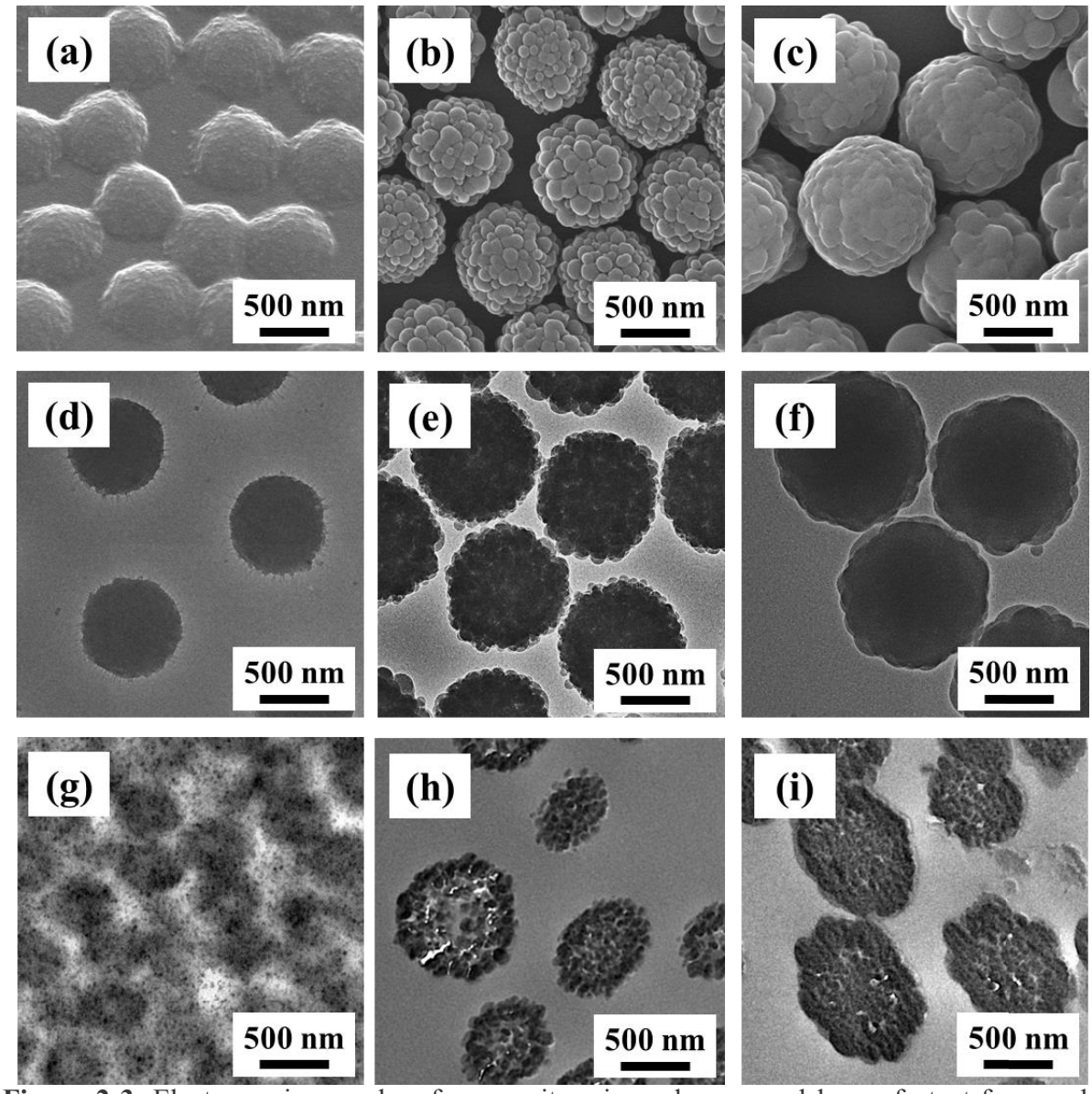


**Figure 2-3**. Electron micrographs of composite microgels prepared by surfactant-free seeded emulsion polymerization in the presence of **NF5** microgels. Styrene concentrations were (a, d, g) 50 mM, (b, e, h) 200 mM, (c, f, i) 300 mM. (a, b, c) FE-SEM images. (d, e, f) TEM images. (g, h, i) TEM images of ultrathin cross sections of composite microgels.

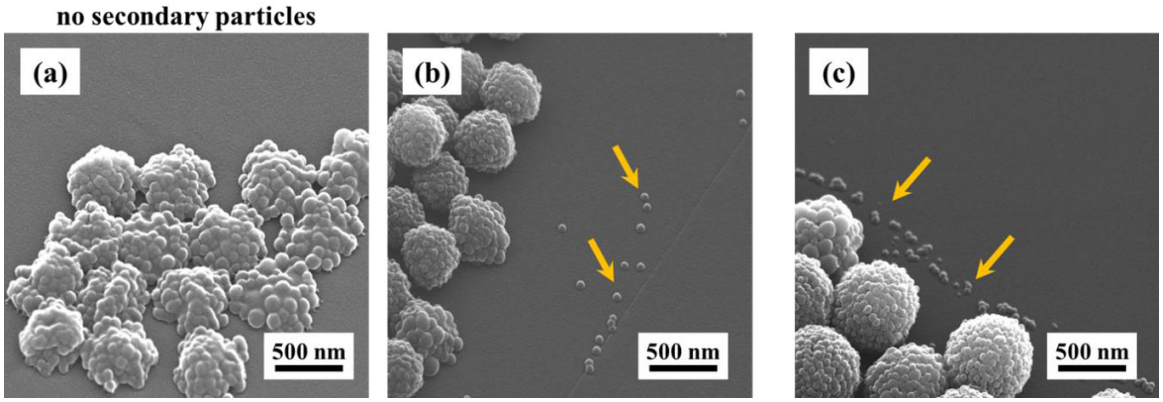


**Figure 2-4**. FE-SEM images of secondary polystyrene nanoparticles: (a) **NM5-S100** (no secondary polystyrene nanoparticles), (b) **NA5-S100**, and (c) **NF5-S100** composite microgels. The secondary nanoparticles were indicated by yellow allows.

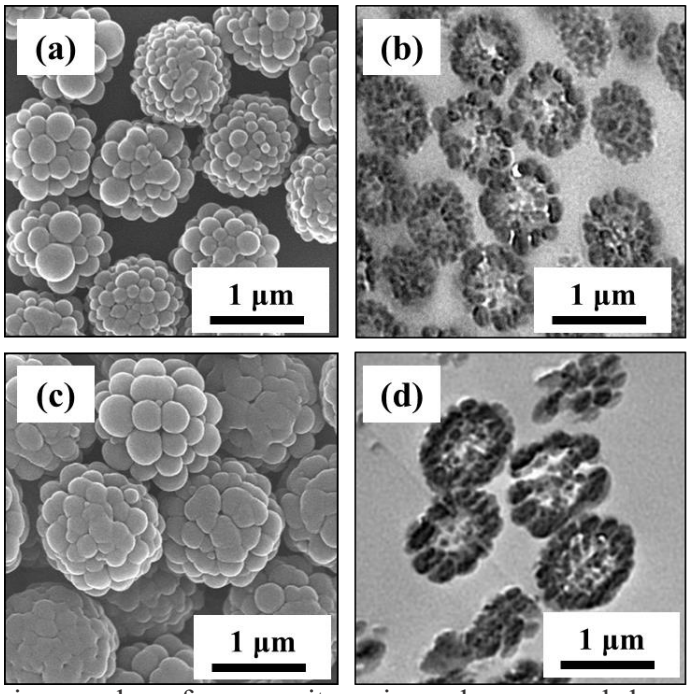


**Figure 2-5**. Electron micrographs of composite microgels prepared by seeded emulsion polymerization of styrene in the presence of **NA5** microgels. Styrene concentrations were fixed at (a, b) 200 mM and (c, d) 300 mM. (a, c) FE-SEM images. (b, d) TEM images of ultrathin cross sections of the composite microgels.

### 2.3.4. Characterization of Stimuli-Responsiveness and Surface Properties of Composite Microgels

Because the author confirmed that the composite microgels were uniform, as determined from electron micrographs, the author subsequently evaluated these composite microgels dispersed in aqueous solution. First, the temperature- and pH-responsiveness of the composite microgels were examined by DLS (**Table 2-4**). Composite microgels with a small amount of polystyrene (i.e., **NF5-S50** microgels) exhibited swelling/deswelling behavior. By contrast, determining whether the other composite microgels exhibited such stimuli-responsiveness on the basis of these changes in hydrodynamic diameters is difficult (**Table 2-4**). Therefore, the author evaluated the EPMs of these composite microgels to clarify the changes in their surface properties

Swollen, neutral microgels are generally acknowledged to exhibit low absolute values of EPM, and the absolute EPM values are known to increase as microgels deswell because of the increase in their surface charge densities, which was also seen from core microgels in this study (**Table 2-4**).[40] Because EPM values are sensitive to the periphery of microgels, whether the composite microgels are covered with hydrogel layers can be determined by comparing their parent core microgels (**Table 2-4**) and free polystyrene particles. [12-14] Notably, the EPM of polystyrene particles synthesized by surfactant-free emulsion polymerization using KPS as an initiator are $-2.97 \pm 0.07 \times 10^{-8}$ $m^2$ $V^{-1}$ $s^{-1}$ at 25 °C and pH 3, and $-3.13 \pm 0.16 \times 10^{-8}$ $m^2$ $V^{-1}$ $s^{-1}$ at 25 °C and pH 10. At 25 °C, where the microgel networks in the composite must be hydrated, the EPM for **NF5-S50** composite microgels did not substantially change at either pH 3 or pH 10 from the EPM of their parent core (i.e., **NF5** microgels), indicating that the surface of the composites were not bound to polystyrene nanoparticles. This result is well consistent with the electron microscopy observations (**Figure 2-3(a),(d)**) indicating that the number of polystyrene nanoparticles bound to core microgels was low and that the resultant composite microgels were highly deformed. With increasing concentration of styrene monomer used during seeded emulsion polymerization (i.e., **NF5-S100**, **NF5-S200** composite microgels), the absolute values of EPM became larger than those of the parent microgels (**NF5**) and were shifted to higher values when the pH was increased from 3 to 10 (**Table 2-4**); by contrast, the values of pure polystyrene particles were virtually constant with changing pH, as previously mentioned. This result indicates that the surfaces of these composite microgels were partially covered with polystyrene, although most of the surfaces was hydrogel layers.

In the case of **NF5-S300** composite microgels, which contained the largest amount of bound polystyrene, the EPM values of the composite microgels approached the EPM value of free polystyrene particles; in particular, the EPM value of the **NF5-S300** microgels measured at pH 10, where the carboxyl groups originating from core **NF5** microgels were deprotonated, became larger than that of free polystyrene particles. This result indicates that the surface of **NF5-S300** composite microgels possess pH-responsive hydrogel layers. This idea is supported by the changes in EPMs with increasing temperature; absolute values of EPM at 70 °C for all composite microgels listed

in **Table 2-4** increased compared to those measured at 25 °C, indicating that these composite microgels were covered with thermoresponsive hydrogel layers. Actually, **NF5-S300** microgels exhibited high colloidal stability at centrifugation process comparing the case of pure polystyrene particles (**Figure 2-6**).

**Table 2-4.** Hydrodynamic Diameters and Electrophoretic Mobilities of Various **NF-S** Composite Microgels

| Code | pH | Hydrodynamic diameter /nm | | electrophoretic mobility / × $10^{-8}$ $m^2$/Vs | |
|---|---|---|---|---|---|
| | | 25 °C | 70 °C | 25 °C | 70 °C |
| NF5 | 3 | 570 ±3.8 | 479 ± 7.2 | -0.70 ± 0.01 | -3.31± 0.06 |
| | 10 | 2605 ±38 | 946 ± 13 | -2.08 ± 0.01 | -3.66 ± 0.09 |
| NF5-S50 | 3 | 867 ±30 | 487 ±13 | -0.69± 0.002 | -3.28 ± 0.004 |
| | 10 | 1444 ±46 | 819 ± 15 | -1.75 ± 0.02 | -4.10± 0.07 |
| NF5-S100 | 3 | 854 ±9 | 743 ± 36 | -1.68 ± 0.02 | -3.59 ± 0.06 |
| | 10 | 957 ±17 | 736 ± 10 | -2.37 ± 0.03 | -4.85 ± 0.32 |
| NF5-S200 | 3 | 1029 ±14 | 1027 ± 24 | -1.73 ± 0.03 | -3.58 ± 0.01 |
| | 10 | 1157 ±14 | 977 ± 13 | -2.23 ± 0.02 | -5.76 ± 0.53 |
| NF5-S300 | 3 | 1198 ± 32 | 1251 ± 34 | -2.68 ± 0.02 | -4.27 ± 0.08 |
| | 10 | 1153± 98 | 1143 ± 35 | -4.69 ± 0.05 | -7.41 ± 0.15 |
| polystyrene particle | 3 | 380 ± 2 | 395 ±1 | -2.97 ± 0.07 | -2.99 ± 0.06 |

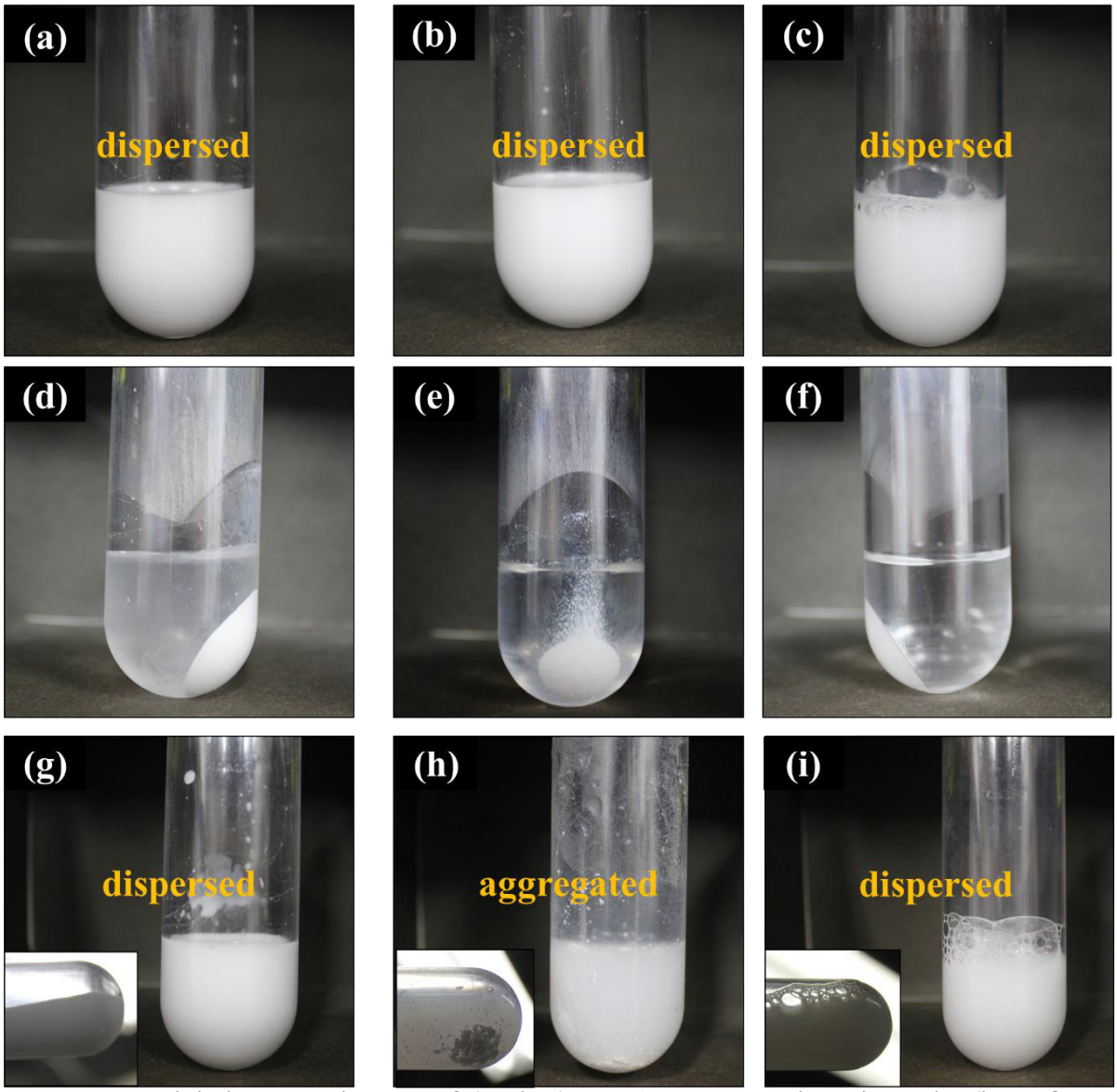


**Figure 2-6**. Digital camera images of (a, d, g) **NF5S300** composite microgels, (b, e, f) pure polystyrene particles , and (c, f, i) **NF5** microgels dispersions (a-c) before centrifugation procedure (70,000×*g*, 30 min, 15 ° C), (d-f) after centrifugation procedure, and (g-i) after re-dispersion procedure (shaking for 30 min), respectively. The pure polystyrene particles could not be re-dispersed and a lot of aggregates were formed (g). By contrast, the **NF5** microgels and **NF5S300** composite microgels could be re-dispersed easily (h, i).

### 2.3.5. Dependence of the Amount of FAc Incorporated in Microgels

The author has clarified that carboxyl-group distribution in core microgels indeed affects the resultant composite microgels synthesized by seeded emulsion polymerization of styrene. Next, to clarify the effect of surface charge densities of core microgels on the resultant composite microgels in greater detail, the author synthesized poly(NIPAm-*co*-FAc) microgels with increased amount of FAc fed during precipitation polymerization; the obtained microgels were subsequently used as cores for the seeded emulsion polymerization of styrene. Wu et al. reported that hydrophobic nitrobenzene can be easily diffused into the center of pNIPAm microgels compared to the case of more hydrophilic 4-nitrophenol when the pNIPAm microgels were deswollen. [41] Therefore, the author speculated that, if the surfaces of the core microgels were more swollen by electrostatic repulsion during seeded emulsion polymerization, then polystyrene nanoparticles would not form at the center of the core microgels because the styrene monomer would not easily diffuse into the microgels.

The recipes for the various poly(NIPAm-*co*-FAc) microgels are listed in **Table 1**. Notably, **NF** microgels were aggregated during precipitation polymerization when 60 mol.% FAc was fed (**Figure 2-7**). **Figure 2-8** shows the electron micrographs of dried **NF20**, **NF40**, and **NF50** microgels. On the basis of these FE-SEM images shown in **Figure 2-8(a)–(c)**, the author measured the diameters of these microgels to be 660 ± 23 nm (**NF20**, CV = 3.5 %, $N$ = 50), 647 ± 36 nm (**NF40**, CV = 5.6%, $N$ = 50), and 678 ± 59 nm (**NF50**, CV = 8.7%, $N$ = 50), indicating that they are uniform microgels. Here, the amount of comonomer incorporated in each microgel increased with increasing amount of comonomer fed during the polymerization, which was determined by conductometric titration (**Table 2-5**). The multi-responsive properties of these microgels were then evaluated to clarify their surface charge.

First, temperature- and pH-responsiveness of the **NF** microgels were examined by DLS (**Table 2-6**). As evident in **Table 2-6**, all microgels exhibit temperature- and pH-responsive changes in hydrodynamic diameters. However, it is difficult to clearly say that the DLS measurements at pH = 10 were accurately performed, which was judged by correlation functions. Some of diffusion coefficients were not calculated accurately by the cumlant approach because the electric-field correlation functions were not proportional to the correlation time (**Figure 2-9**). Therefore, instead of using DLS measurements, the author measured apparent diameters of these **NF** microgels attached at the air/water interface from optical microscope images to evaluate the pH responsivities of the microgels (**Table 2-5** and **Figure 2-10**). In all cases, these diameters of various **NF** microgels became larger as the pH was increased from 3 to 10. Additionally, the pH-swelling ratio ($V_{\mathrm{pH10,\ 25\ ^\circ C}}/V_{\mathrm{pH3,\ 25\ ^\circ C}}$) of these microgels increased with increasing amount of FAc incorporated into the microgels (**Table 2-5**). Moreover, the author evaluated the EPM values of these composite microgels to clarify the charge density of the core microgel surfaces. At 25 °C, where the microgels are highly swollen by water, the absolute values of EPM for **NF*X*** microgels ($X$ = 20, 40, 50) were shifted to higher values at pH 10, where carboxyl groups were deprotonated, as compared to that of **NF5** microgels (**Table 2-5**), indicating that the microgels with higher

surface charge densities were obtained. In particular, the absolute values of EPM measured at pH 10 and at 70 °C, where the microgels were more or less deswollen, as indicated by DLS measurements (**Table 2-6**), increased with increasing amount of FAc introduced into the microgels. These results indicate that the amount of charged groups located near the surface of the microgels increased with increasing amount of FAc fed during precipitation polymerization.

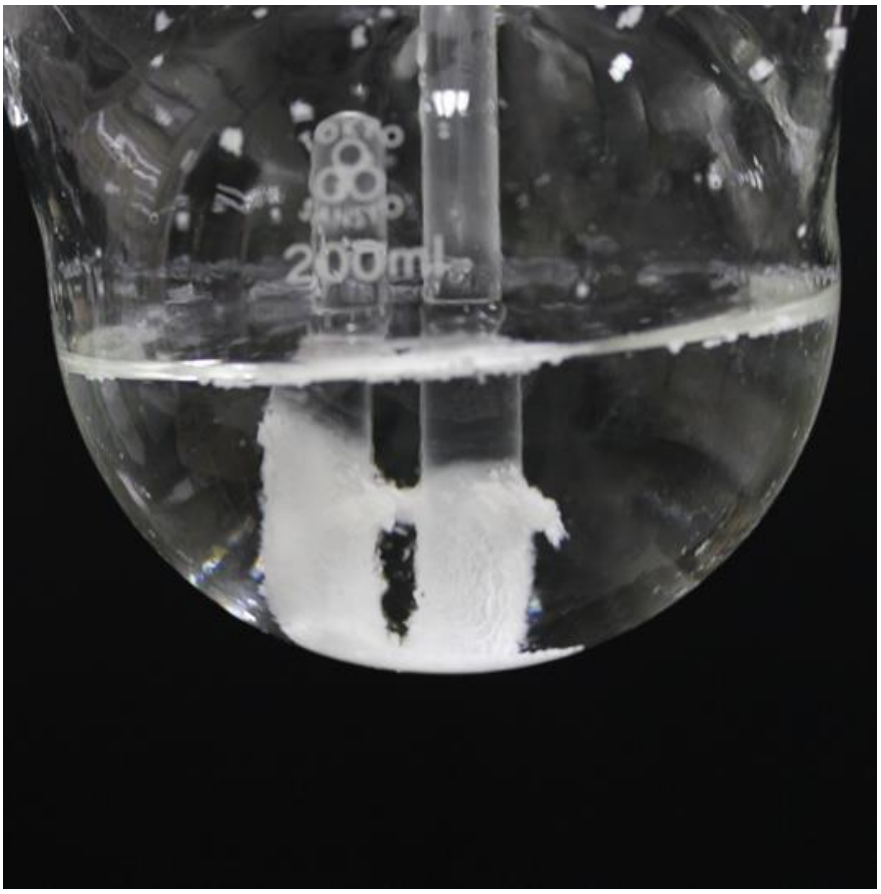


**Figure 2-7.** Photograph of aggregation of **NF60** microgel dispersion.

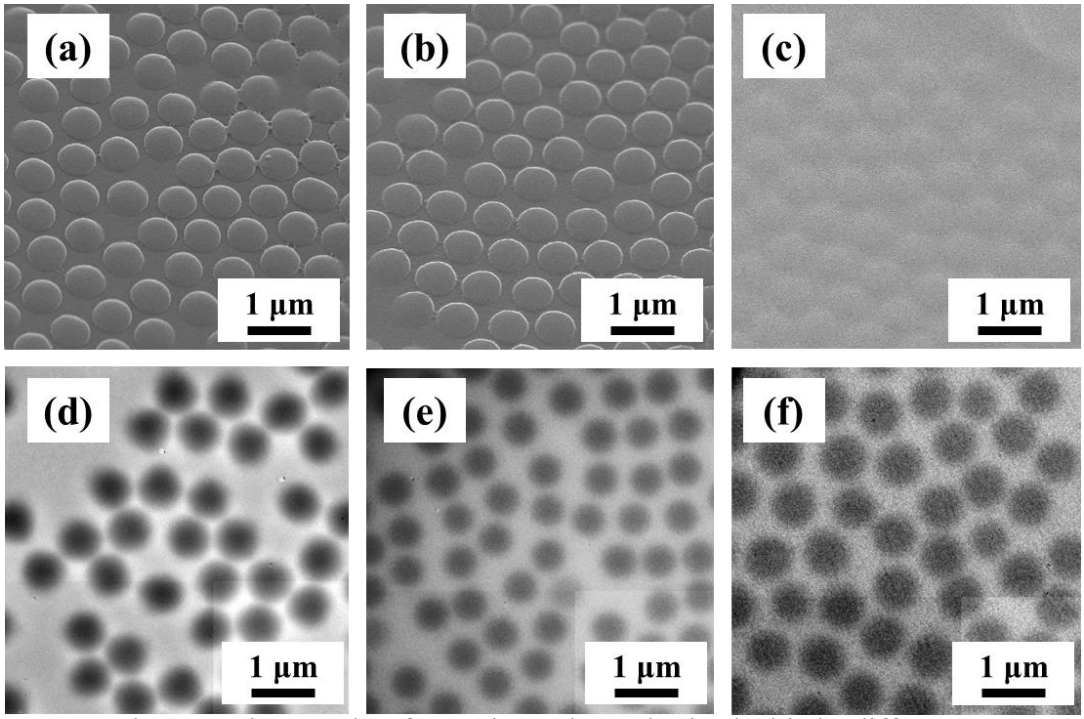


**Figure 2-8**. Electron micrographs of **NF** microgels synthesized with the different amount of FAc fed during precipitation polymerization. (a, d) **NF20**, (b, e) **NF40**, (c, f) **NF50** microgels. (a-c) FE-SEM images. (e-f) TEM images.

**Table 2-5**. Characterization of Each **NF** Microgel.

| Code | pH | diameter at 25 °C ※1 /nm | electrophoretic mobility / × $10^{-8}$ $m^2$/Vs 25 ° C | 70 ° C | swelling ratio ($V_{pH10, 25°C}$/ $V_{pH3, 25°C}$) | content of –COOH in microgel mmol/g |
|---|---|---|---|---|---|---|
| NF5 | 3 | 981 ±58 | -0.70 ± 0.01 | -3.31± 0.06 | 1.6 | 0.44 |
| | 10 | 1150 ±101 | -2.08 ± 0.01 | -3.66 ± 0.09 | | |
| NF20 | 3 | 954 ±58 | -1.10± 0.03 | -3.34± 0.02 | 2.3 | 2.0 |
| | 10 | 1263 ±103 | -2.88 ± 0.04 | -4.31 ± 0.06 | | |
| NF40 | 3 | 821 ±53 | -0.76 ± 0.02 | -3.4 ± 0.03 | 3.3 | 3.6 |
| | 10 | 1220 ±71 | -3.05 ± 0.06 | -4.39 ± 0.13 | | |
| NF50 | 3 | 836 ±88 | -0.93 ± 0.03 | -3.26 ± 0.04 | 5.9 | 4.2 |
| | 10 | 1512 ±108 | -2.76 ± 0.004 | -4.82 ± 0.18 | | |

※1 : Determined with optical microscope image in **SI Figure 5** in the supporting information.

**Table 2-6**. Hydrodynamic Diameters of NF Microgels at Different pH Condition.

| Code | pH | Hydrodynamic diameter /nm | |
|---|---|---|---|
| | | 25 °C | 70 °C |
| NF5 | 3[a] | 570 ±3.8 | 479± 7.2 |
| | 10[a] | 2605 ±38 | 796 ± 9.2 |
| NF20 | 3[a] | 1034 ±38 | 490 ±6.1 |
| | 10[a] | 3825 ±409 | 2654 ± 308 |
| NF40 | 3[a] | 1167 ±29 | 439 ± 1.6 |
| | 10[a] | 2873 ±166 | 2332 ± 119 |
| NF50 | 3[a] | 1842 ±107 | 535 ± 9.2 |
| | 10[a] | 3798 ±512 | 3977 ± 119 |

a) Ionic strength 1 mM

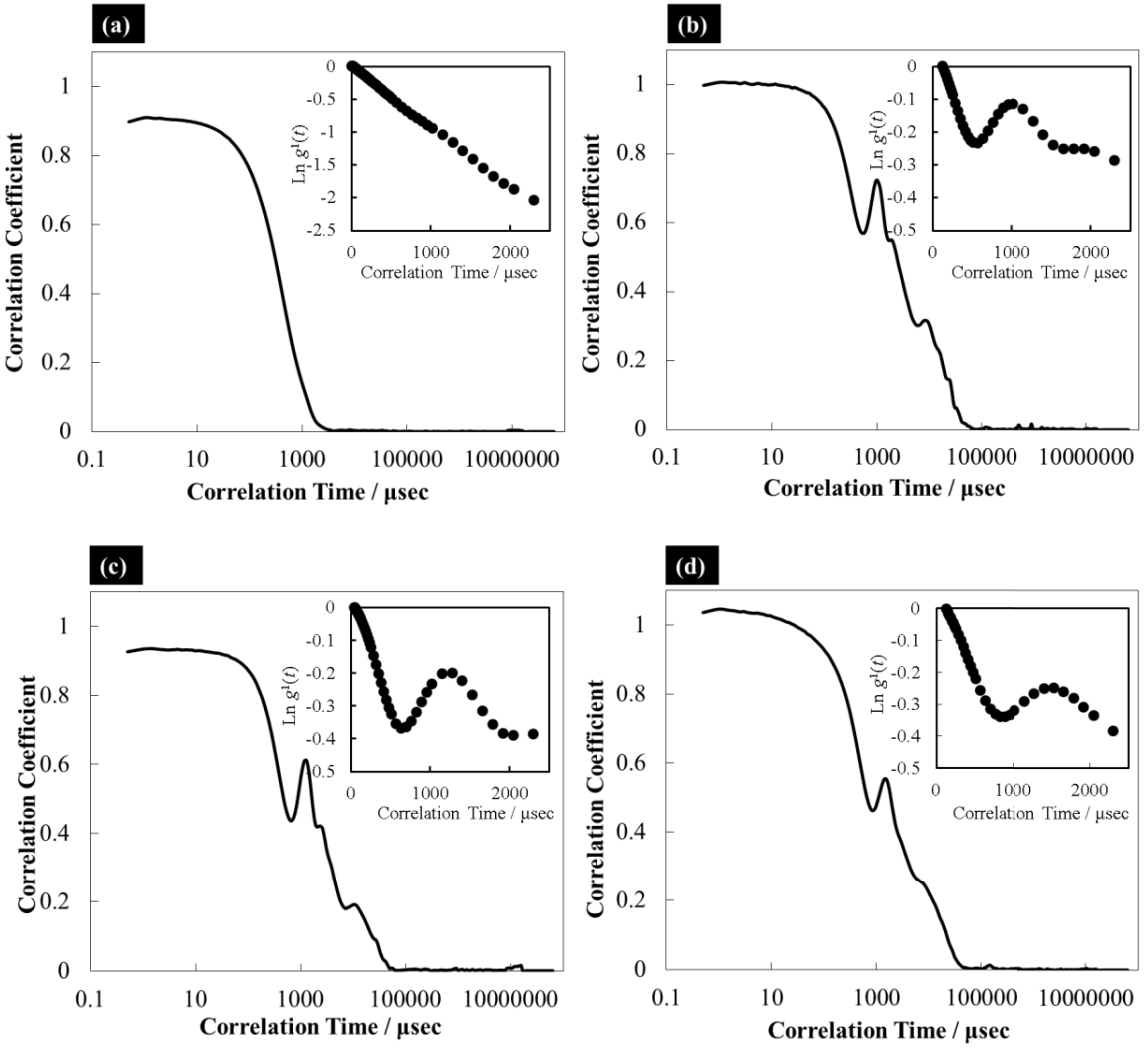


**Figure 2-9**. Intensity correlation functions of (a) **NF5**, (b) **NF20**, (c) **NF40**, and (d) **NF50** microgels measured at pH 10 and 70 °C. Insets are the electric-field time correlation function of these microgels. In the case of **NF5** microgel, the electric-field correlation function was proportional to the correlation time ($t$) in the low $t$ region ($t$/μsec $\leq$ 2500), indicating that the microgel diffusion coefficient was accurately measured because the cumlant approach was performed in the time range of 1 $\leq$ $t$/μsec $\leq$ 2000. In contrast, in the cases of **NF20**, **NF40, NF50** microgels, the diffusion coefficients were not calculated accurately by the cumlant approach because the electric-field correlation functions were not proportional to the correlation time in $t$ > ~ 500.

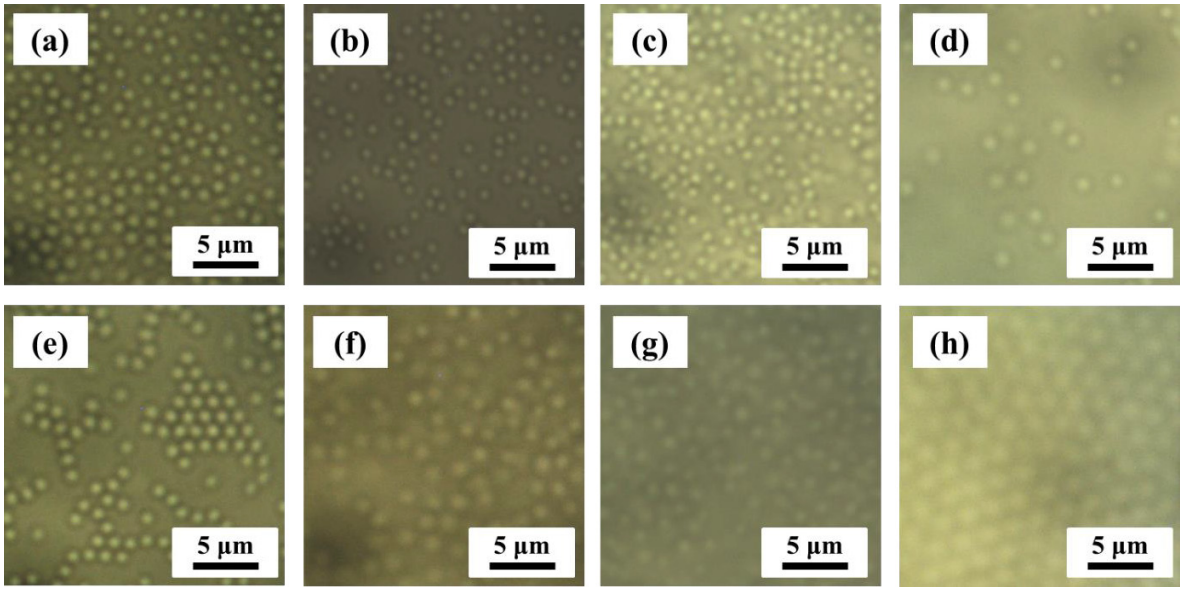


**Figure 2-10**. The optical microscope images of various **NF** microgels attached at the air/water interface at room temperature (a, e) **NF5**, (b, f) **NF20**, (c, g) **NF40**, (d, h) **NF50** microgels, under different pH conditions (a-d) pH3, (e-h) pH10. The microgel concentration was approximately 0.001 wt. %. The microgel morphologies at the air/water interface were observed with an optical microscope (BX51, Olympus) equipped with a digital camera (ImageX Earth Type S-2.0 M Ver. 3. 0. 5, Kikuchi-Optical Co., Ltd.). For the sample preparation, the microgel concentration was appropriately adjusted to 0.001 wt.%, and the ionic strength was adjusted to 1 mM using NaOH, HCl, and NaCl solutions. The microgels attached at the air/water interface were then observed after the microgel dispersions (2 µL) were put on the polystyrene substrate.

### 2.3.6. Composite Microgels Synthesized in the Presence of NF Microgels Having Different Amounts of FAc

Electron micrographs of these composite microgels are shown in **Figure 2-11**. The mean diameters of the composite microgels and polystyrene nanoparticles were calculated from these images and shown in **Table 2-3**. Diameters of both composite microgels and polystyrene nanoparticles increased with increasing amount of FAc fed during precipitation polymerization; however, the composites containing microgels with high FAc contents (i.e., **NF40-S100** and **NF50-S100**) were highly deformed on the solid substrates under high-vacuum conditions (**Figure 2-11(b),(c)**). Moreover, the amount of secondary (or individual) polystyrene nanoparticles during seeded emulsion polymerization of styrene also increased with increasing amount of FAc incorporated into the core microgels, as determined quantitatively by thermogravimetric analysis (**Figure 2-12 and 2-13**). This result supports that styrene monomer could be dissolved in neutral (deswollen) pNIPAm microgel phase and the amount of styrene monomer dissolved in water phase was increased with increasing amount of FAc incorporated into the core microgels. Additionally, the results also indicated that the surfaces of the composite microgels with high FAc contents (i.e., **NF40-S100** and **NF50-S100**) were not completely covered with polystyrene nanoparticles. Polystyrene secondary (or individual) particles were not observed by TEM after two centrifugal purification procedures (**Figure 2-11(d)–(f)**). Notably, given the monomer/comonomer copolymerization curves (**Scheme 2-1(A)**), the author assumed that a portion of the FAc monomer was also present at the center of the microgels when the amount of FAc monomer fed during precipitation polymerization was high. For example, in the case of **NF50** microgels, ~10% of FAc was expected to be incorporated at the center of the core microgels because of the mechanism of precipitation polymerization. Therefore, styrene monomer might not easily diffuse into the polyelectrolyte cores of the **NF40** and **NF50** microgels; thus, the amount of polystyrene bound to core microgels decreased.

The author also visualized the internal structures of the composite microgels by preparing ultra-thin cross sections (**Figure 2-11(g)–(i)**). Similar to the **NF5-S100** composite microgels (**Figure 2-2(i)**), polystyrene nanoparticles were also formed inside the core microgels in the case of **NF20-S100** composite microgels (**Figure 2-11(g)**). In contrast, in the case of **NF40-S100** composite microgels, the center of the composite microgels was not entirely occupied by polystyrene as compared to **NF20-S100** composite microgels; thus, spaces (i.e., white regions) were present in which polystyrene domains did not exist. Furthermore, in the case of **NF50-S100** composite microgel, the internal structure was not clearly investigated although the author attempted to prepare cross sections several times; our difficulty in cross-sectioning this composite microgel implies that it was not entirely covered with polystyrene nanoparticles and not occupied by polystyrene.

Thus far, the structures of the composite microgels had been observed by TEM and SEM, where the only dehydrated microgels were imaged in the high-vacuumed EM columns. In this study,

composite microgels of **NF5-S100** and **NF40-S100** were examined using cryo-TEM in order to clarify the morphology of the hydrated composite microgels (**Figure 2-14**). Compared with their appearance in the FE-SEM images shown in **Figure 2-2(c)** and **Figure 2-11(b)**, the shapes of the hydrated composite microgels appeared more spherical. The size of **NF40-S100** composite microgels determined by cryo-TEM image (528 ± 35 nm, CV = 6.7 %, $N$ = 25, **Figure 2-14(b)**) was significantly smaller than that by TEM image (872 ± 43 nm, CV = 4.9 %, $N$ = 50, **Figure 2-11(e)**). It suggests that the **NF40-S100** composite microgels would be deformed by drying and flattened on the support film during TEM sample preparation. Similarly, the size of **NF5-S100** composite microgels determined by cryo-TEM image (525 ± 16 nm, CV = 3.0 %, $N$ = 25, **Figure 2-14(a)**) was also smaller than that by TEM image (627 ± 45 nm, CV = 7.2 %, $N$ = 50, **Figure 2-2(f)**), which was thought to be the same reason with **NF40-S100** composite microgels. Moreover, the center-to-center distances among the polystyrene nanoparticles presented around **NF5-S100** and **NF40-S100** composite microgels were measured to be 53 ± 9 nm ($N$=50, from cryo-TEM image, **Figure 2-14(a)**), and 76 ± 9 nm ($N$=50, from cryo-TEM image, **Figure 2-14(b)**), respectively. These distances were both larger than the size of the original polystyrene nanoparticles, indicating that the polystyrene nanoparticles did not completely cover the **NF-*X*** microgels when they were dispersed in aqueous solution as is the case with **NM-S** composite microgels.[14]

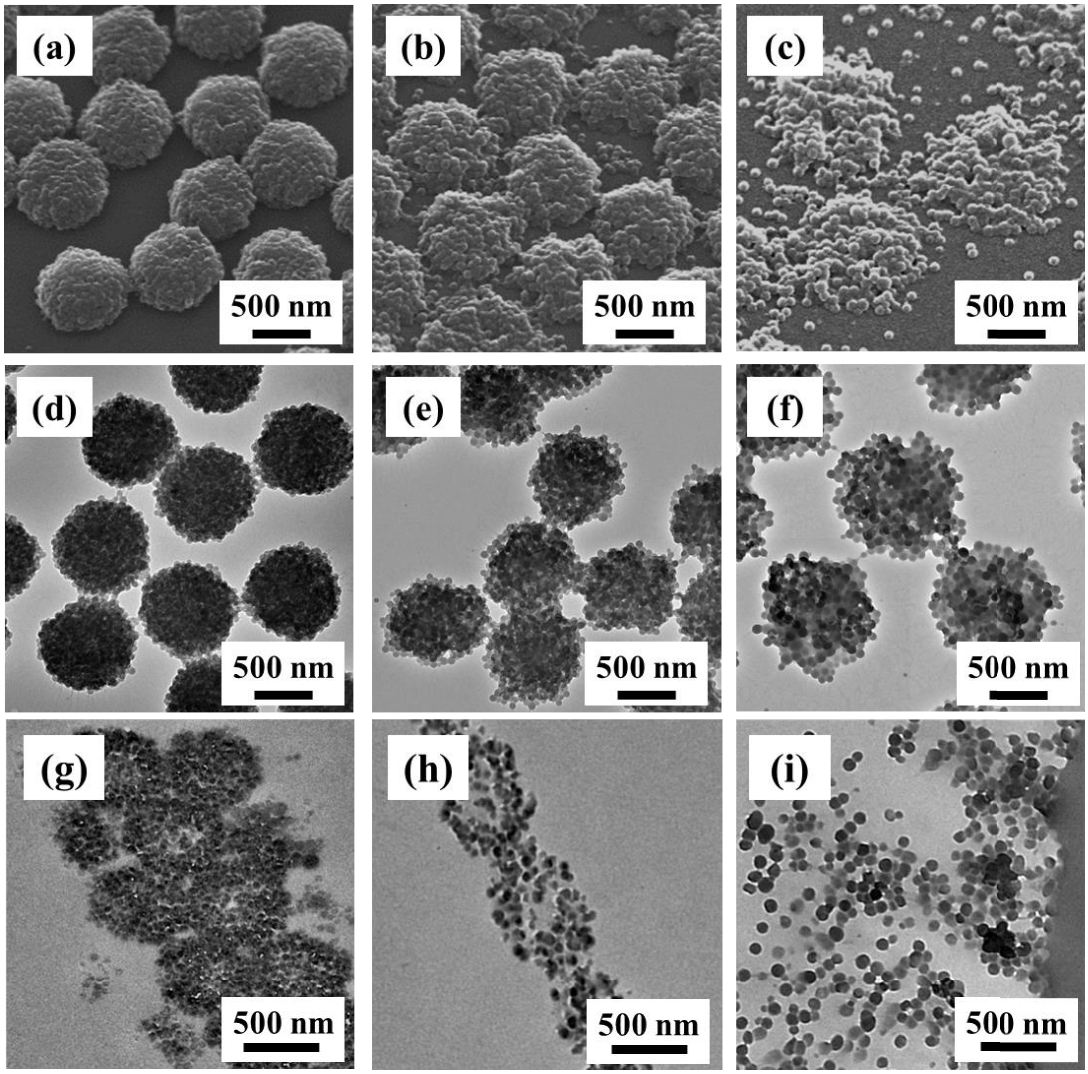


**Figure 2-11.** Electron micrographs of (a, d, g) **NF20-S100**, (b, e, h) **NF40-S100**, and (c, f, i) **NF50-S100** composite microgels. (a, b, c) FE-SEM images. (d, e, f) TEM images. (g, h, i) TEM images of ultra-thin cross sections of the composite microgels.

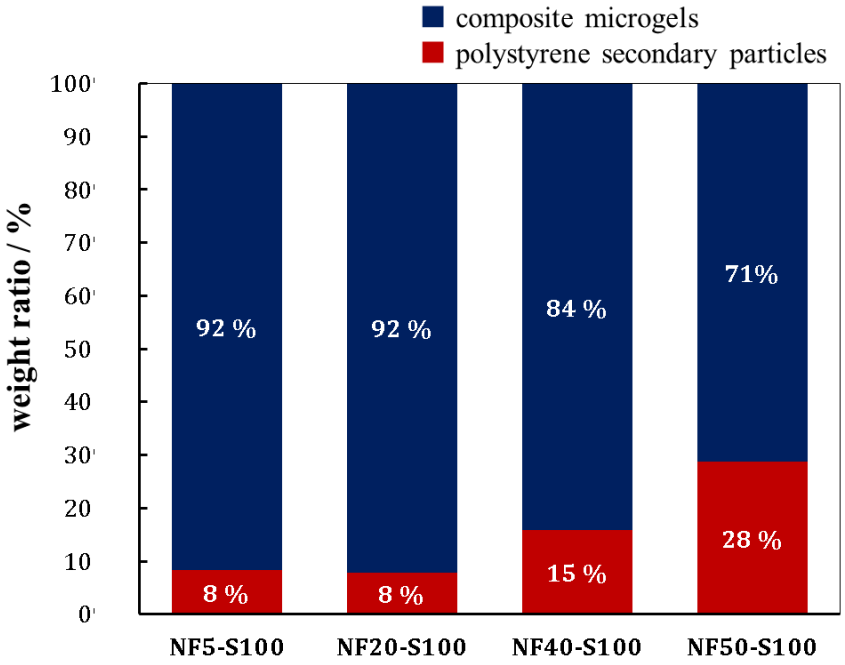


**Figure 2-12**. Weight ratios of composite microgels and secondary polystyrene nanoparticles in **NF-S** systems. For sample preparations, these composite microgel dispersions were centrifuged (20,000×*g*, 10 min) to separate the composite microgels and secondary polystyrene particles. The thermo gravimetric analysis was performed on Shimadzu analyzer DYG-60H under $N_2$ atmosphere using platinum crucibles with heating rate of 10 °C/min from room temperature to 90 °C.

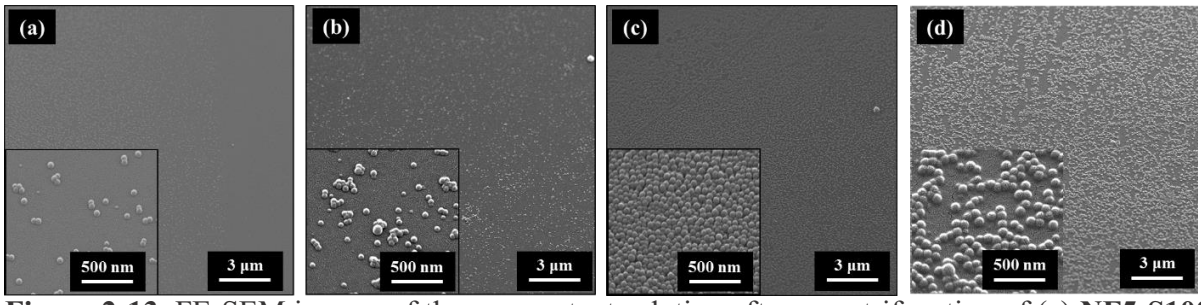


**Figure 2-13.** FE-SEM images of the supernatant solution after a centrifugation of (a) **NF5-S100**, (b) **NF20-S100**, (c) **NF40-S100**, and (d) **NF50-S100** microgel dispersions, which were samples for the TGA measurements. The supernatant solutions were dried on the polystyrene substrates at room temperature. The diameters of the composite microgels were determined to be 54.8 ± 4 nm (CV = 8 %, *N* = 50, **(a)**), 57.2 ± 4 nm (CV = 8 %, *N* = 50, **(b)**), 54.6 ± 5 nm (CV = 8 %, *N* = 50, **(c)**), and 85.0± 8 nm (CV = 9 %, *N* = 50, **(d)**).

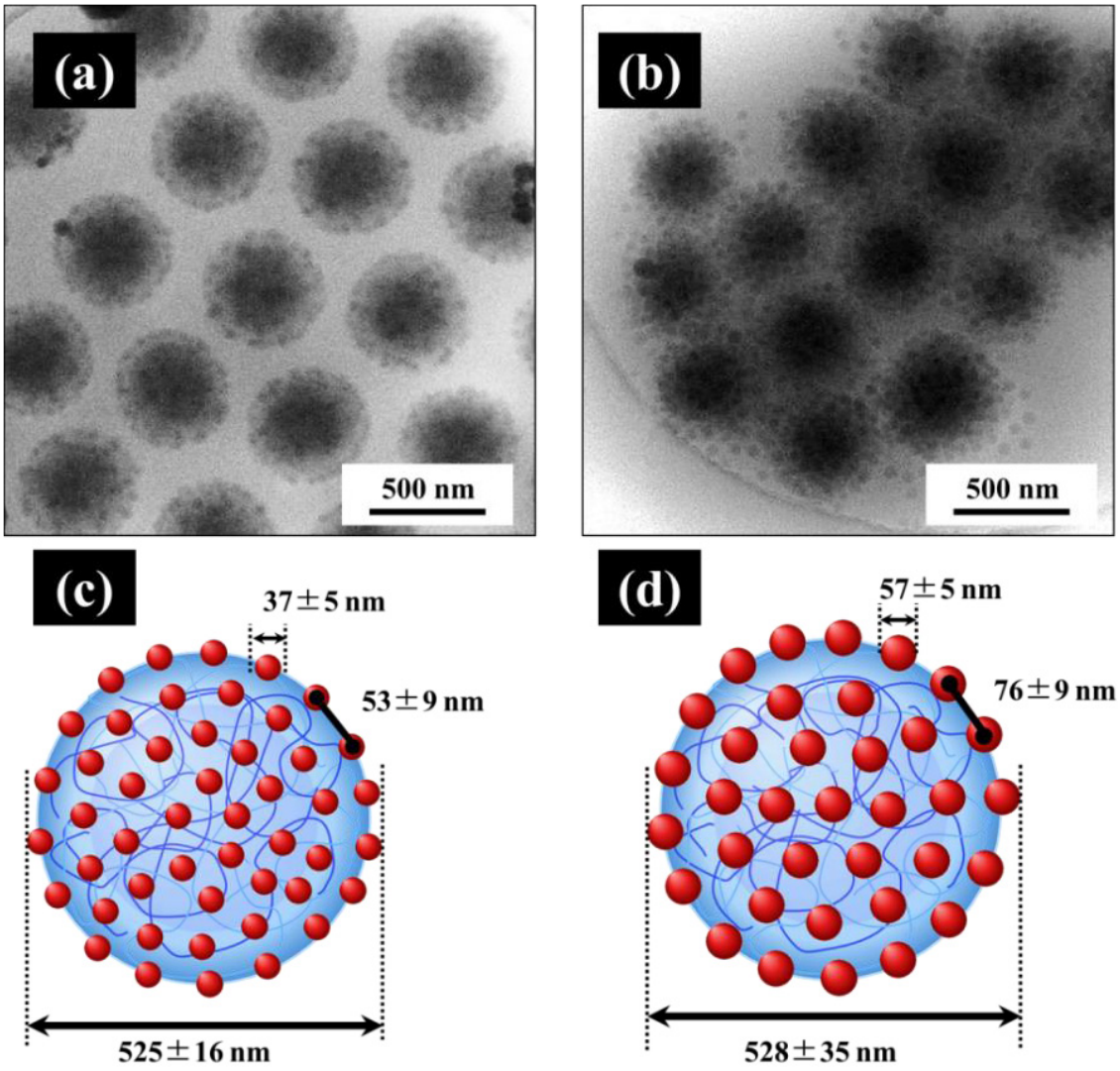


**Figure 2-14**. (a, b) Cryo-TEM images and (c, d) schemes of composite microgel structures of (a, c) **NF5-S100** composite microgels and (b, d) **NF40-S100** composite microgels.

### 2.3.6. Composite Microgels Synthesized in the Presence of Core/Shell Microgels Having Highly Charged Thicker Shell

As previously mentioned, the number of carboxyl groups appeared to be increased not only on the surface of the microgels but also inside the microgels when the amount of FAc fed during precipitation polymerization was increased. Therefore, to eliminate the possibility of the presence of charged groups inside the core microgels, a cross-linked poly(NIPAm-*co*-AAc) shell was added onto **NF5** microgels by semi-batch seeded precipitation polymerization and the resultant core–shell microgels were used as cores for the seeded emulsion polymerization of styrene. The author fed 40 mol.% AAc during semi-batch seeded precipitation polymerization because microgels were not obtained stably when 50 mol.% AAc was fed during the core synthesis (**Table 2-1**); with 40 mol.% AAc, the shell was indeed attached onto **NF5** microgels without forming secondary particles, as confirmed by FE-SEM observations (**SI Figure 2-15)** and by DLS measurements. Additionally, from the DLS measurements, hydrodynamic diameters of the core (**NF5**) and core–shell (**NF5-NA40**) microgel were measured to be $D_h$ = 483 ± 3.3 nm (core, pH 3, 70 °C) and $D_h$ = 619 ± 9.5 nm (core–shell, pH 3, 70 °C). From these values, the shell thickness under these conditions is approximately 68 nm (shell thickness was denoted as $R_{h\ \text{core-shell, pH3}} - R_{h\ \text{core, pH3}}$). Moreover, almost all of the carboxyl-group-containing monomer fed during the polymerization for shell synthesis was incorporated (core microgel: 0.44 mmol/g (refer to **Table 2-2**, **NF5** microgel)), shell of microgel: 3.04 mmol/g), indicating that a polyelectrolyte hydrogel layer with high charge density was indeed formed on the **NF5** core microgels.

**Figure 2-16** shows the electron micrographs of composite microgels prepared by seeded emulsion polymerization of styrene (200 mM) in the presence of the core–shell (**NF5-NA40**) microgels under alkali conditions. From the FE-SEM image (**Figure 2-16(a)**), the diameter of the composite microgels was determined to be 1248 ± 52 nm ($N$ = 50, CV = 4.1 %) and that of the polystyrene nanoparticles was determined to be 61 ± 9 nm ($N$ = 50, CV = 14 %).Note that larger polystyrene particles (~120 nm) were also observed (**Figure 2-16 (a),(b)**); however, these were not included in the mean diameter, as previously shown. The formation of larger polystyrene particles might be linked to the core–shell structure of the core microgels used for seeded emulsion polymerization; however, the reason for the formation of these larger polystyrene particles remains unclear. Most importantly, the TEM images of the ultra-thin cross section (**Figure 2-16(c)**) clearly show that polystyrene nanoparticles were formed at the inside of core–shell microgels despite the fact that a highly charged polyelectrolyte shell existed on the microgels. These results clearly demonstrate that styrene monomer can diffuse into the center of core microgels even though the surface of core microgels is hydrophilic and greatly swollen by electrostatic repulsion, which is a new finding in this study.

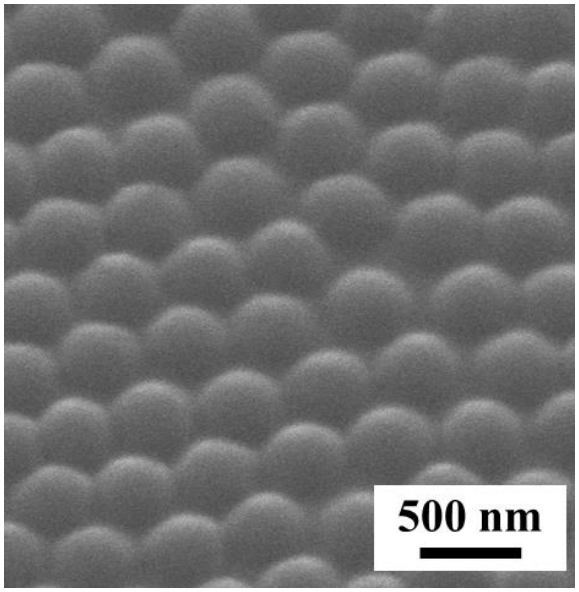


**Figure 2-15**. FE-SEM image of **NF5-NA40** microgels dried on the polystyrene substrate at room temperature.

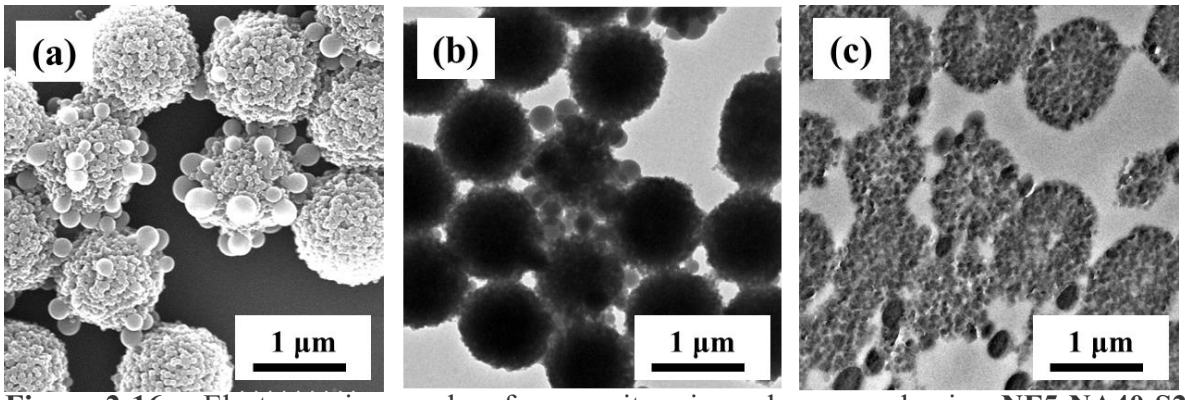


**Figure 2-16.** Electron micrographs of composite microgels prepared using **NF5-NA40-S200** core–shell microgels as cores for seeded emulsion polymerization of styrene. The styrene concentration was fixed at 200 mM. **(a)** FE-SEM image. **(b)** TEM image. **(c)** TEM image of ultra-thin cross section of composite microgels.

### 2.3.7. Formation Process of Composite Microgels Synthesized by Seeded Emulsion Polymerization of Styrene in the Presence of Microgels Possessing Charged Groups Localized on the Surface.

Finally, to clarify how seeded emulsion polymerization of styrene proceeds in the presence of **NF** microgels, where charged groups are localized on the surface, the author monitored the structures of composite microgels at various polymerization times (**Figure 2-13**, **2-15 and 2-17**). Notably, the author attempted to measure the conversion of styrene monomer by gas chromatographic analysis. However, the author did not obtain meaningful conversion data because the polymerization system was a heterogeneous system containing water and styrene; the author did not collect oil drops of styrene from the reaction mixture (i.e., styrene conversion was nearly 100 % at 5 min from the polymerization). **Figure 2-17** summarizes the mean diameters of composite microgels and polystyrene nanoparticles ($N$ = 50, from FE-SEM images) and the number of polystyrene nanoparticles on the microgels surface ($N$ = 50, from FE-SEM images) at different polymerization times for **NF5-S100** composite microgels. The size of composite microgels decreased slightly during the early polymerization stage (until 30 min) because the composite microgels with a low amount of polystyrene nanoparticles were deformed by drying; thus, the apparent diameters increased. Therefore, the diameter of composite microgels decreased because the shape of the composite became spherical with increasing size and number of polystyrene nanoparticles attached on core microgels. The size of the composite microgels then increased with increasing polymerization time after 30 min as the size and number of polystyrene nanoparticles attached to core microgels increased. Here, polystyrene nanoparticles were observed on core microgels at 5 min, and they grew from ~23 nm at 5 min to ~46 nm at 60 min (**Figure 2-17(d)**). Notably, polystyrene nanoparticles also appeared around core microgels during the early stage (i.e., 5 and 15 min) of seeded emulsion polymerization (**Figure 2-17(a)**). However, they were not observed by TEM (**Figure 2-17(b)**), which means that these polystyrene nanoparticles were removed easily by the centrifugal purification process described in the Experimental section. pNIPAm-based microgels are known to exhibit non-close-packed ordered structures when they are dried onto solid substrates. [31,42] More recently, Mourrran et al. reported that dried, hemispherical pNIPAm microgels on a solid substrate were surrounded by low-cross-linked pNIPAm networks.[43] The low-cross-linked pNIPAm networks cannot be observed by FE-SEM or TEM, but can be observed by AFM. In the present study, secondary (or individual) polystyrene nanoparticles were not observed in the other areas. Therefore, the author assumed that the polystyrene nanoparticles were weakly bound to or included in the core microgel surfaces. Moreover, the author visualized the internal structures of the composite microgels at different polymerization times from their ultra-thin cross sections (**Figure 2-17 (c)**). The author confirmed that polystyrene nanoparticles were formed not only on the core microgels surface but also inside the core microgels and that they grew from ~32 nm (30 min) to ~47 nm (60 min) to ~46 nm (24 h, **Figure 2-2(i)**). Moreover, the polystyrene occupied areas were also increased from ~57 ± 5 % (30 min, CV = 9 %) to ~70 ± 6 % (60 min, CV = 8 %). Additionally, from the results of **Figure 2-17 (d)** and **2-18**, the diameter

of composite microgels at 1 h ($D$ = 691 nm, CV = 5.9 %, $N$ = 50) was nearly same as one of these at 2 h ($D$ = 699 nm, CV = 4.4 %, $N$ = 50), 4h ($D$ = 694 nm, CV = 5.0 %, $N$ = 50), and 24 h ($D$ = 709 nm, CV = 5.6 %, $N$ = 50), indicating that almost all of styrene monomer was consumed within 1 hour after starting polymerization.

Conversely, when pNIPAm-based microgels with carboxyl groups localized at their center (i.e., **NM*X***: $X$ = 1, 5) were used as cores, the number of polystyrene nanoparticles formed on the surface of the core microgels decreased and the sizes of the polystyrene nanoparticles markedly increased as polymerization time proceeded (**Figure 2-18**, and in reference 14). These tendencies were similar to the case of the pure pNIPAm microgel system (**Figure 2-19**). By contrast, in the case of **NM50** microgels used as cores, which were highly swollen during seeded emulsion polymerization, the number of small polystyrene nanoparticles on the core surface did not substantially decrease because methacrylic acid was incorporated not only at the center but also on the surface of **NM50** microgels in terms of the reactivity ratio (**Scheme 2-1(A)**); thus, the charged groups prevented fusion of the polystyrene nanoparticles. These results indicate that the distribution of charged groups in core microgels affect not only the formation of polystyrene particles in the core microgels[14] but also the size of polystyrene nanoparticles formed on the surface of the core microgels, which is an important parameter for obtaining raspberry-shaped particles.

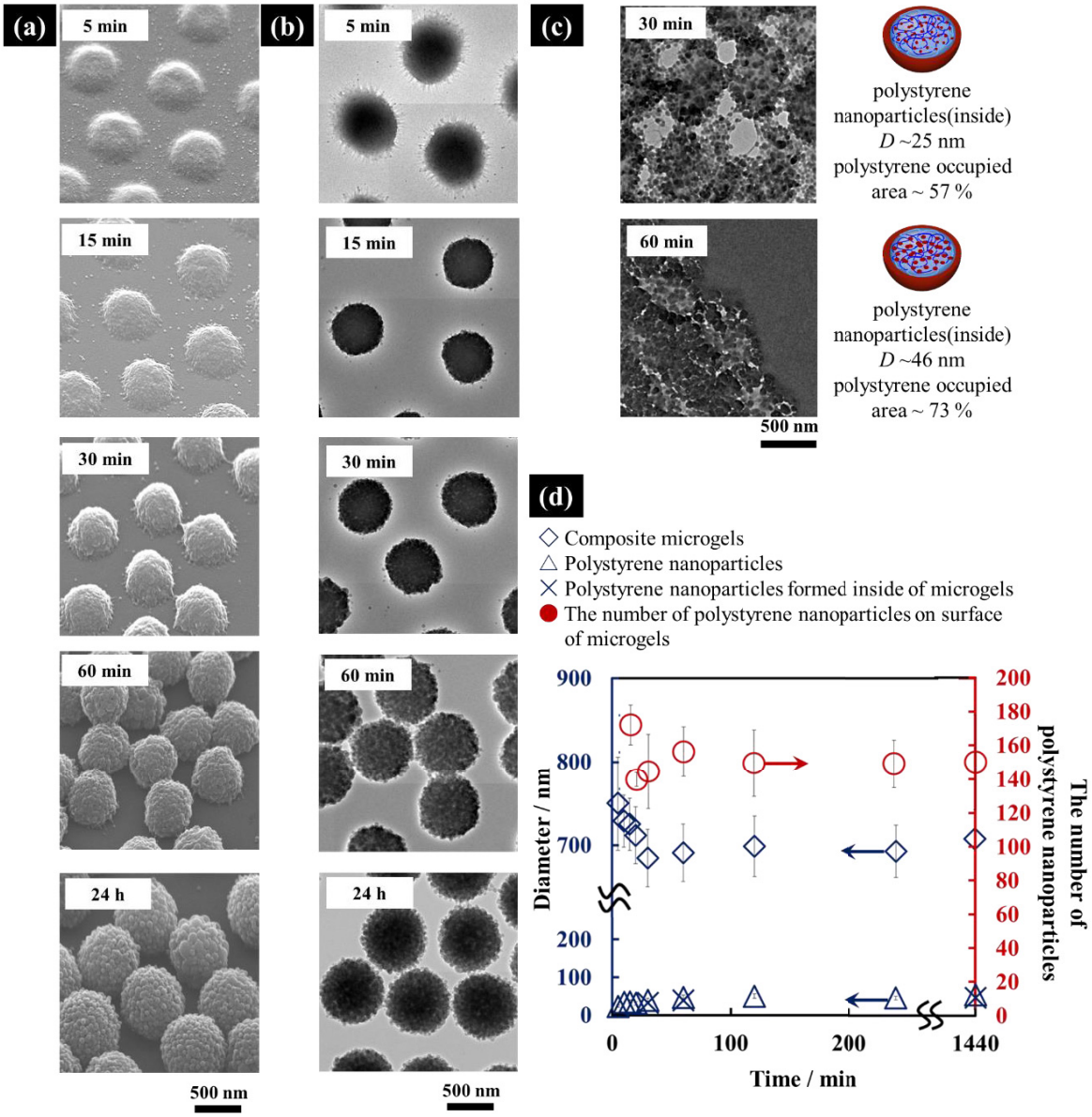


**Figure 2-17**. **(a)** FE-SEM, **(b)** TEM images of **NF5-S100** composite microgels, and **(c)** TEM images of ultra-thin cross sections of **NF5-S100** composite microgels at different polymerization times. **(d)** Diameters of the composite microgels (blue diamonds), polystyrene nanoparticles formed on the core surface (blue triangles), polystyrene nanoparticles formed inside the composite microgels (blue crosses), and the number of polystyrene nanoparticles attached on the core microgel (red circles) at different polymerization times.

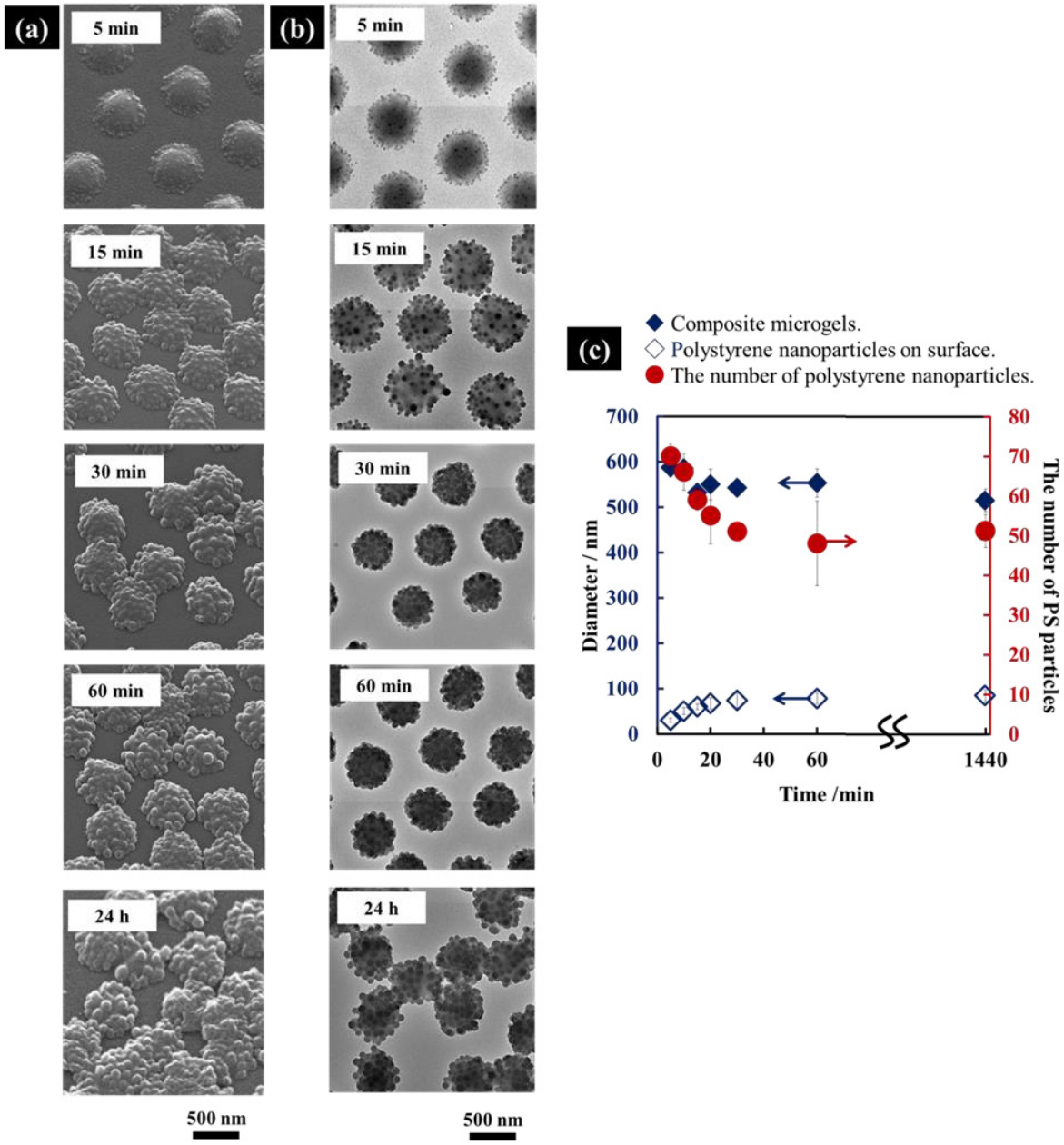


**Figure 2-18**. (a) FE-SEM and (b) TEM images of **NM5-S100** microgels at different polymerization times. The graph shows mean diameters of composite microgels (blue ◆ ), polystyrene nanoparticles (blue◇), and the number of polystyrene nanoparticles on the core microgel (red●) at different polymerization times.

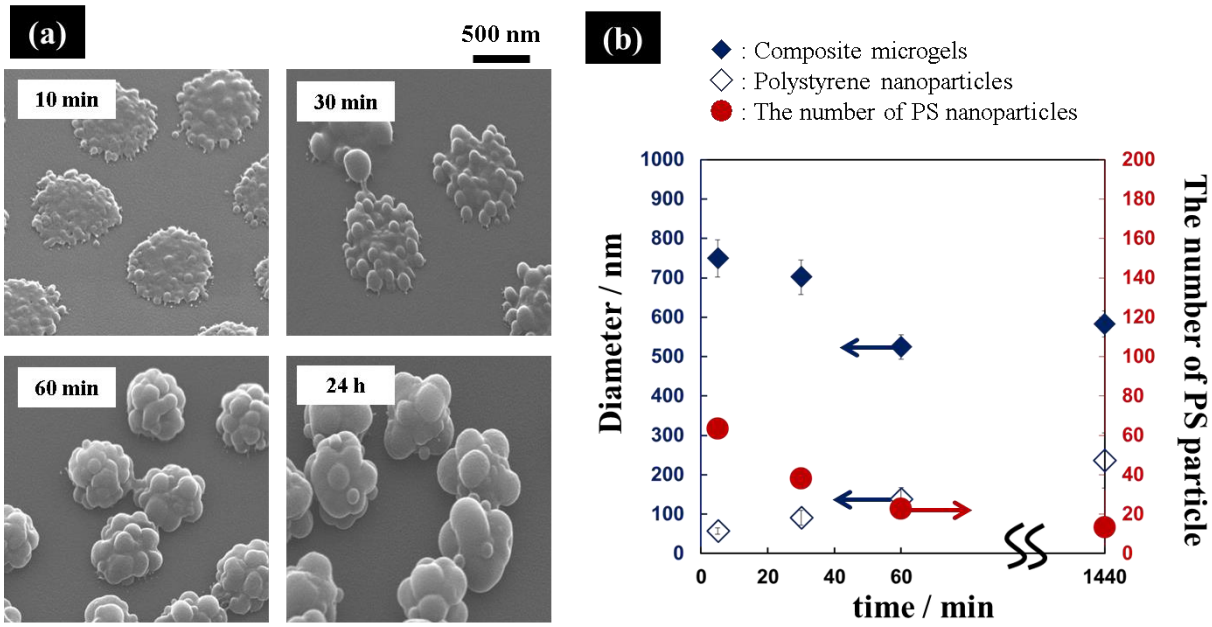


**Figure 2-19**. (a) FE-SEM images of **N-S100** microgels at different polymerization times. (b) The graph shows mean diameters of composite microgels (blue◆), polystyrene nanoparticles (blue◇), and the number of polystyrene nanoparticles on the seed microgel (red ● ) at different polymerization times.

Given the results of this study and those of our previous studies, [13,14] the polymerization mechanism of seeded emulsion polymerization of styrene in the presence of hydrogel particles has gradually become clear. These results enable control of the surface and internal structures of resultant stimuli-responsive composite microgels (**Scheme 2-2**). When pure, deswollen pNIPAm microgels are used as cores for the polymerization, raspberry-shaped composite microgels with an irregular surface are obtained (**Scheme 2-2(a)**). [14] Uniform polystyrene nanoparticles are then formed not only on the surface but inside the cores when an anionic surfactant, SDS, is added during the polymerization (**Scheme 2-2(b)**). [14] In the present study, the author investigated whether the surface and internal structures of composite microgels were similarly changed when SDS was added during seeded emulsion polymerization of styrene in the presence of **NF5** microgels (**Figure 2-20**). As expected, the resultant composite microgels contained a lot of polystyrene nanoparticles in their interior, which means that SDS surfactants were adsorbed to core **NF5** microgels to form SDS aggregates.[44] Moreover, the carboxyl group distribution in the core microgels was also observed to play a substantial role in the formation of polystyrene nanoparticles in the presence of microgels. When poly(NIPAm-*co*-MAc) microgels, whose carboxyl groups are localized at their

center, are used as cores, polystyrene nanoparticles do not form at the center of the core microgels and polystyrene nanoparticles cover the core microgel as a monolayer (**Scheme 2-2(c)**).[14] Conversely, in this study, when pNIPAm-based microgels, whose carboxyl groups are localized on their surfaces, are used as cores, polystyrene nanoparticles are formed not only on the surface but inside the microgels and the amount of composited polystyrene can be increased because colloidal stability of resultant composite microgels are enhanced by electrostatic repulsion originating from the charged groups on the surface (**Scheme 2-2(d)**). Additionally, the size of polystyrene nanoparticles attached to the surface of the core microgels can be controlled by changing the core microgels' surface charge densities: less hydrophobic surfaces (or an increase in charged groups) result in smaller polystyrene nanoparticles formed on the surface.

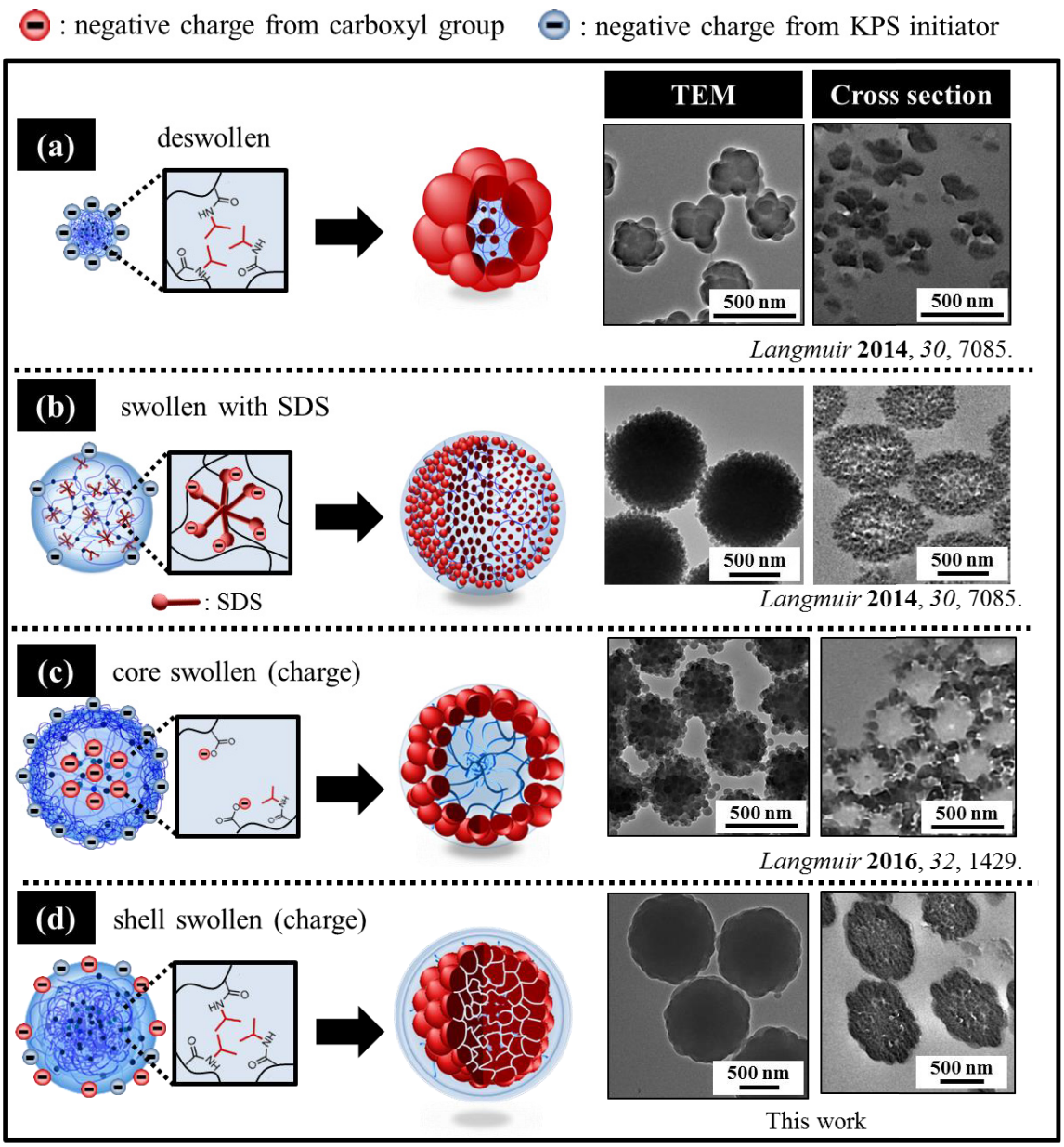


**Scheme 2-2**. Summary of the composite microgels prepared by seeded emulsion polymerization of styrene in the presence of various microgel cores.

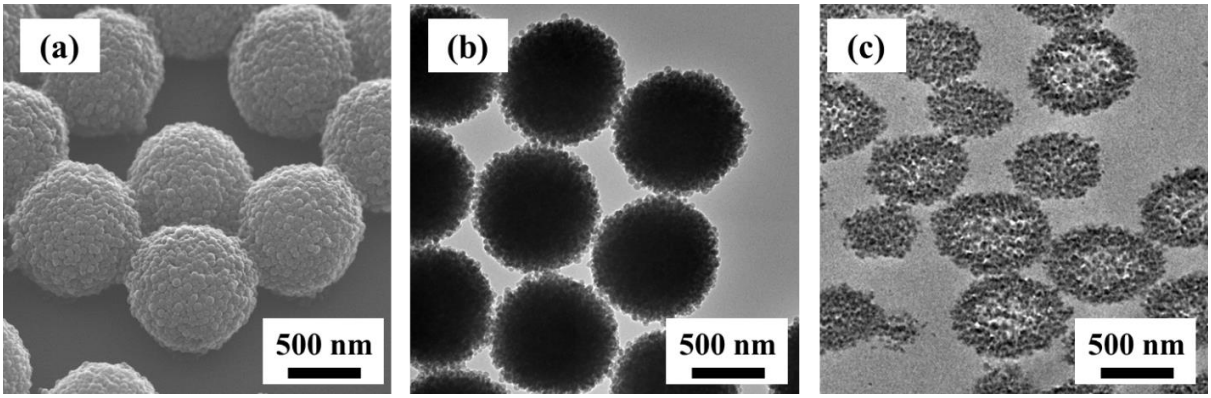

**Figure 2-20**. Electron micrographs of **NF5-S300-SDS** microgels prepared by the seeded emulsion polymerization of styrene with anionic surfactant SDS. (a) FE-SEM image. TEM images of (b) composite microgels, and (c) ultrathin cross section of composite microgels. From the FE-SEM image, the diameter of the composite microgels and polystyrene nanoparticles were determined to be 875 ± 41 nm ($N$ = 50, CV = 4.7 %) and 46 ± 6 nm ($N$ = 50, CV = 13 %), respectively.

## 2.4. Conclusions

Various pNIPAm-based microgels with different spatial distributions of carboxyl groups were used in the seeded emulsion polymerization of styrene to clarify the effects of charge distribution in core microgels on the resultant composite microgels (**Scheme 2-2** and **Scheme 2-3**). Unlike the case of poly(NIPAm-*co*-MAc) microgels,[14] whose carboxyl groups are located at the center of the microgel, polystyrene nanoparticles did form at the center of the core microgels when poly(NIPAm-*co*-FAc) microgels, whose carboxyl groups are located on the surface of the core microgel, were used. Additionally, the poly(NIPAm-*co*-FAc) microgels could be combined with a larger amount of polystyrene compared to the poly(NIPAm-*co*-MAc) microgels because the poly(NIPAm-*co*-FAc) microgels exhibited high colloidal stability stemming from their high surface charge densities. Furthermore, polystyrene nanoparticles were formed inside the core microgels even though the number of charged groups was substantially greater; the author clarified this process using core–shell microgels. These facts indicate that styrene monomer can penetrate into polyelectrolyte hydrogel layers; however, the resultant polystyrene nanoparticles do not favor combination with polyelectrolyte hydrogels. The author also clarified that the size of polystyrene nanoparticles decreases with increasing surface charge densities of the core microgels. As a result, the author clarified that spatial distribution of charged groups in pNIPAm-based microgels indeed affects the resultant structures of composite microgels not only on the surface but also inside the core microgels. The design strategy of stimuli-responsive raspberry-shaped composite microgels will be useful not only for creating well-defined functional particles but also for understanding the

interaction of hydrogel particles and water-immiscible materials such as oils, which will lead to new developments in fields such as cosmetics and drug delivery systems.

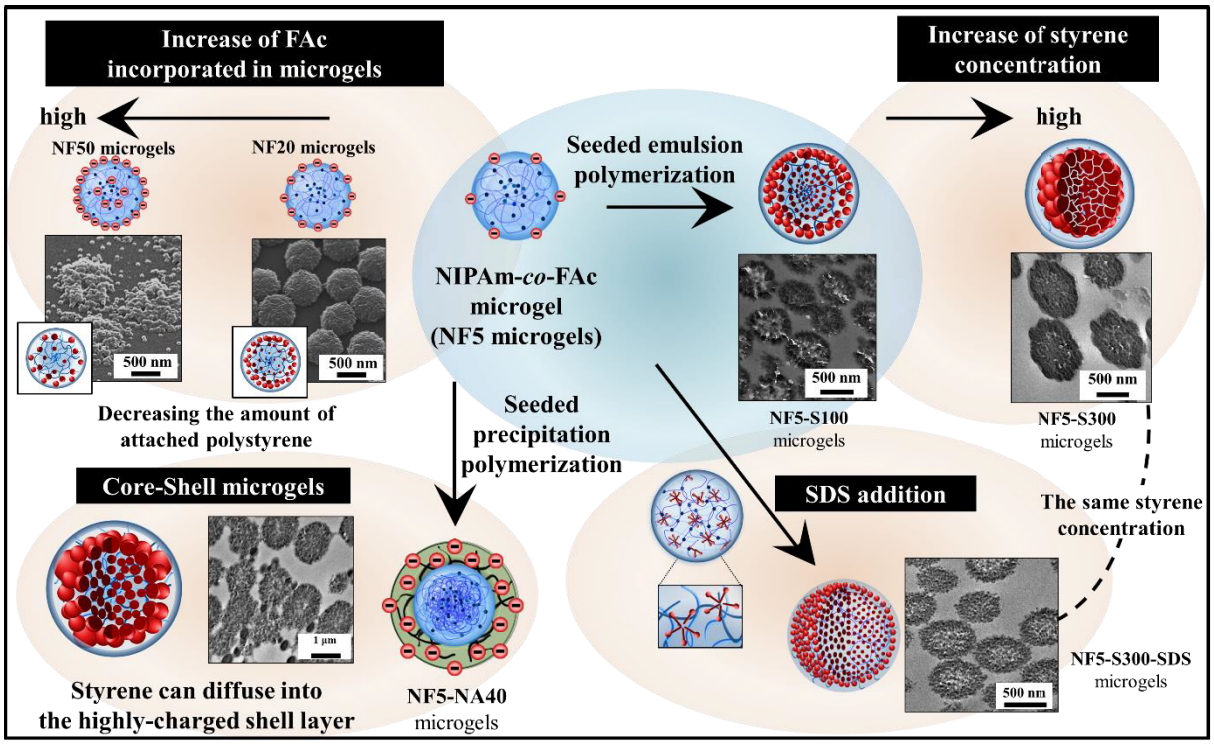


**Scheme 2-3.** Summary of results in this study.

## 2.5. References


1. Jones, C. D.; Lyon, L. A. Synthesis and Characterization of Multiresponsive Core-Shell Microgels. *Macromolecules* **2000**, *33*, 8301-8306.
2. Jones, C. D.; Lyon, L. A. Shell-Restricted Swelling and Core Compression in Poly(*N*-isopropylacrylamide) Core-Shell Microgels. *Macromolecules* **2003**, *36*, 1988-1993.
3. Keerl, M.; Pedersen, J. S.; Richtering, W. Temperature Sensitive Copolymer Microgels with Nanophase Separated Structure. *J. Am. Chem. Soc*. **2009**, *131*, 3093–3097.
4. Bradley, M.; Vincent, B.; Burnett, G. Uptake and Release of Anionic Surfactant into and from Cationic Core-Shell Microgel Particles. *Langmuir* **2007***, 23,* 9237-9241.
5. Hu, X.; Tong, Z.; Lyon, L. A. One-Pot Synthesis of Microcapsules with Nanoscale Inclusions. *Macromol. Rapid Commun*. **2011**, *32*, 1461-1466.
6. Smith, M. H.; Lyon, L. A. Multifunctional Nanogels for siRNA Delivery. *Accounts of Chemical Research* **2011**, *45*, 985-993.
7. Hellweg, T. Responsive Core-Shell Microgels: Synthesis, Characterization, and Possible Applications. *J. Polym. Sci., Part B: Polym. Phys.* **2013**, *51*, 1073-1083.
8. Saxena, S.; Hansen, C. E.; Lyon, L. A. Microgel Mechanics in Biomaterial Design. *Acc.Chem. Res*. **2014**, *47*, 2426-2434.
9. Dubbert, J.; Nothdurft, K.; Karg, M.; Richtering, W. Core-Shell-Shell and Hollow Double-Shell Microgels with Advanced Temperature Responsiveness. *Macromol. Rapid Commun*. **2015**, *36*, 159-164
10. Clarke, K. C.; Dunham, S. N.; Lyon, L. A. Core/Shell Microgels Decouple the pH and Temperature Responsivities of Microgel Films. *Chem. Mater.* **2015**, *27*, 1391-1396.
11. Calculated using Advanced Chemistry Development (ACD/Labs) Software V11.02 (©22 1994-2015 ACD/Labs) as implemented in SciFinder.
12. Suzuki, D.; Yamagata, T.; Murai, M. Multilayered Composite Microgels Synthesized by Surfactant-Free Seeded Polymerization. *Langmuir* **2013**, *29*, 10579-10585.
13. Suzuki, D.; Kobayashi, C. Raspberry-Shaped Composite Microgel Synthesis by Seeded Emulsion Polymerization with Hydrogel Particles. *Langmuir* **2014**, *30*, 7085-7092.
14. Kobayashi, C.; Watanabe, T.; Murata, K.; Kureha, T.; Suzuki, D. Localization of Polystyrene Particles on the Surface of Poly(*N*-isopropylacrylamide-*co*-methacrylic acid) Microgels Prepared by Seeded Emulsion Polymerization of Styrene, *Langmuir* **2016**, *32*, 1429-1439.
15. Hwang, H. S.; Lee, S. B.; Park, I. Fabrication of Raspberry-like Superhydrophobic Hollow Silica Particles. *Materials Letters* **2010**, *64*, 2159-2162.
16. Bao, Y.; Li, Q.; Xue, P.; Huang, J.; Wang, J.; Guo, W.; Wu, C. Tailoring the Morphology of Raspberry-like Carbon Black/Polystyrene Composite Microspheres for Fabricating Superhydrophobic Surface. *Mater. Res. Bull.* **2011**, *46*, 779-785.
17. Esteves, A. C. C.; Luo, Y.; Van de Put, M. W. P.; Carcouët, C. C. M.; de With, G. Self-Replenishing Dual Structured Superhydrophobic Coating Prepared by Drop-Casting of an All-In-One Dispersion. *Adv. Funct. Mater.* **2014**, *24*, 986-992.

18. Liu, Y.; Li, M.; Chen, G. A New Type of Raspberry-like Polymer Composite Sub-Microspheres with Tunable Gold Nanoparticles Coverage and Their Enhanced Catalytic Properties. *J. Mater. Chem. A*, **2013**, *1*, 930-937.
19. Cao, Z.; Chen, H.; Zhu, S.; Chen, Z.; Xu, C.; Qi, D.; Ziener, U. Inverse Miniemulsion-Based Preparation of Raspberry-Like Au/$SiO_2$ Nanocomposite Particles with High Catalytic Activity Towards Reduction of *p*-nitrophenol. *Colloid and Surfaces A: Physicochem. Eng. Aspects* **2016**, *489*, 223-233.
20. Arpornwichanop, T.; Polpanich, D.; Thiramanas, R.; Suteewong, T.; Tangboriboonrat, P. Enhanced Antibacterial Activity of NR Latex Gloves with Raspberry-Like PMMA-*N*,*N*,*N*-trimethyl chitosan Particles. *Internal Journal of Biological Macromolecules* **2015**, *81*, 151-158.
21. Tu, F.; Lee, D. Shape-Charging and Amphiphilicity-Reversing Janus Particles with pH-Responsive Surfactant Properties. *J. Am. Chem. Soc*. **2014**, *136*, 9999-10006.
22. Kaewsaneha, C.; Bitar, A.; Tangboriboonrat, P.; Polpanich, D.; Elaissari, A. Fluorescent-magnetic Janus Particles Prepared via Seed Emulsion Polymerization. *Journal of Colloid and Interface Science* **2014**, *424*, 98-103.
23. Niu, Q.; Pan, M.; Yuan, J.; Liu, X.; Wang, X.; Yu, H. Anisotropic Nanoparticles with Controllable Morphologies from Non-Cross-Linked Seeded Emulsion Polymerization. *Macromol. Rapid Commun*. **2013**, *34*, 1363-1367.
24. Duracher, D.; Sauzedde, F.; Elaissari, A.; Perrin, A.; Pichot, C. Cationic Amino-Containing *N*-isopropyl-acrylamide-Styrene Copolymer Latex Particles: 1-Particle Size and Morphology vs. Polymerization Process. *Colloid Polym. Sci*. **1998**, *276*, 219-231.
25. Mock, E. B.; De Bruyn, H.; Hawkett, B. S.; Gilbert, R. G.; Zukoski, C. F. Synthesis of Anisotropic Nanoparticles by Seeded Emulsion Polymerization. *Langmuir* **2006**, *22*, 4037-4043.
26. Liu, Y.; Ma, Y.; Liu, L.; Yang, W. Facile Synthesis of Core-Shell/Hollow Anisotropic Particles via Control of Cross-Linking during One-pot Dispersion Polymerization. *Journal of Colloid and Interface Science* **2015**, *445*, 268-276.
27. Minami, H,; Wang, Z.; Yamashita, T.; Okubo, M. Thermodynamic analysis of the morphology of monomer-adsorbed, cross-linked polymer particles prepared by the dynamic swelling method and seeded polymerization. *Colloid Polym. Sci.* **2003**, *281*, 246-252.
28. Okubo, M. and Minami, H. Control of Hollow Size of Micron-Sized Monodispersed Polymer Particles Having a Hollow Structure. *Colloid Polym. Sci*. **1996**, *274*, 433-438.
29. Li, B.; Xu, Y.; Wang, M.; Ge, X. Morphological Control of Multihollow Polymer Latex Particles through Controlled Phase Separation in the Seeded Emulsion Polymerization. *Langmuir* **2013**, *29*, 14787-14794.
30. Okubo, M.; Kanaida, K.; Matsumoto, T. Production of Anomalously Shaped Carboxylated Polymer Particles by Seeded Emulsion Polymerization. *Colloid and Polym. Sci*. **1987**, *265*, 876-881.

31. Horigome, K.; Suzuki, D. Drying Mechanism of Poly(*N*-isopropylacrylamide) Microgel Dispersions. *Langmuir* **2012**, *28*, 12962−12970.
32. Suzuki, D.; Kawaguchi, H. Stimuli-Sensitive Core/Shell Template Particles for Immobilizing Inorganic Nanoparticles in the Core. *Colloid Polym. Sci*. **2006**, *284*, 1443-1451.
33. Hoare, T.; Pelton, R. Highly pH and Temperature Responsive Microgels Functionalized with Vinylacetic Acid. *Macromolecules* **2004**, *37*, 2544-2550.
34. Hoare, T.; Pelton, R. Titrametric Characterization of pH-Induced Phase Transitions in Functionalized Microgels. *Langmuir* **2006**, *22*, 7342-7350.
35. Hoare, T.; Pelton, R. Characterizing Charge and Crosslinker Distributions in Polyelectrolyte Microgels. *Current Opinion in Colloid & Interface Science* **2008**, *13*, 413-428.
36. Ponratnam, S.; Kapur, S. L. Reactivity Ratios of Ionizing Monomers in Aqueous Solution. Copolymerization of Acrylic and Methacrylic Acid with Acrylamide. *Macromol. Chem*. **1977**, *178*, 1029-1038.
37. Machida, S.; Narita, H. Studies on the Water-Soluble Polymers. X. Copolymerization of Maleic Acid or Fumaric Acid with Acrylamide. *J. Synth. Org. Chem. Jpn.* **1966**, *24*, 467-470.
38. Lyon, L. A.; Debord, J. D.; Debord, S. B.; Jones, C. D.; McGrath, J. G. and Serpe, M. J. Microgel Colloidal Crystals. *J. Phys. Chem. B* **2004**, *108*, 19099-19108.
39. Stubbs, J.; Karlsson, O.; Jönsson, J. E.; Sundberg, E.; Durant, Y.; Sundberg, D. Non-equilibrium Particle Morphology Development in Seeded Emulsion Polymerization. 1: Penetration of Monomer and Radicals as a Function of Monomer Feed Rate during Second Stage Polymerization. *Colloids Surfaces A: Physiochem. Eng. Aspects* **1999**, *153*, 255-270.
40. Daly, E.; Saunders, B. R. Temperature-Dependent Electrophoretic Mobility and Hydrodynamic Radius Measurements of poly(*N*-isopropylacrylamide) Microgel Particles: Structural Insights. *Phys. Chem. Chem. Phys*. **2000**, *2*, 3187-3193.
41. Wu, S.; Dzubiella, J.; Kaiser, J.; Drechsler, M.; Guo, X.; Ballauff, M.; Lu, Y. Thermosensitive Au-PNIPA Yolk–Shell Nanoparticles with Tunable Selectivity for Catalysis. *Angew. Chem. Int. Ed*. **2012**, *51*, 2229-2233.
42. Tsuji, S.; Kawaguchi, H. Self-Assembly of Poly(*N*-isopropylacrylamide)-Carrying Microspheres into Two-Dimensional Colloidal Arrays. *Langmuir* **2005**, *21*, 2434−2437.
43. Mourran, A.; Wu, Y.; Gumerov, R. A.; Rudov, A. A.; Potemkin, I. I.; Pich, A.; Möller, M. When Colloidal Particles Become Polymer Coils. *Langmuir* **2016**, *32*, 723-730.
44. Gilányi, T.; Varga, I.; Meszaros, R.; Filipcsei, G.; Zrinyi, M. Interaction of Monodisperse Poly(*N*-isopropylacrylamide) Microgel Particles with Sodium Dodecyl Sulfate in Aqueous Solution. *Langmuir* **2001**, *17*, 4764-4769.

# 3. Chapter II

# " Seeded Emulsion Polymerization of Styrene in the Presence of Water-swollen Hydrogel Microspheres"

*Part of this work was published in " Takumi Watanabe, Chihong Song, Kazuyoshi Murata, Takuma Kureha, and Daisuke Suzuki, *Langmuir* **2018**, *34*, 8571-8580."


## 3.1. Introduction

Initially, SEP was studied predominantly to clarify the polymerization kinetics of emulsion polymerizations.[1,2] However, many researchers have recently aimed at controlling the morphology of microspheres by SEP, which has led to a variety of unique structures such as snowman-like,[3-6] octopus-ocellatus-like,[7] hollow,[8,9] and raspberry-like microspheres.[10] The particle morphology is usually determined by the relationship between thermodynamic and kinetic aspects during the SEP. Changing the polymerization conditions (e.g. temperature, stirring speed, and/or solvent) and particle properties (e.g. size, hydrophobicity/philicity, and/or polarity) is accordingly an important factor to control the particle morphology in most cases.[11,12] Therefore, clarifying the effect of each polymerization conditions on the morphology of resultant microspheres is crucial.

In **Chapter I**, it was found that the charged group distribution of core microgels on the morphology of nanocomposite microgels is key factor for controlling of morphology of nanocomposite microgels prepared by SEP in the presence of microgels. However, ,in the previous studies,[13-16] pNIPAm-based microgels have been partially or mostly deswollen and dehydrated during the SEP, as all polymerizations were conducted at ~70 °C, which is well above the volume phase transition temperature (VPTT) of pNIPAm microgels (~32 °C),[17,18] the deswollen and hydrophobic regions within the microgels might therefore serve as nucleation sites for the formation of polystyrene. Consequently, it is still unclear whether water-swollen and hydrophilic microgels can serve as nucleation sites for the formation of hydrophobic polystyrene; a clarification of this topic should improve our understanding of the role of microgels in the SEP of hydrophobic monomers. In contrast to the SEP with microgels reported by Kraft *et al.*,[19] our method does not require a swelling period for the seed microgels in the hydrophobic monomer. A systematic investigation of our polymerization system should thus improve our understanding of the dynamics of diffusion of the hydrophobic monomers in the water-swollen microgels. Moreover, visualizing microgels or composite microgels in the water-swollen state on the nanoscale is challenging. Herein, the author introduces a cryo-tomography technique that allows recording 3D images of individual composite microgels in order to evaluate the size and shape of water-swollen composite microgels.

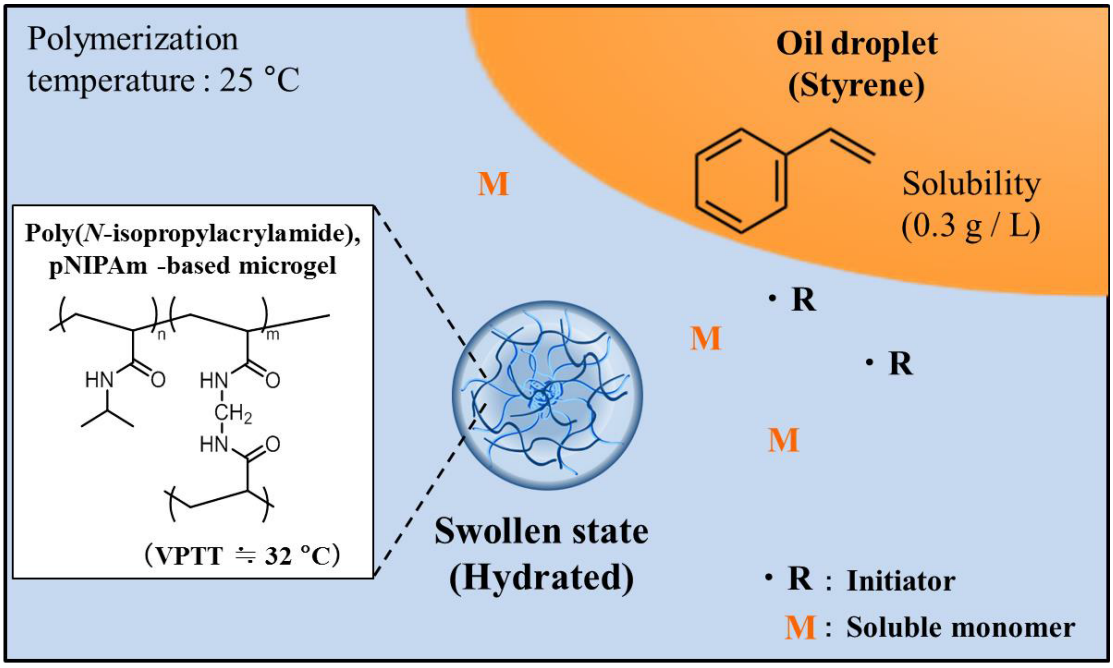


**Scheme 3-1.** SEP of water-immiscible monomers in the presence of water-swollen pNIPAm microgels.

### 3.2. Experimental Section

**Materials.** *N*-isopropyl acrylamide (NIPAm, 98 %), *N*,*N*′-methylenebis(acrylamide) (BIS, 97%), styrene (99%), ammonium peroxodisulfate (APS, 95%), methacrylic acid (MAc, 99%), sodium dodecyl sulfate (SDS, 95%), and fumaric acid (FAc, 98%) were purchased from Wako Pure Chemical Industries Ltd. (Japan). *N*,*N*,*N*',*N*'-Tetramethyl ethylenediamine (TEMED, 99 %) was purchased from Sigma-Aldrich and used as received. A stabilized aqueous solution (0.5 %) of ruthenium tetroxide ($RuO_4$) was purchased from Electron Microscopy Sciences and used as received. For all experiments, water was distilled and ion-exchanged (EYELA, SA-2100E1) prior to use.

Microgels based on pNIPAm were synthesized by aqueous free radical precipitation polymerization[18] according to the conditions outlined in **Table S1**. Initially, monomer solutions containing NIPAm, BIS, a carboxyl-group-containing comonomer, and water were poured into a three-necked round-bottom flask (1 L) equipped with a mechanical stirrer, a condenser, and a

nitrogen gas inlet, which was subsequently immersed in an oil-bath. The monomer solutions were heated to 70 °C, stirred at 250 rpm, and sparged with nitrogen gas for 30 min to remove any oxygen. Then, 5 mL of a solution of the water-soluble initiator KPS were added to the monomer solutions to start the polymerizations. All reactions were run with stirring for 4 h, before the microgel dispersions were allowed to cool to room temperature using an ice-bath. The microgel dispersions were purified by two centrifugations (70,000 × g, 15 °C) using pure water. In this manuscript, all microgels are denoted as **N*XY***, where **N** refers to pNIPAm, while ***X*** denominates the comonomer in the microgels and ***Y*** denominates the amount of comonomer (in mol%).

**Synthesis of the Core-shell Microgels by Seeded Precipitation Polymerization**

Microgels based on pNIPAm were synthesized by aqueous free radical precipitation polymerization[18] according to the conditions outlined in **Table 3-1**. Initially, monomer solutions containing NIPAm, BIS, a carboxyl-group-containing comonomer, and water were poured into a three-necked round-bottom flask (1 L) equipped with a mechanical stirrer, a condenser, and a nitrogen gas inlet, which was subsequently immersed in an oil-bath. The monomer solutions were heated to 70 °C, stirred at 250 rpm, and sparged with nitrogen gas for 30 min to remove any oxygen. Then, 5 mL of a solution of the water-soluble initiator KPS were added to the monomer solutions to start the polymerizations. All reactions were run with stirring for 4 h, before the microgel dispersions were allowed to cool to room temperature using an ice-bath. The microgel dispersions were purified by two centrifugations (70,000 × g, 15 °C) using pure water. In this manuscript, all microgels are denoted as **N*XY***, where **N** refers to pNIPAm, while ***X*** denominates the comonomer in the microgels and ***Y*** denominates the amount of comonomer (in mol%).

**Table 3-1.** Chemical Composition and Polymerization Conditions of the Core Microgels.

| **Code** | **Monomer** | | | | | | | **Initiator** | | | **Water** | **Result** |
|---|---|---|---|---|---|---|---|---|---|---|---|---|
| | NIPAm | | BIS | | **comonomer** | | | | | | | |
| | mol% | g | mol% | g | | mol% | g | type | mM | g | mL | |
| **N** | 95 | 12.90 | 5 | 0.93 | - | - | - | KPS | 2 | 0.43 | 800 | dispersed |
| **NM5** | 90 | 7.64 | 5 | 0.58 | MAc | 5 | 0.32 | KPS | 2 | 0.27 | 500 | dispersed |
| **NF5** | 90 | 7.64 | 5 | 0.58 | FAc | 5 | 0.44 | KPS | 2 | 0.27 | 500 | dispersed |

**Preparing microgel-stabilized emulsions.** Microgel-stabilized emulsions were prepared by homogenizing 1 mL of microgel dispersion (2 wt%) and styrene monomer (1 mL) strained with Nile red (0.5 mM) using an Ultra Turrax T25 homogenizer (8000 rpm; 1 min). Then, 50 µL of 1 M NaOH or HCl solution were added to adjust the pH value of the microgel solution. The obtained emulsion was examined using an optical microscope (BX53, Olympus) with a fluorescence system (wavelength: 451~485 nm and 541~565 nm).

**Synthesis of the Composite Microgels Under Swollen-Microgel Conditions.** As the VPTT of pNIPAm microgels is ~32 °C,[17,18] composite microgels were synthesized by a SEP in the presence of pNIPAm-based microgels at room temperature (25 °C), where the core microgels are completely hydrated. Water was poured into a three-necked round-bottom flask (200 mL) equipped with a mechanical stirrer, a condenser, and a nitrogen gas inlet. The monomer solution was stirred (250 rpm) at room temperature (25 °C) and sparged for 30 min with nitrogen to remove any oxygen. Subsequently, sufficient aqueous NaOH (1 M) was added to adjust the pH ~ 10 in order to deprotonate the carboxyl groups within the core microgels. Then, the microgel dispersion was added to the system so that the solid content of microgels was 0.17 wt%. Subsequently, 5 mL of the initiator solution (0.0228 g APS dissolved in 5 mL water; [APS] = 1 mM) and TEMED were added. In order to improve the dispersion stability, SDS (0.0124 g, [SDS] = 0.5 mM) was added as required. Immediately, the styrene monomer was added to the flask to start the polymerization. The polymerization was allowed to proceed for 24 h. Then, the composite microgels were purified by two times centrifugations (20,000 × g, 15 °C) using pure water. The composite microgels are denoted as **(microgel code)-S*Z***, where **S** indicates polystyrene and ***Z*** indicates the concentration of styrene (in mM) during the polymerization.

**Measurements.** The hydrodynamic diameters ($D_h$) of the core microgels and composite microgels were determined by dynamic light scattering (DLS) using a Zetasizer Nano S (Malvern Instruments Ltd., UK). The DLS data correspond to an average of 15 independent measurements of the intensity autocorrelation acquired over 30 s, and the values given represent averages of three independent measurements. The scattering intensity was detected at a total scattering angle of 173°. For the sample preparation, the particle concentration was adjusted to ~0.005 wt% and the ionic strength was adjusted to 1 mM using NaOH, HCl, and/or NaCl solutions. $D_h$ values were calculated on the basis of the measured diffusion coefficients using the Stokes–Einstein equation (Malvern, Zetasizer software v. 6.12).

The electrophoretic mobility (EPM) was measured using a Zetasizer NanoZS (Malvern, Zetasizer software v. 4.20). For the sample preparation, the particle concentration was adjusted to ~0.005 wt% and the ionic strength was adjusted to 1 mM using NaOH, HCl, and/or NaCl solutions. The EPM data correspond to an average of 20 independent measurements, and an average of three replicate the measurements. Prior to all measurements, the sample was allowed to equilibrate for 5 min at a specific temperature.

The contact angle between the water droplet (5 μL) and the polystyrene substrates coated with different microgels was measured using a contact angle meter (DMo-701, Kyowa Interface Science Co., Ltd.). The average contact angle corresponds to an average of ten independent measurements.

The equilibrium surface tension of each particle dispersion was determined using the Wilhelmy method with a surface tensiometer (CBVP-Z, Kyowa Interface Science Co., Ltd.,). 5 mL of each dispersion were deposited in a glass dish for 1 day. The measurement was conducted at 25 °C and the average surface tension values (γ) were calculated from five independent measurements. For these measurements, highly concentrated microgel dispersions (2 wt% ~) were used to determine the equilibrium surface tension.

The particle morphology in the dried state was examined by field emission scanning electron microscopy (FE-SEM, Hitachi Ltd., S-5000), transmission electron microscopy (TEM, JEOL2010, operated at 200 kV), and Cryo-TEM (JEOL2200FS, operated at 200kV). For the FE-SEM measurements, the microgels were dried on a polystyrene substrate at room temperature, before they were washed with pure water. The sample substrates were sputtered with Pt/Pd prior to the measurements (15 mA, 6 Pa, 80 s). In the FE-SEM measurements, the composite microgel dispersions were not centrifuged and purified in order to determine the potential presence of secondary polystyrene particles. Conversely, for TEM measurements, the microgel dispersions were purified by centrifugation to remove impurities such as unreacted monomers and polymer chains, before the purified dispersions were dried on a carbon-coated copper grid (Okenshoji Co., Ltd).

Lyophilized composite microgels were stained for 30 min with $RuO_4$ vapor, and then dispersed in epoxy matrices (EPON812, TAAB Laboratories Equipment). The matrices were kept at 40 °C for 6 h, and finally solidified at 70 °C for 24 h. Then, the matrices were microtomed into ultrathin cross sections and observed by TEM (JEOL JEM-2100, operated at 200 kV). The density values of polystyrene-occupied area were calculated by ImageJ (ver.1.50) from TEM images of ultra-thin cross sections. It should be noted that the calculated polystyrene areas were used as a reference, given that these ultra-thin cross section images were 2D images of 3D particles.

Hydrated composite microgels were observed by cryo-TEM. 2.5 μL of the aqueous samples were applied onto R 3.5/1 Quantifoil grids (Quantifoil Micro Tools) glow-discharged beforehand. Colloidal gold (15 nm) was mixed with the sample as a fiducial marker. The grid was blotted for 10 s and quick frozen in liquid ethane using a Vitrobot Mark IV (FEI Company, USA) set at 95% humidity and a temperature of 4 °C. The frozen grid was mounted on the side-entry Gatan 914 cryo-specimen holder (Gatan Inc., USA) and examined with a JEM2200FS electron microscope (JEOL Inc., Japan) equipped with a field-emission gun operated at 200 kV accelerating voltage and an in-column energy filter operated in a zero-energy loss mode with a slit width of 15 eV. A tilt series of hydrated microgels was collected in the range of -60° and +60° with a 2° increment step using a low dose mode, where the total electron dose was less than 100 $e^-/Å^2$ on the specimen. Images were recorded on a DE20 direct-detector CMOS camera (Direct Electron LP. USA) with a detector magnification of 9,566 corresponding to 6.84 Å per pixel. Image alignment and

tomographic reconstruction were performed by IMOD software[38] by using fiducial markers. The final tomograms were calculated by a filtered back projection algorithm using images of 41.04 Å per pixel after applying a pixel-binning of 6. The 3-D reconstructions were generated using IMOD software version 4.7.15. The image segmentation in the 3-D reconstructions was performed with IMOD software.

## 3.3. Results and discussion

### 3.3.1. Synthesis and Characterization of the Microgel Cores

In order to investigate the influence of hydrated pNIPAm-based microgels on the polymerization of hydrophobic monomers, the author prepared three types of core microgels (**Table 3-1**), which differ with respect to the charge distribution within the microgels: i) an almost uncharged pNIPAm microgel (**Figure 3-1(a)**), ii) a poly(NIPAm-*co*-MAc) microgel, where carboxyl groups are located at the center of the microgels (**Figure 3-1(b)**); iii) a poly(NIPAm-*co*-FAc) microgel, where carboxyl groups are located on the surface of the microgels (**Figure 3-1(c)**). These microgels are similar to those that the author have used previously.[16] It should be noted that controlling the spatial distribution of the carboxyl groups within the microgels was achieved by choosing appropriate types of *co*-monomers in terms of reactivity ratio,[15,16,21,22] and the amount of *co*-monomer fed during the synthesis of the core microgel was fixed at 5 mol% to clarify the charge distribution among these three types of microgels.

**Figure 3-1** shows the FE-SEM images, and the electrophoretic mobilities (EPM) of the **N**, **NM5**, and **NF5** microgels, respectively. From these FE-SEM images (**Figure 3-1(a)-(c)**), the size of these microgels were determined as 433 nm (**N**, CV = 7.1 %, $N$ = 50), 434 nm (**NM5**, CV = 5.1 %, $N$ = 50), and 608 nm (**NF5**, CV = 5.3 %, $N$ = 50), indicating that uniform and submicron-sized microgels were obtained in all cases. Moreover, at pH = 10, the absolute EPM value of the **NF5** microgels was higher than that of the other microgels, even though the EPM values of **N**, **NM5**, and **NF5** at pH = 3 were almost identical (**Figure 3-1**). In addition, the author determined by conductometric titration that the **NM5** and **NF5** microgels incorporate almost the same content of carboxyl group (**NM5**: 0.40 mmol/g; **NF5**: 0.44 mmol/g). These results indicate that the surface-charge density of the **NF5** microgels is the highest among the three types of microgel cores, and that the charge distribution between the **NF5** and **NM5** microgels is different (**Figure 3-1**).

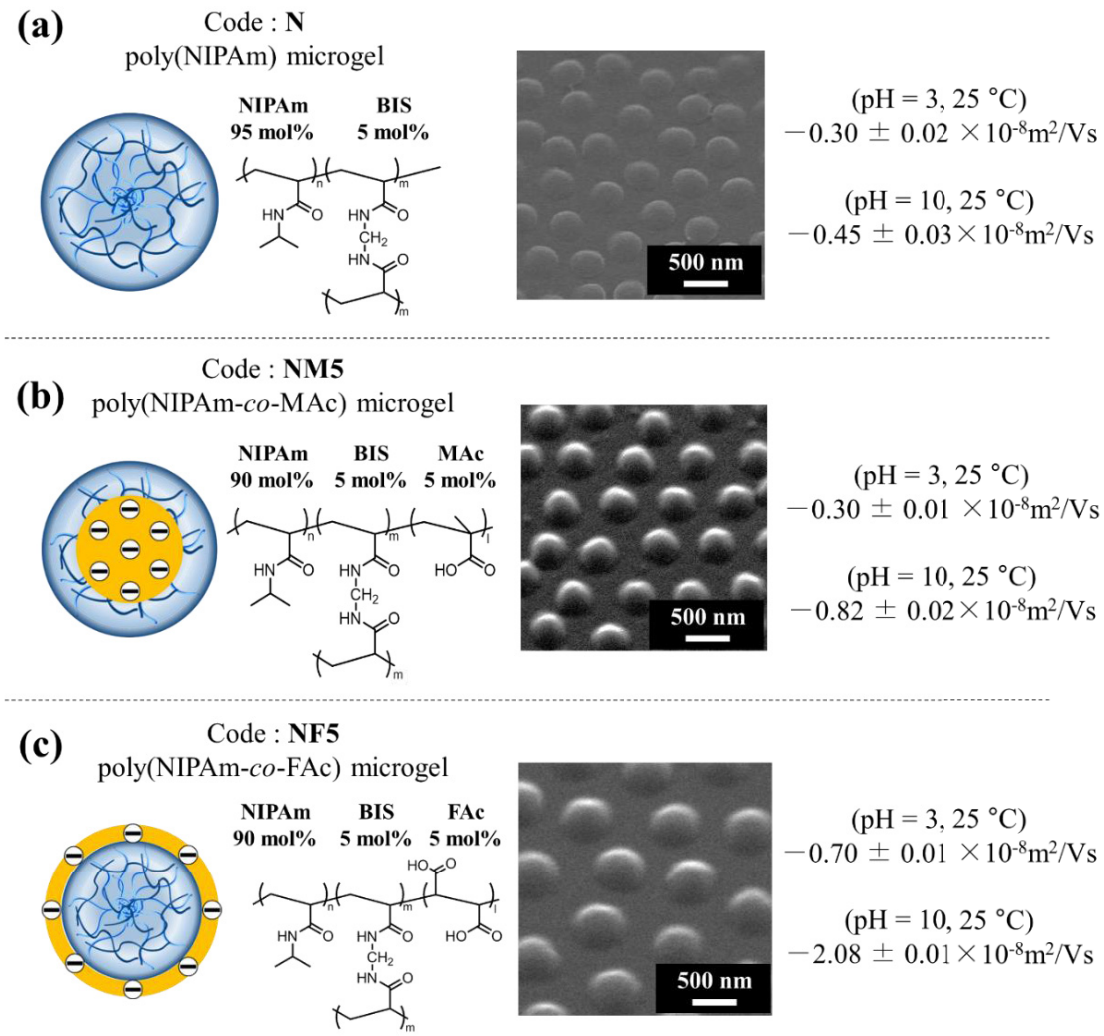


**Figure 3-1**. Characteristics of the microgel cores used for the SEP of styrene in the present study.

### 3.3.2. The Effect of the Charge Distribution in Hydrated Microgel Cores on the Colloidal Stability of the Composite Microgels

The author have already reported that composite microgels aggregate during the SEP of styrene when **N** microgels are used as seeds ($[styrene]_{conc.}$ = 200 mM, $[microgel]_{conc.}$ = 0.1 or 0.17 wt%, 25 °C).[14] Therefore, the author initially confirmed that the SEP of styrene in the presence of **N** microgels at lower styrene concentrations ($[styrene]_{conc.}$ = 50 mM or 100 mM) and lower seed concentration (0.1 wt%) prevent particle aggregation. However, the resulting composite microgels aggregated during the SEP, despite the fact that stable composite microgels were obtained for the same styrene concentration (200 mM) at 70 °C.[14] Similarly, the resulting composite microgels also aggregated during the SEP at 25 °C, when **NM5** microgels were used as seeds (**NM5-S50** microgels in **Table3- 2** and **Figure 3-2(a)**). These results suggest that the polystyrene nanoparticles are attached to the microgel surfaces during the polymerization, resulting in decrease in colloidal stability. Conversely, when **NF5** microgels were used as seeds, the resulting composite microgels were colloidally stable, even when the concentration of the styrene monomer was increased to 200 mM (**Figure 3-2(b)**). These results suggest that sufficient surface-charge density of the core microgels is necessary to obtain colloidally stable composite microgels when water-swollen microgels are used for the SEP as cores. It should also be noted that colloidally stable composite microgels were not obtained for a styrene concentration of 300 mM (**Figure 3-2(c)** and **Table 3-2**). It should be noted that stable microgel-stabilized emulsions were formed only in the case of **NF5** microgels when the styrene monomer was used as an oil phase, while the emulsions were unstable when **N** and **NM5** microgels were used as stabilizers (**Figure 3(a)-(c)**). These results indicate that the charge-group distribution in core microgels is important to determine the colloidal stability of microgel-related materials.

**Table 3-2**. Polymerization Conditions and Results of the SEP

| code | concentration / mM | | | seed | | pH | Note |
|---|---|---|---|---|---|---|---|
| | APS | TEMED | styrene | type | solid content /wt.% | | |
| N-S100 | 1 | 5 | 100 | **N** | 0.1 | pure water | aggregated |
| N-S50 | 1 | 5 | 50 | **N** | 0.1 | pure water | aggregated |
| NM5-S50 | 1 | 5 | 50 | **NM5** | 0.17 | pH = 10 | aggregated |
| NF5-S50 | 1 | 5 | 50 | **NF5** | 0.17 | pH = 10 | stable |
| NF5-S100 | 1 | 5 | 100 | **NF5** | 0.17 | pH = 10 | stable |
| NF5-S200 | 1 | 5 | 200 | **NF5** | 0.17 | pH = 10 | stable |
| NF5-S300 | 1 | 5 | 300 | **NF5** | 0.17 | pH = 10 | aggregated |

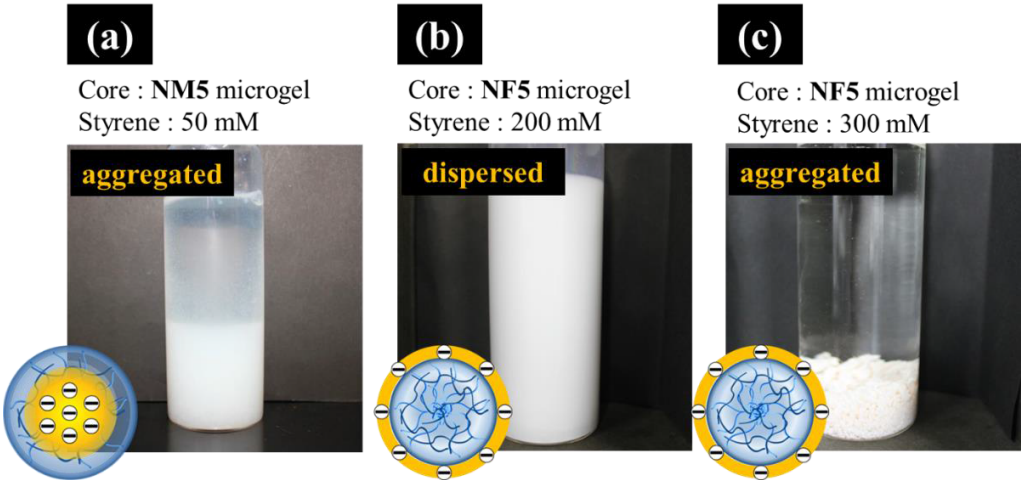


**Figure 3-2.** The photographs of colloidal dispersions of (a) **NM5-S50** microgels, (b) **NF5-S200** microgels, and (c) **NF5-S300** microgels. All polymerizations were conducted at pH = 10.

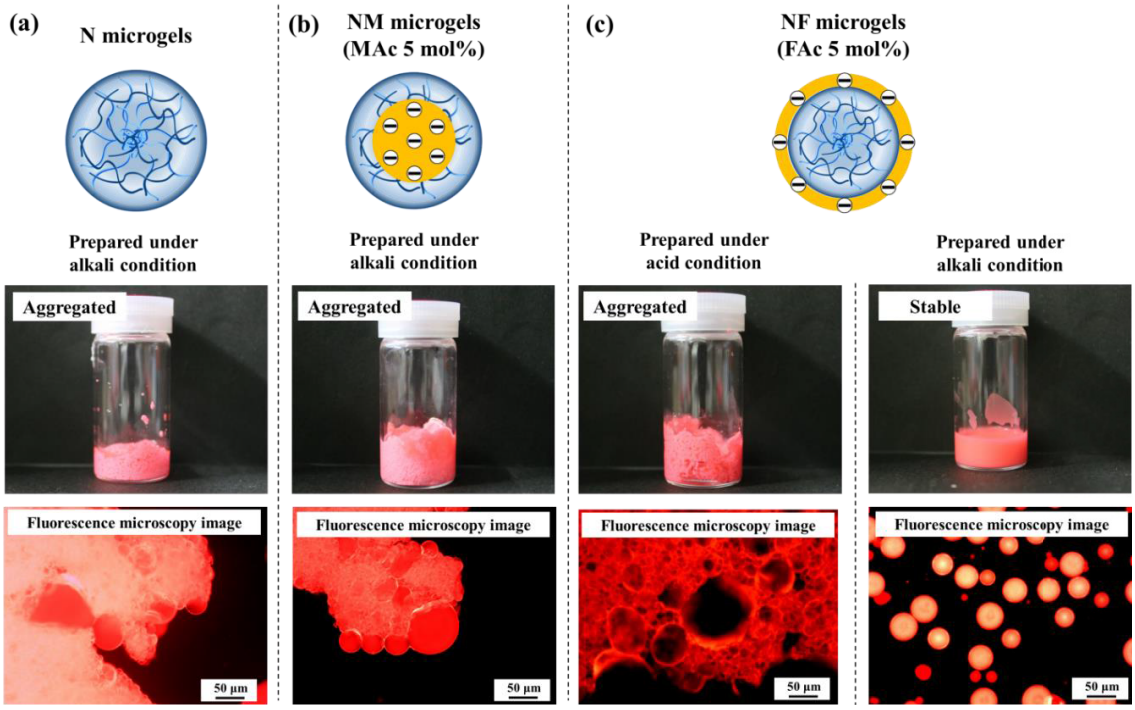


**Figure 3-3**. Formation of microgel-stabilized emulsions with (a) **N**, (b) **NM5**, and (c) **NF5** microgels as emulsifiers. Therein, the styrene monomers were stained using Nile red.

### 3.3.3. Morphology of the Composite Microgels Prepared in the Presence of Swollen NF Microgels

The FE-SEM images (**Figure 3-4(a)-(c)**) show that raspberry-shaped composite microgels, containing decanano-sized polystyrene particles attached to their parent microgel cores, were obtained from the SEP of styrene in the presence of water-swollen **NF5** microgels. The size of the polystyrene particles increased as the concentration of the styrene monomer fed into the polymerization increased (**Table 3-3**), while secondary (or individual) polystyrene particles were hardly observed in all cases (**Figure 3-5**). Additionally, the morphology of the **NF5-S*X*** composite microgels did not change after the centrifugation/re-dispersion purification process (**Figure 3-6**), indicating that the polystyrene particles are strongly attached to the **NF5** microgel cores.

Next, ultra-thin cross sections of these composite microgels were examined by TEM in order to clarify the inner structures of these composite microgels (**Figure 3-4(d)-(f)**). For that purpose, the polystyrene was stained with $RuO_4$. In all cases, the polystyrene nanoparticles attached to the microgel cores were formed in the entire microgel core. Here, it was possible to use these images to roughly estimate the polystyrene-occupied areas, and these values increased as the concentration of the styrene monomer during the polymerization increased (**Table 3-3**). It should be noted that the calculated occupied area and distribution of the polystyrene particles within the microgels were used as a reference, as it was uncertain whether the images of the cross-sections showed the center of the composite microgels. To determine the particle morphology in the swollen state, the morphology of the composite microgels was observed by cryo-TEM images (**Figure 3-4(g)-(i)**). The diameters of the composite microgels are shown in **Table 3-3**. The mean diameters of the **NF5-S50** and **NF5-S100** composite microgels determined by cryo-TEM images (**Figure 3-4(g)-(i)**) were greater than those determined using the FE-SEM images (**Figure 3-4(a)-(c)**) and the obtained values indicated that the **NF5-S50** and **NF5-S100** composite microgels swell in water and deform during drying similar to the seed microgels, unlike the case of **NF5-S200** composite microgels. Moreover, the contact angles between the water droplets and polystyrene substrates coated with different microgels were investigated. The contact angle increases with increasing proportion of the polystyrene composite (**Figure 3-7**). Similarly, the surface tension of each particle dispersion was determined: 41.6 mN/m (**NF5**), 42.3 mN/m (**NFS50**), 46.5 mN/m (**NFS100**), and 57.0 mN/m (**NFS200**), and 71.9 mN/m (polystyrene microspheres). These results indicate that the hydrophobicity (or amphiphilicity) of the composite microgels can be tuned by changing the polymerization condition during the SEP. It should be noted that the morphology of the composite microgels did not change as much when core **NF5** microgels with a different cross-link density (1 or 10 mol%) were used for the SEP (**Figure 3-8**).

The author further examined the thermo- and pH-responsiveness of the composite microgels by EPM measurements in order to investigate the surface properties of the composite microgels. Swollen microgels exhibit low absolute EPM values due to their low surface polymer

density, and the absolute EPM value increases upon deswelling the microgels on account of the increase of the surface-charge density.[23] Indeed, the absolute EPM values of all composite microgels changed upon varying the temperature and pH value (**Table 3-4**), suggesting that these composite microgels were covered with a hydrogel layer.[16] In fact, all composite microgels exhibited high colloidal stability; the composite microgels can be easily redispersed via centrifugation as compared with the polystyrene particles (**Figure 3-9**). Due to the remaining hydrogel layer on the surface of the microgels, stable composite microgels were obtained when **NF5** microgels were used as seeds (50 ~ 200 mM, **Table 3-2**). These results suggest that pNIPAm serves as the nucleation site for polystyrene, and the polystyrene domains (or nanoparticles) form not only the surface of microgels but also center of microgels.

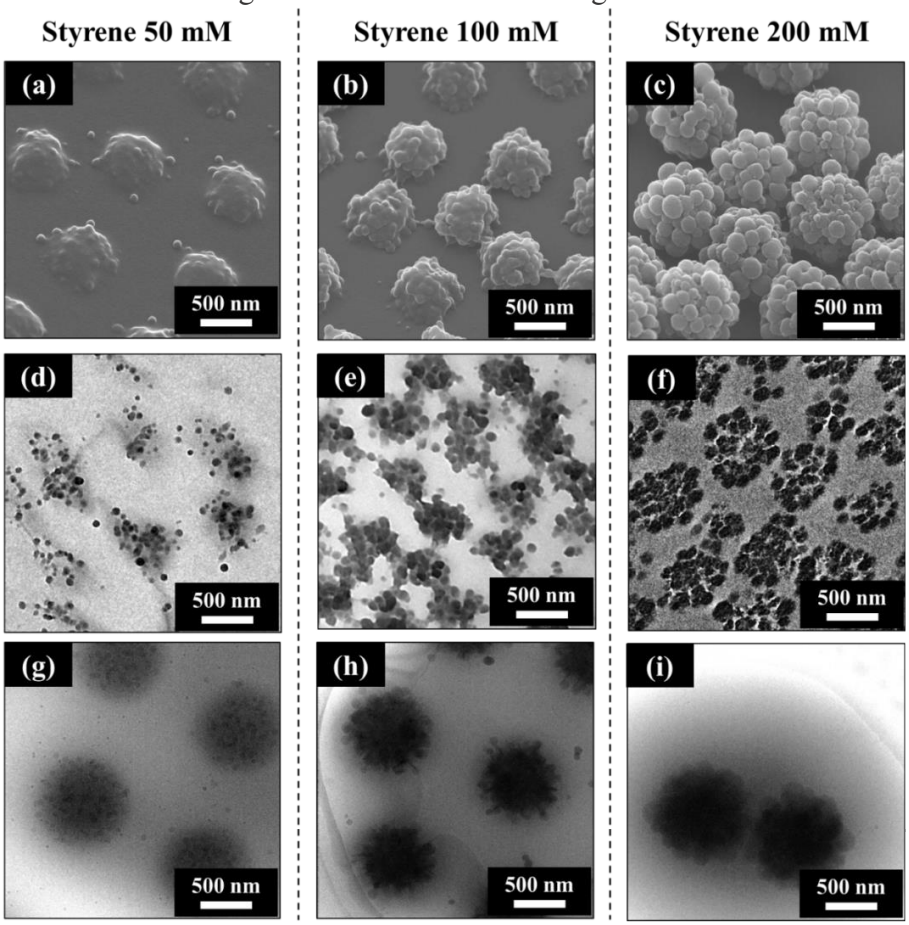


**Figure 3-4**. Electron microscopy images of **NF5-S*X*** composite microgels prepared by the soap-free SEP of styrene. During the SEP, the styrene concentration fed during SEP was (a, d, g) 50 mM, (b, e, h) 100 mM, or (c, f, i) 200 mM; (a-c) FE-SEM images; (d-f) TEM images of ultra-thin cross sections of the composite microgels; (g-i) Cryo-TEM images of the composite microgel.

**Table 3-3.** Characterization Results of **NF-S*X*** Composite Microgels ($N = 50$).

| Code | Composite microgels (determined by FE-SEM) | | Small polystyrene particles (determined by FE-SEM) | | Polystyrene-occupied area (determined by cross-section) | | Composite microgels (determined by cryo-TEM) | |
|---|---|---|---|---|---|---|---|---|
| | diameter / nm | CV / % | diameter / nm | CV / % | area / % | CV / % | diameter / nm | CV / % |
| NF5-S50 | 666 ± 40 | 6.0 | 67 ± 12 | 18 | 30 | 6.1 | 873 ± 18 | 2.0 |
| NF5-S100 | 638 ± 32 | 5.0 | 79 ± 21 | 26 | 58 | 18 | 740 ± 44 | 5.9 |
| NF5-S200 | 846 ± 41 | 4.9 | 115 ± 47 | 41 | 74 | 5.5 | 853 ± 20 | 2.4 |

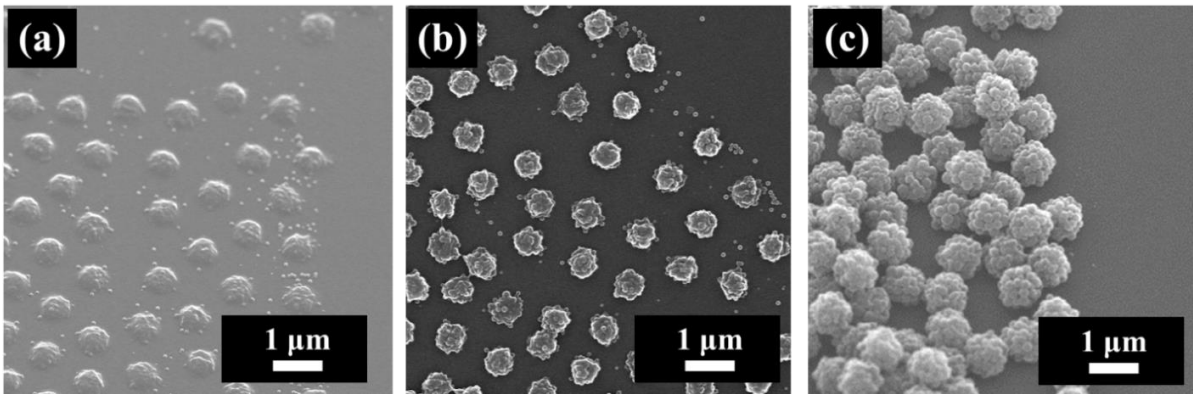


**Figure 3-5.** FE-SEM images of the edge of the samples: (a) **NF5-S50**, (b) **NF5-S100**, and (c) **NF5-S200** composite microgels in the dry state. Byproducts such as secondary polystyrene nanoparticles were virtually not observed in all cases, not even near the edge of the droplets.

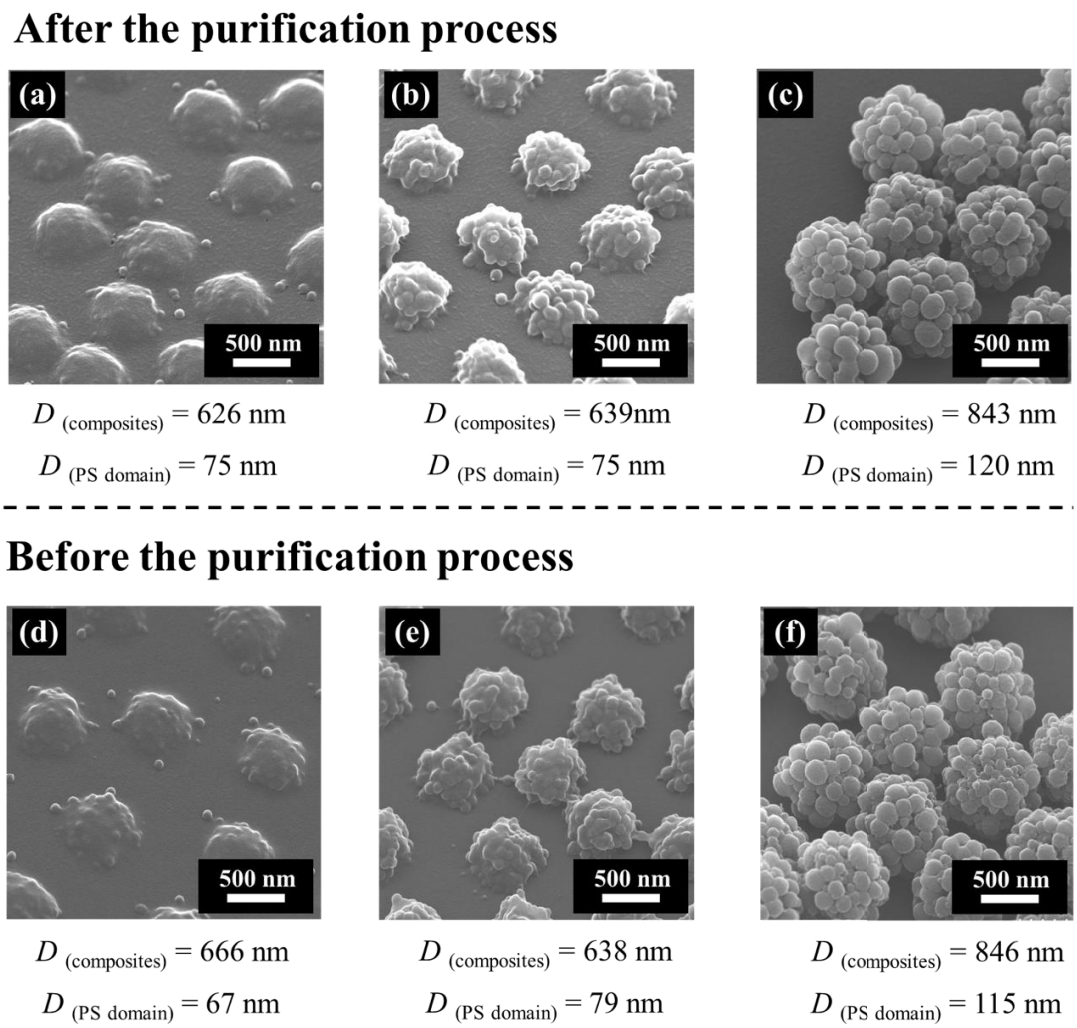


**Figure 3-6.** FE-SEM images of (a) **NF5-S50**, (b) **NF5-S100**, and (c) **NF5-S200** composite microgels after two purification (centrifugation/redispersion) processes. These morphologies did not change after the centrifugation. The morphologies of the composite microgels before the centrifugation/redispersion are shown in **Figure 3-2 (d)-(f)**.

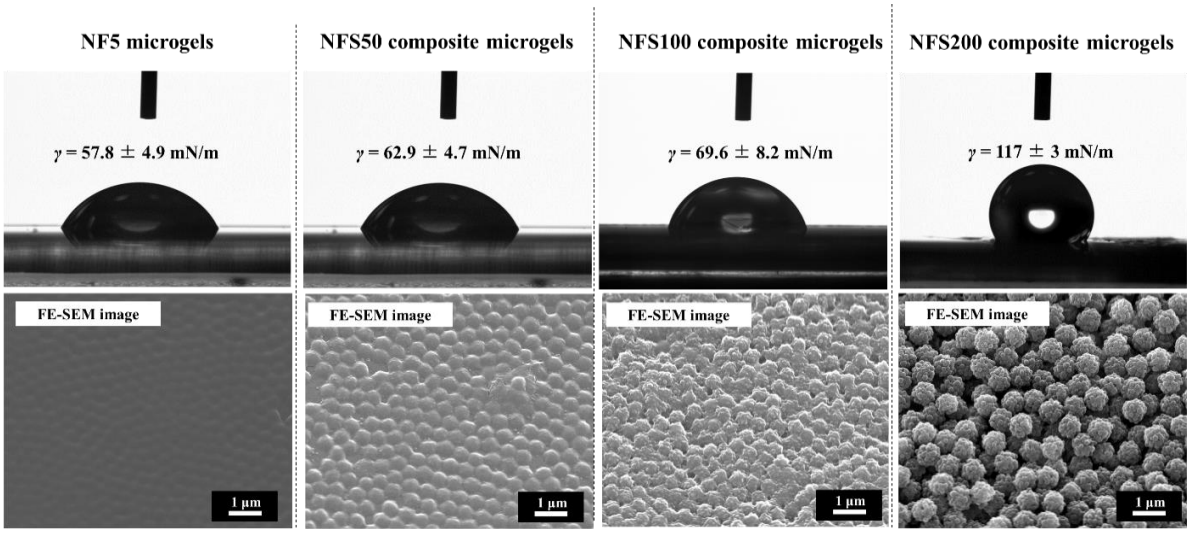


**Figure 3-7.** Measuring the contact angle of microgel or composite microgel-coated polystyrene substrates. The surface of the polystyrene substrates was completely covered by each type of microspheres, which was determined by FE-SEM. Here, the contact angle was measured immediately after a water droplet (5 μL) was deposited on the substrate.

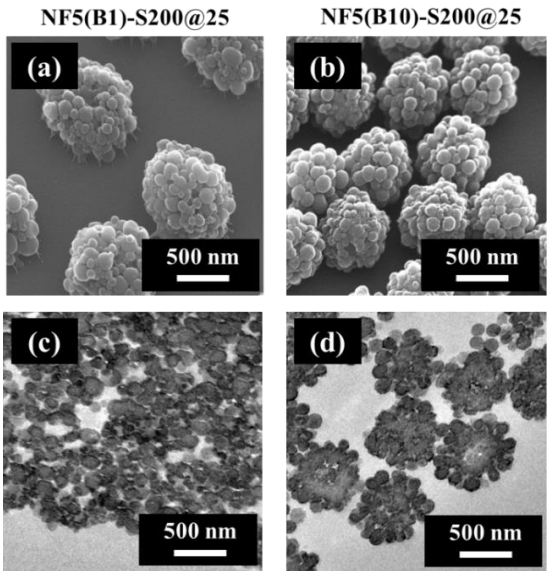


**Figure 3-8.** Electron micrographs of (a, c) **NF5(B1)-S200** and (b, d) **NF5(B10)-S200** composite microgels. (a, b) FE-SEM and (c, d) TEM images of ultra-thin cross sections of composite microgels. The diameter of the composite microgels were calculated to be 926 nm (CV = 4.2 %, **Figure 3-8(a)**) and 688 nm (CV = 4.5 %, **Figure 3-8(b)**), respectively.

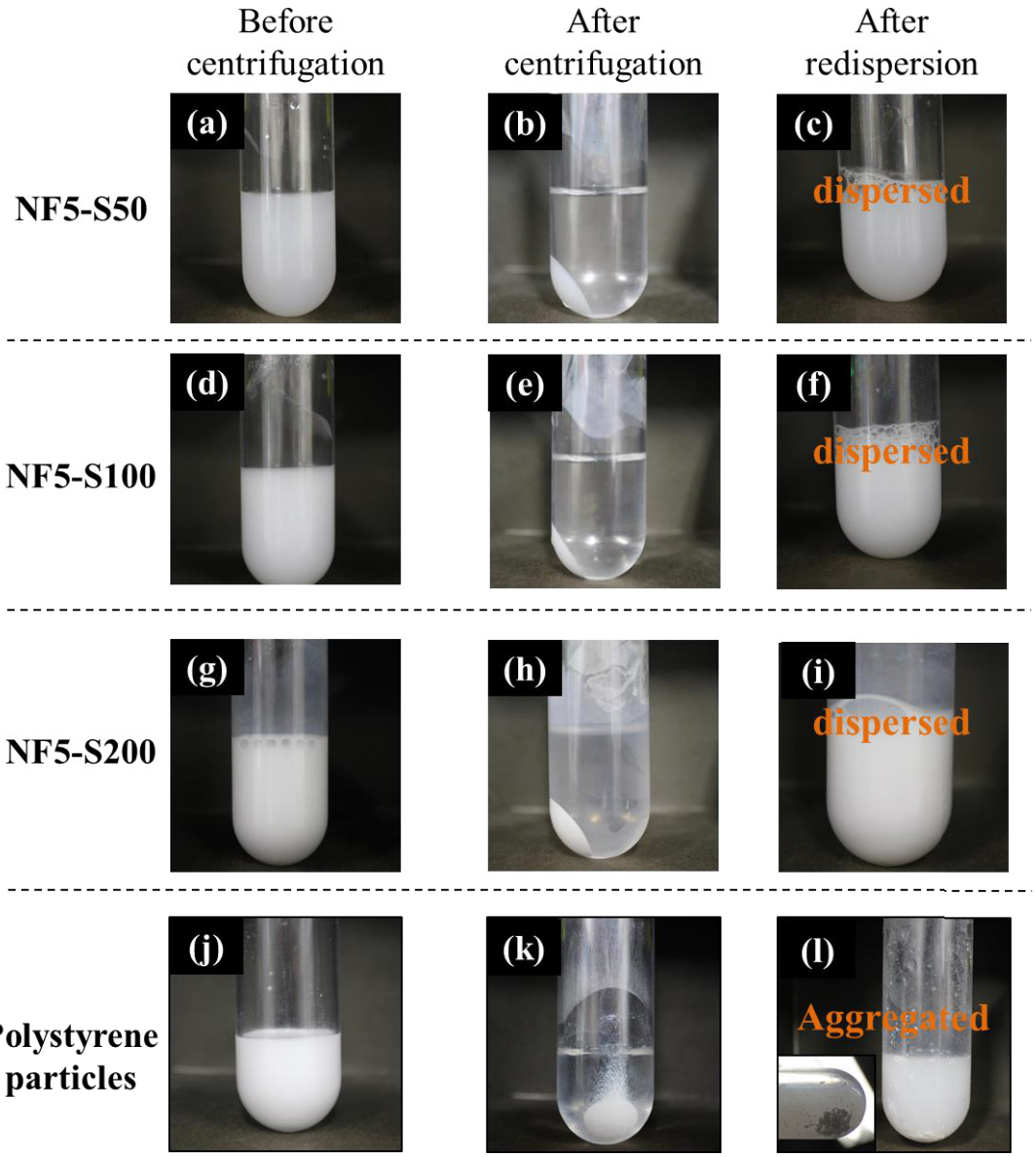


**Figure 3-9.** Photographic images of dispersions of (a-c) **NF5-S50**, (b-f) **NF5-S100**, and (g-i) **NF5-S200** composite microgels as well as (j-l) polystyrene particles (a, d, g, j) before centrifugation, (b, e, h, k) after centrifugation (70,000 × *g*, 30 min, 15 °C), and (c, f, i, l) after redispersion (~20 times pipetting). The polystyrene particles could not be redispersed even after shaking for 30 min and numerous aggregates remained (l). In contrast, all composite microgels could be easily redispersed by pipetting (c, f, i).

**Table 3-4.** Hydrodynamic Diameters and Electrophoretic Mobilities of **NF-S*X*** Composite Microgels.

| code | pH | Electrophoretic mobility × $10^{-8}m^2(Vs)$ | |
|---|---|---|---|
| | | 25 °C | 70 °C |
| **NF** | 3 | -0.70 ± 0.01[a] | -3.31 ± 0.06[a] |
| | 10 | -2.08 ± 0.01[a] | -3.66 ± 0.09[a] |
| **NF-S50** | 3 | -0.78 ± 0.02 | -3.76 ± 0.09 |
| | 10 | -1.88 ± 0.02 | -3.29 ± 0.06 |
| **NF-S100** | 3 | -0.69 ± 0.04 | -3.35 ± 0.06 |
| | 10 | -2.00 ± 0.01 | -3.97 ± 0.01 |
| **NF-S200** | 3 | -1.07 ± 0.04 | -2.78 ± 0.09 |
| | 10 | -1.86 ± 0.02 | -4.02 ± 0.12 |
| **Polystyrene particle** | 3 | -2.97 ± 0.07[a] | -2.99 ± 0.06[a] |

a : Reproduced with permission from *Langmuir* **2016**, *32*, 12760-12773. Copyright 2016 American Chemical Society.

### 3.3.4. Effect of the Charge Distribution in the Hydrated Microgel Cores on the Morphology of the Composite Microgels

In order to clarify the effect of the charge distribution within the hydrated microgels on the morphology of the composite microgels in more detail, the author tried to stabilize the **NM5-S** composite microgels. When the SDS concentration was kept at 0.5 mM, i.e., below the critical micelle concentration, during the SEP in the presence of the **NM5** microgels, colloidally stable **NM5** composite microgels were obtained (**Figure 3-10(a)**). It should be noted that the concentration of 0.5 mM SDS did not affect the morphology when **NF5** microgels were used as seeds (**Figure 3-11**). Their diameter was calculated to be 510 nm (**Figure 3-10(a)**; CV = 6.4 %, *N* = 50), while that of the polystyrene nanoparticles attached to the **NM5** microgels was calculated to be 69 nm (**Figure 3-10(a)**, CV = 6.0 %, *N* = 50). More importantly, the TEM images of the ultra-thin cross sections (**Figure 3-10(b)**) clearly show that the polystyrene nanoparticles mainly form on the surface of the microgels and not in the center of the microgels, which is different from the case when **NF5-S*X*** composite microgels were used (**Figure 3-4(d)-(f)**).

Furthermore, when the amount of SDS during the SEP was increased to 16 mM, the size of the polystyrene nanoparticles attached to the obtained composite microgels decreased (**Figure 3-10(c),(d)**), while the number of polystyrene nanoparticles increased. In addition, the monomer-to-polymer conversion of styrene improved relative to the SEP without SDS (**Table 3-5**). Thus, compared to the previous case (**Figure 3-10(a),(b)**), the polystyrene density of the shell in the composite microgels was improved, and the dimple structure appeared (**Figure 3-10(c)**). The dimple structure was presumably formed during the drying process due to the density difference within the composites, which has already been reported in a previous study on hollow microspheres.[42] These results indicate that SDS molecules were adsorbed onto the core microgels avoiding the polyelectrolytes, and the formed SDS associations serve as nucleation sites for the formation of polystyrene.[33] It should also be noted that the size of the polystyrene nanoparticles decreased upon addition of SDS during the SEP when the **NF5** microgels were used as seeds (**Figure 3-10(e),(f)**).

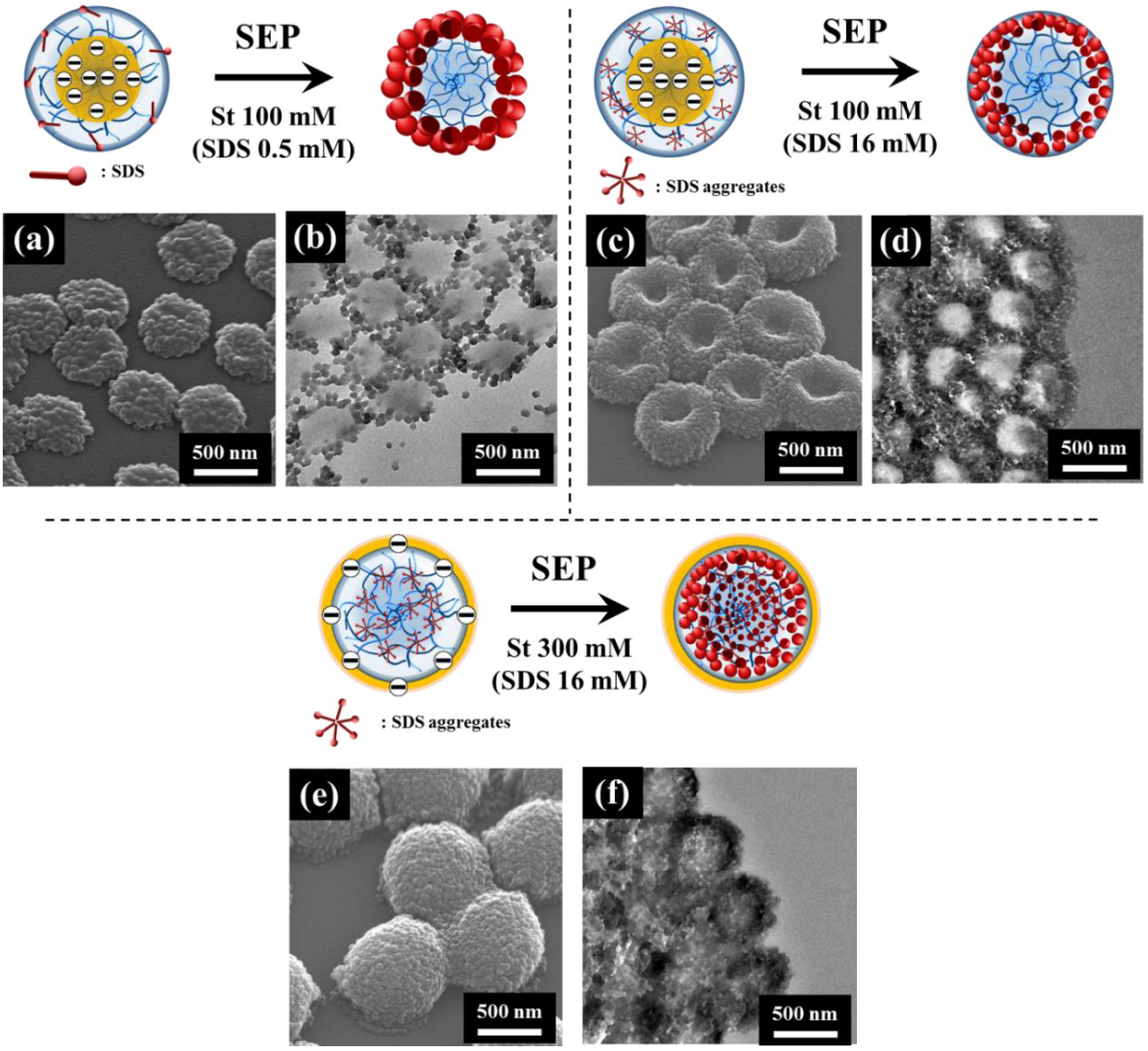


**Figure 3-10.** Electron micrographs of (a,b) **NM5-S100-SDS0.5mM**, (c,d) **NM5-S100-SDS16mM**, and (e, f) **NF5-S300-SDS16mM** composite microgels; (a,c,e) FE-SEM images and (b,d,f) TEM images of ultra-thin cross sections of the composite microgels.

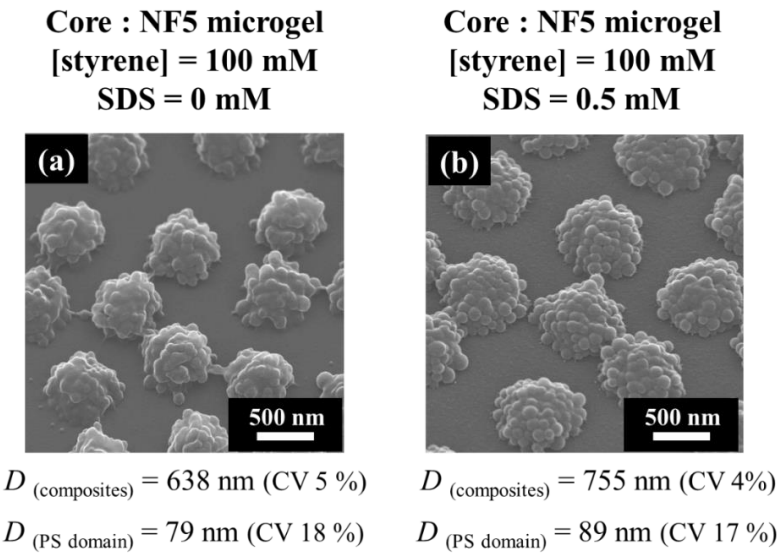


**Figure 3-11.** FE-SEM images of **NF5-S100** composite microgels prepared by SEP without SDS (a) and with 0.5 mM SDS (b). The addition of small amount SDS did not have any significant effect on the morphology of composite microgels.

**Table 3-5.** Styrene monomer conversion for each SEP system.

| Code | Polymerization temperature / ° C | Conversion / % |
|---|---|---|
| **NF5-S50** | 25 | 31 |
| **NF5-S100** | 25 | 20 |
| **NF5-S200** | 25 | 24 |
| **NM5-S100 (SDS16 mM)** | 25 | 82 |
| **NF5-S300 (SDS16 mM)** | 25 | 79 |

### 3.3.5. Investigation of the Diffusion of Styrene into the Core-shell Microgels

The effect of surface charged density of core microgels on the diffusion of the styrene monomers into the core microgels was investigated. Based on the results obtained from the **NM5** microgel system (**Figure 3-10(a)-(b)**), the author hypothesized that the hydrophilic gel layer composed of hydrated pNIPAm and polyelectrolytes may interrupt the diffusion of the hydrophobic styrene monomer into the center of the microgels. In order to increase the surface-charge density of the core microgels, a cross-linked **NA40** gel shell was deposited on the surface of the **NF5** core microgels by seeded precipitation polymerization (**Figure 3-12(a)**). The FE-SEM image of the thus obtained **NF5-NA40** core-shell microgels indicated that the formation of uniform micron-sized microgels without any secondary microgels (**Figure 3-12(b)**). From the DLS measurements, the shell thickness was ~200 nm in deswollen state (shell thickness: $R_{\text{core-shell, pH=3, 70 °C}}$ - $R_{\text{core, pH=3, 70 °C}}$). It should be noted that the shell-thickness of core-shell microgels in polymerization condition (pH = 10, 25 °C) could not be determined by DLS measurement. Some of diffusion coefficients were not calculated accurately by the cumlant approach because the electric-field correlation functions were not proportional to the correlation time (**Figure 3-13**). These results indicated that the sufficient thickness of highly hydrated shell layer was existed on the **NF5** microgels during SEP. Moreover, the EPM of the microgels increased upon the addition of the shell ($EPM_{\text{core-shell}} = -2.9 \times 10^{-8}$ $m^2/Vs$; pH = 10; 25 °C), indicating that the charge density of the surface of the microgels increased upon the addition of shell-gels in the swollen state ($EPM_{\text{core}} = -2.1 \times 10^{-8}$ $m^2/Vs$; pH = 10; 25 °C). Based on the FE-SEM images (**Figure 3-12(c)**), raspberry-shaped composite microgels were obtained. The diameter of these composite microgels and the polystyrene nanoparticles was determined to be 933 nm (CV = 6 %) and 95 nm (CV = 26 %), respectively. Notably, the formation of secondary polystyrene nanoparticles was not observed for this system. Most importantly, the TEM images suggest that the polystyrene nanodomains or nanoparticles are formed not only on the surface of the core-shell microgels but also at the center (**Figure 3-12(d)**). Thus, these results (**Figure 3-12**) clearly suggest that hydrophobic styrene monomers can diffuse into the microgels despite the presence of a highly charged and "hydrated" shell on the microgels; thereafter, the neutral microgels serve as polymerization sites for the formation of polystyrene.

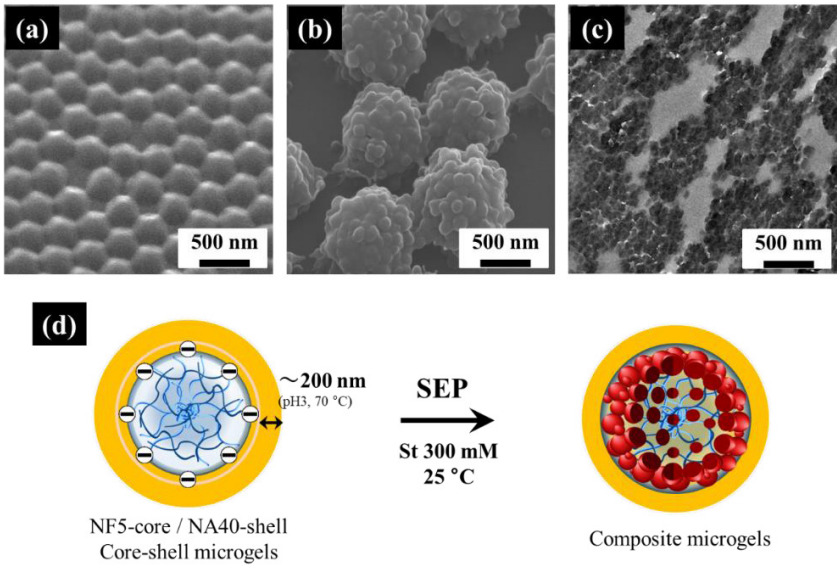


**Figure 3-12.** Electron micrographs of **NF5-NA40** core-shell microgels and **NF5-NA40-S300** composite microgels; (a) FE-SEM image of **NF-NA40** microgels, (b) FE-SEM images of **NF5-NA40-S300** composite microgels, (c) TEM image of ultra-thin cross section of **NF5-NA40-S300** composite microgels, respectively. (d) Scheme of core-shell microgels and obtained composite microgels.

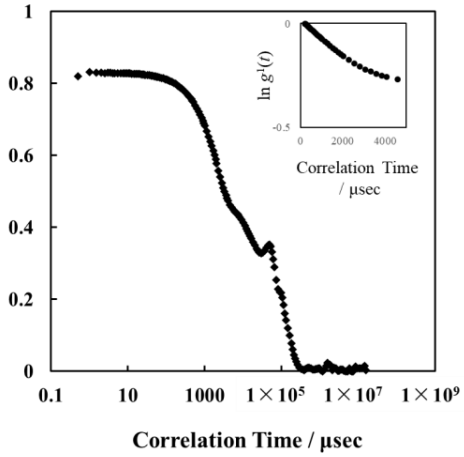


**Figure 3-13.** Intensity correlation functions of **NF5-A40** core-microgels measured at pH = 10 and 25 °C. The inset shows the electric-field time correlation function of these microgels. The diffusion coefficients were not calculated accurately by the cumlant approach because the electric-field correlation functions were not proportional to the correlation time in $t > \sim 5000$.

### 3.3.6. The Three-Dimensional Morphology of the Composite Microgels in the Swollen State

Cryo-electron tomography (cryo-ET) was applied to evaluate the three-dimensional morphology of composite microgels for this study. Unlike the general characterization techniques, this allows to observe the composite microgels in hydrated swollen state by embedding samples in vitreous ice using a plunge-freezing apparatus. Moreover, the reconstruction from a tilt series of two-dimensional projections collected at a tilt angle range of -60° to +60°, three-dimensional structural information of composite microgels was obtained in details.[25]

Segmentation images are shown in **Figure 3-14**. These results indicate that the spaces between the individual polystyrene nanoparticles immobilized in each microgel decrease as the styrene monomer concentration increased (**Figure 3-14**). In addition, the segmentations revealed the accurate size of the polystyrene nanoparticles ($D_{seg}$) for **NF5-S50** (49 nm; CV = 23 %; **Figure 3-14(a)**), **NF5-S100** (69 nm; CV = 24 %; **Figure 14(b)**), and **NF5-S200** (124 nm; CV 90 %; **Figure 14(c)**). There were no differences in size between at the surface of microgels and the center. However, the mean CV in the case of the **NF5-S200** composites was larger than that of the other composites, which should be attributed to the particle formation process (**Figures 3-15** and **3-16**). When the styrene concentration was kept constant at 100 mM during the SEP in the presence of the **NF5** microgels (**Figure 3-15**), the number of polystyrene nanoparticles attached to the core microgels remained almost constant during the polymerization, from initially 49 counts / microgel ($D$ = 38 nm, 30 min, $N$ = 50) to 50 counts / microgel ($D$ = 79 nm, 24 h, $N$ = 50). In contrast, when the concentration of the styrene monomer was kept constant at 200 mM during the SEP (**Figure 3-16**), the number of polystyrene nanoparticles attached to the microgels decreased during the polymerization from 52 counts / microgel ($D$ = 78 nm, 1 h, $N$ = 50) to 41 counts / microgel ($D$ = 115 nm, 24 h, $N$ = 50). Thus, these result strongly supported our hypothesis that hydrated and highly swollen pNIPAm-based microgels can serve as polymerization fields to hydrophobic styrene monomer regardless of swollen state.

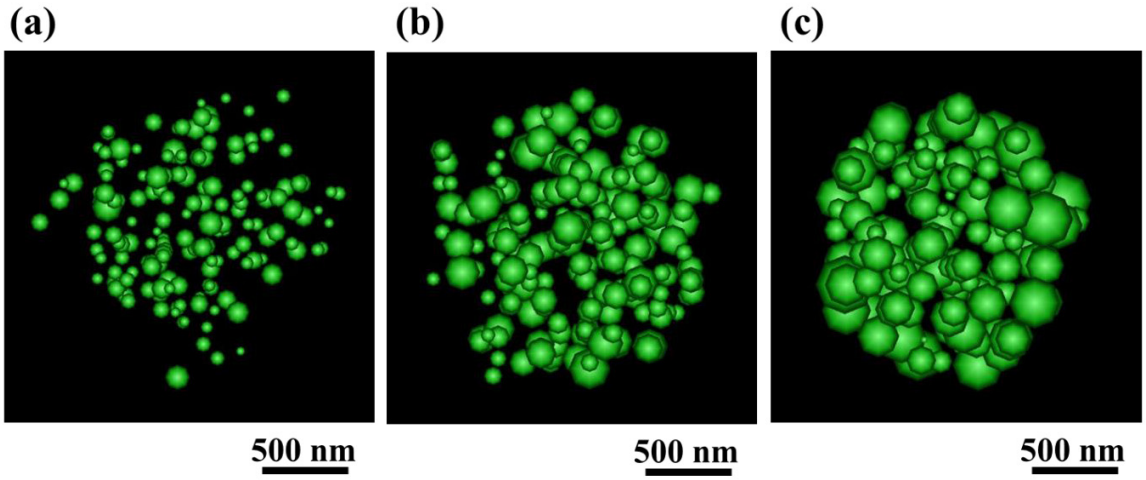


**Figure 3-14.** Segmentation image of **NF5-S*X*** composite microgels. (a) **NF5-S50**, (b) **NF5-S100**, and (c) **NF5-S200** composite microgels.

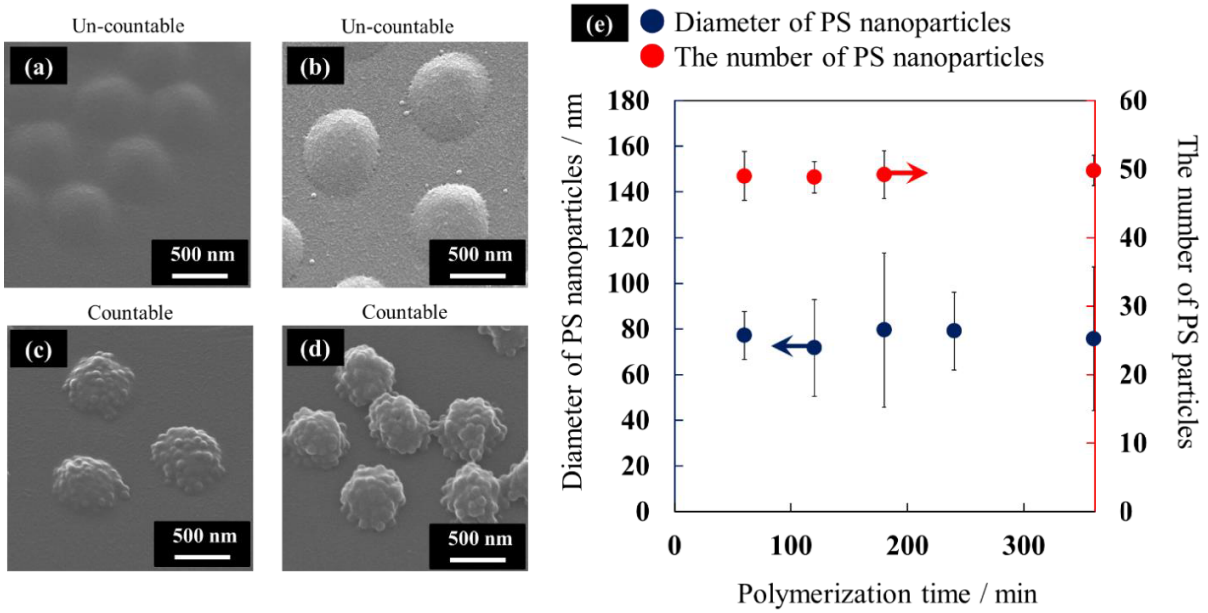


**Figure 3-15.** (a-d) FE-SEM images of **NF(B5)-S100** microgels after (a) 15 min, (b) 30 min, (c) 1 h, and (d) 2 h of polymerization. (e) The graph shows the mean diameters of the composite microgels (blue circles) and the number of polystyrene nanoparticles on the seed microgel (red circles) after different polymerization periods.

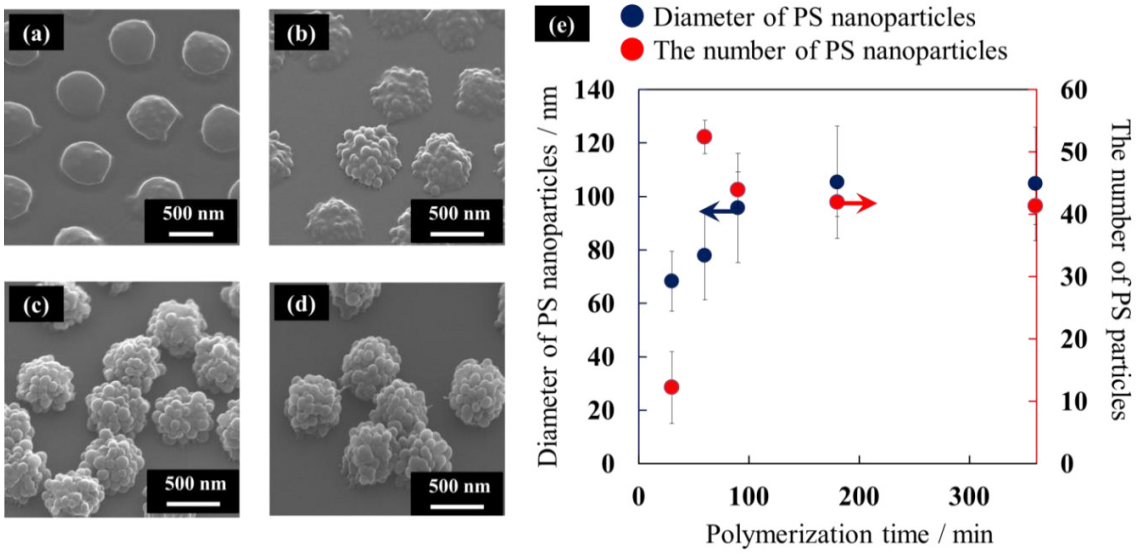


**Figure 3-16.** (a-d) FE-SEM images of **NF(B5)-S200** microgels after (a) 30 min, (b) 1 h, (c) 2 h, and (d) 4 h of polymerization. (e) The graph shows the mean diameters of the composite microgels (blue circles) and the number of polystyrene nanoparticles on the seed microgel (red circles) after different periods of polymerization.

### 3.4. Conclusions

The results of the present study allow drawing the following conclusion: (**Figure 3-17**): (1) during the SEP of styrene, water-swollen pNIPAm microgels can serve as the polymerization environment for hydrophobic styrene monomers; (2) different from the high-temperature polymerization system,[13-16] the surface-charged density of the microgel seeds strongly affects the colloidal stability of the resulting composite microgels; when **N** and **NM5** microgels were used as seeds, the resulting colloidal dispersion were unstable, even though stable composite microgels were obtained using **NF5** microgels seeds at pH < 10; (3) polystyrene nanoparticles cannot combine with the polyelectrolytes in the hydrated microgels, indicating that the charge distribution of the microgel cores is key factor for the morphological design of the composite microgels; (4) three-dimensional images of water-swollen composite microgels were obtained for the first time from a cryo-tomography TEM analysis, which delivered the accurate size ($D_{seg}$) and size distribution of the generated polystyrene nanoparticles. The difference of total number of polystyrene nanoparticles, which was calculated using $D_{seg}$ and the monomer conversion, between the soap-free EP and the SEP with microgels also supported the notion that microgels aid the formation of polystyrene nanoparticles.

These results clearly demonstrate that a series of raspberry-shaped composite microgels are obtained even when the seed microgels are swollen and hydrated during the SEP of styrene, and the key factor for determining the structures of the composite microgels by the SEP is the distribution of the polyelectrolytes in the core microgels, not the swelling state of core microgels. Therefore, this study will help to i) design new composite microgels, which should be useful for applications of non-spherical microspheres and microgels in e.g. sensors,[26,27] drug carriers,[28-30] reactors,[31-34] coating materials,[35] and autonomous oscillators,[36-40] and ii) improve the understanding of the properties of the local environment in swollen microgels.

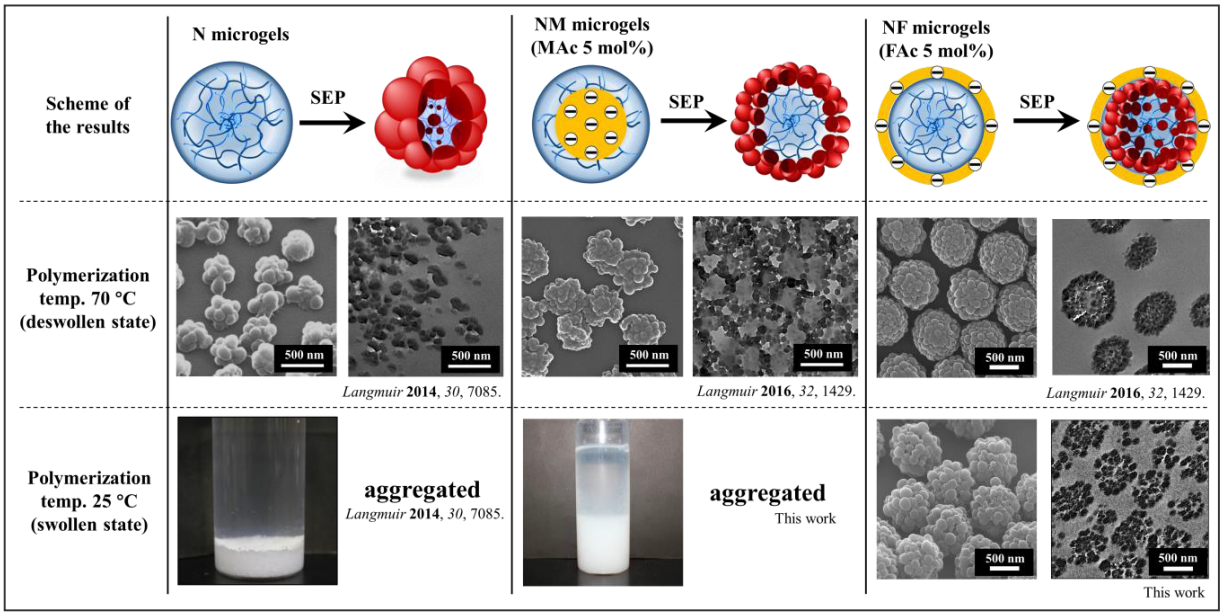


**Figure 3-17.** SEP in the presence of pNIPAm microgels. Reproduced with permission from *Langmuir* **2016**, *32*, 12760-12773. Copyright 2016 American Chemical Society and *Langmuir* **2014**, *30*, 7085-7092. Copyright 2014 American Chemical Society.

### 3.5. References


1. Smith, W. V.; Ewart, R. H. Kinetics of Emulsion Polymerization. *J. Chem. Phys.* **1948**, *16*, 592-599.
2. Thickett, S. C.; Gilbert, R. G., Emulsion Polymerization: State of the Art in Kinetics and Mechanisms. *Polymer* **2007**, *48*, 6965-6991.
3. Mock, E. B.; De Bruyn, H.; Hawkett, B. S.; Gilbert, R. G.; Zukoski, C. F. Synthesis of Anisotropic Nanoparticles by Seeded Emulsion Polymerization. *Langmuir* **2006**, *22*, 4037-4043.
4. Liu, Y.; Ma, Y.; Liu, L.; Yang, W. Facile Synthesis of Core-Shell/Hollow Anisotropic Particles via Control of Cross-Linking during One-pot Dispersion Polymerization. *J. Coll. Int. Sci.* **2015**, *445*, 268-276.
5. Minami, H.; Wang, Z.; Yamashita, T.; Okubo, M. Thermodynamic Analysis of the Morphology of Monomer-adsorbed, Cross-linked Polymer Particles Prepared by the Dynamic Swelling Method and Seeded Polymerization. *Colloid Polym. Sci.* **2003**, *281*, 246-252.
6. Tu, F.; Lee, D. Shape-Charging and Amphiphilicity-Reversing Janus Particles with pH-Responsive Surfactant Properties. *J. Am. Chem. Soc*. **2014**, *136*, 9999-10006.
7. Okubo, M.; Kanaida, K.; Matsumoto, T. Production of Anomalously Shaped Carboxylated Polymer Particles by Seeded Emulsion Polymerization. *Colloid and Polym. Sci*. **1987**, *265*, 876-881.
8. Okubo, M. and Minami, H. Control of Hollow Size of Micron-sized Monodispersed Polymer Particles Having a Hollow Structure. *Colloid Polym. Sci*. **1996**, *274*, 433-438.
9. Li, B.; Xu, Y.; Wang, M.; Ge, X. Morphological Control of Multihollow Polymer Latex Particles through Controlled Phase Separation in the Seeded Emulsion Polymerization. *Langmuir* **2013**, *29*, 14787-14794.
10. Duracher, D.; Sauzedde, F.; Elaissari, A.; Perrin, A.; Pichot, C. Cationic Amino-Containing *N*-isopropyl-acrylamide-Styrene Copolymer Latex Particles: 1-Particle Size and Morphology vs. Polymerization Process. *Colloid Polym. Sci*. **1998**, *276*, 219-231.
11. Sheu, H. R.; El-Aasser, M. S.; Vanderhoff, J. W. Phase Separation in Polystyrene Latex Interpenetrating Polymer Networks. *J. Polym. Sci.: Part A: Polym. Chem*. **1990**, *28*, 629-651.
12. Ravensteijn, B. G. P.; Kegel, W. K. Tuning Particle Geometry of Chemically Anisotropic Dumbbell-Shaped Colloids. *J. Coll. Int. Sci.* **2017**, *490*, 462-477.
13. Suzuki, D.; Yamagata, T.; Murai, M. Multilayered Composite Microgels Synthesized by Surfactant-Free Seeded Polymerization. *Langmuir* **2013**, *29*, 10579-10585.
14. Suzuki, D.; Kobayashi, C. Raspberry-Shaped Composite Microgel Synthesis by Seeded Emulsion Polymerization with Hydrogel Particles. *Langmuir* **2014**, *30*, 7085-7092.
15. Kobayashi, C.; Watanabe, T.; Murata, K.; Kureha, T.; Suzuki, D. Localization of Polystyrene Particles on the Surface of Poly(*N*-isopropylacrylamide-*co*-methacrylic acid) Microgels Prepared by Seeded Emulsion Polymerization of Styrene, *Langmuir* **2016**, *32*, 1429-1439.

16. Watanabe, T.; Kobayashi, C.; Song, C.; Murata, K.; Kureha, T.; Suzuki, D. Impact of Spatial Distribution of Charged Groups in Core Poly(*N*-isopropyl acrylamide)-Based Microgels on the Resultant Composite Structures Prepared by Seeded Emulsion Polymerization of Styrene. *Langmuir* **2016**, *32*, 12760-12773.
17. Heskins, M.; Guillet, J. E.; Solution Properties of Poly(N-isopropylacrylamide). *J. Macromol. Sci.-Chem.* **1968**, *2*, 1141-1455.
18. Pelton, R. H. Temperature-Sensitive Aqueous Microgels. *Adv. Colloid Interface Sci.* **2000**, *85*, 1-33.
19. Kraft, D. J.; Hilhorst, J.; Heinen, M. A. P.; Hoogenraad, M. J.; Luigjes, B.; Kegel, W. K. Patchy Polymer Colloids with Tunable Anisotropy Dimensions. *J. Phys. Chem. B* **2011**, *115*, 7175-7181.
20. Kremer, J. R.; Mastronarde, D. N.; Mcintosh, J. R. Computer Visualization of Three-dimensional Image Data Using IMOD. *J Struct Biol*, **1996**, 116, 71-76.
21. Hoare, T.; Pelton, R. Characterizing Charge and Crosslinker Distributions in Polyelectrolyte Microgels. *Curr Opin. Colloid Interface Sci.* **2008**, *13*, 413-428.
22. Hoare, T.; Pelton, R. Functional Group Distributions in Carboxylic Acid Containing Poly(*N*-isopropylacrylamide) Microgels. *Langmuir* **2004**, *20*, 2123-2133.
23. Daly, E.; Saunders, B. R. Temperature-Dependent Electrophoretic Mobility and Hydrodynamic Radius Measurements of poly(*N*-isopropylacrylamide) Microgel Particles: Structural Insights. *Phys. Chem. Chem. Phys*. **2000**, *2*, 3187-3193.
24. Okubo, M.; Minami, H.; Morikawa, K. Influence of Shell Strength on Shape Transformation of Micron-Sized, Monodisperse, Hollow Polymer Particles. *Colloid Polym. Sci.* **2003**, *281*, 214-219.
25. Lučič, V.; Rigort, A.; Baumeister, W. Cryo-electron tomography: the challenge of doing structural biology in situ. *J. Cell Biol.* **2013**, *202 (3)*, 407–419.
26. Holtz, J. H.; Asher, S. A. Polymerized Colloidal Crystal Hydrogel Films as Intelligent Chemical Sensing Materials. *Nature* **1997**, *389*, 829-832.
27. Li, X.; Gao, Y.; Serpe, M. J. Responsive Polymer-Based Assemblies for Sensing Applications. *Macromol. Rapid Commun*. **2015**, *36*, 1382-1392.
28. Walta, S.; Pergushov, D. V.; Oppermann, A.; Steinschulte, A. A.; Geisel, K.; Sigolaeva, L. V.; Plamper, F. A.; Woll, D.; Richtering, W. Microgels Enable Capacious Uptake and Controlled Release of Architecturally Complex Macromolecular Species. *Polymer* **2017**, *119*, 50-58.
29. Kataoka, K.; Harada, A.; Nagasaki, Y. Block Copolymer Micelles for Drug Delivery: Design, Characterization and Biological Significance. *Adv. Drug Delivery Rev.* **2001**, *47*, 113-131.
30. Otsuka, H.; Nagasaki, Y.; Kataoka, K. PEGylated Nanoparticles for Biological and Pharmaceutical Applications. *Adv. Drug Delivery Rev.* **2012**, *64*, 246-255.
31. Zhang, J.; Xu, S.; Kumacheva, E. Polymer Microgels: Reactors for Semiconductor, Metal, and Magnetic Nanoparticles. *J. Am. Chem. Soc.* **2004**, *126*, 7908-7914.

32. Seto, H.; Imai, K.; Hoshino, Y.; Miura, Y. Polymer Microgel Particles as Basic Catalysts for Knoevenagel Condensation in Water. *Polymer Journal* **2016**, *48*, 897-904.
33. Lu, Y.; Ballauff, M. Spherical Polyelectrolyte Brushes as Nanoreactors for the Generation of Metallic and Oxidic Nanoparticles: Synthesis and Application in Catalysis. *Prog. Polym. Sci.* **2016**, *59*, 86-104.
34. Klinger, D.; Landfester, K. Stimuli-Responsive Microgels for the Loading and Release of Functional Compounds: Fundamental Concepts and Applications. *Polymer* **2012**, *53*, 5209-5231.
35. Cors, M. Wrede, O.; Genix, A. C.; Anselmetti, D.; Oberdisse, J.; Hellweg, T. Core-Shell Microgel-Based Surface Coatings with Linear Thermoresponse. *Langmuir* **2017**, *33*, 6804-6811.
36. Suzuki, D.; Sakai, T.; Yoshida, R. Self-Flocculating/self-Dispersing Oscillation of Microgels. *Angew. Chem., Int. Ed*. **2008**, *47*, 917-920.
37. Suzuki, D.; Taniguchi, H.; Yoshida, R. Autonomously Oscillating Viscosity in Microgel Dispersions. *J. Am. Chem. Soc*. **2009**, *131*, 12058-12059.
38. Suzuki, D.; Kobayashi, T.; Yoshida, R.; Hirai, T. Soft Actuators of Organized Self-Oscillating Microgels. *Soft Matter* **2012**, *8*, 11447-11449.
39. Matsui, S.; Kureha, T.; Nagase, Y.; Okeyoshi, K.; Yoshida, R.; Sato, T.; Suzuki, D. Small-Angle X-ray Scattering Study on Internal Microscopic Structures of Poly(*N*-isopropylacrylamide-*co*-tris(2,2'-bipyridyl))ruthenium( Ⅱ ) Complex Microgels. *Langmuir* **2015**, *31*, 7228-7237.
40. Suzuki, D.; Horigome, K.; Kureha, T.; Matsui, S.; Watanabe, T. Polymeric Hydrogel Microspheres: Design, Synthesis, Characterization, Assembly and Applications. *Polymer Journal* **2017**, *49*, 695-702.

# 4. Chapter III

# " Hydrophobized Nanocomposite Hydrogel Microspheres as Particulate Stabilizers for Water-in-Oil Emulsions "

*Part of this work was submitted in " Watanabe Takumi, Masaya Takizawa, Hang Jiang, To Ngai, and Daisuke Suzuki, *Chemical Communications*, **2019**, *55*, 5990-5993." Reprinted with permission from Copyright (2019), The Royal Society of Chemistry.

## 4.1. Introduction

Through **Chapter I** and **II**, a series of nanocomposite microgels with different polystyrene distribution inside of microgels have been synthesized by SEP of styrene in the presence of microgels under various polymerization conditions. As described in the introductory remarks, nanocomposite microgels have some potential on applications because nanocomposite microgels have non-spherical shaped with hydrophobicity. However, importance and superior properties of nanocomposite microgels in the colloidal applications have been uncertain. Therefore, in present chapter, the emulsion properties of nanocomposite microgels were investigated for stable emulsions which used in various applications such as drug delivery, and chemical reaction.

Emulsions stabilized by colloidal particles[1,2] hold great potential for a variety of applications in materials science[3-6] owing to their fascinating properties, which include an extremely high adsorption energy of colloidal particles at oil/water interfaces (~ $10^2$–$10^6$ $k_BT$) leading long-term stability of these emulsions. In particular, interest has been growing in soft-hydrogel-microsphere- (microgel-)stabilized emulsions (henceforth: MS-Es) as they show several advantages relative to emulsions stabilized by solid microspheres made of polystyrene or silica.[7-10] For instance, the remarkably stable MS-Es can be demulsified by applying external stimuli such as changes in temperature or pH value.[11-13] In addition, compared to emulsions stabilized by solid microspheres, stable MS-Es can be obtained with a lower energy input since highly swollen microgels spontaneously adsorb at oil/water interfaces.[14-16] Furthermore, porous bulk materials have been obtained from highly concentrated MS-Es as templates,[7,17] which is possible due to the high colloidal stability of MS-Es originating from steric stabilization effects.

However, several unresolved issues remain that hamper the practical utility of **MS-E**s. One of the challenges is that generally only oil-in-water (O/W) emulsions are obtained when microgels are used as emulsion stabilizers, as it is difficult to prepare microgels that meet the requirements to produce water-in-oil (W/O) emulsions. In general, particle wettability is considered a key factor for controlling the type of emulsions (O/W or W/O) stabilized by the particles.[4,18,19] Thus, in order to prepare W/O emulsions with water-swollen microgels, the microgels should display good affinity toward the biphasic interface; for that purpose, the

microgels need to hydrophilic to be dispersible in water and also sufficiently hydrophobic to adsorb strongly at the water/oil interface. However, it is difficult to realize such a combination of features in conventional microgels, given that these are typically highly hydrophilic and swollen by water.[20] Thus, when the microspheres display greater affinity toward the water phase than the oil phase, O/W emulsions are obtained. Consequently, it is practically impossible to prepare W/O emulsions with highly water-swollen conventional microgels. Although few studies on W/O emulsions prepared with microgels as emulsifiers have been reported, these reports a restricted to polar oils such as undecanol,[13] octanol,[21] and other fatty alcohols.[15]

Therefore, in this chapter, the author applied nanocomposite microgels[22-27] to emulsion stabilizer for various kind of oils. There is some possibility that a series of nanocomposite microgels can serve as particulate emulsifiers for water-in-oil (W/O) emulsions with different types of oils, including non-polar oils, which usually do not form W/O emulsions with conventional microgels.

## 4.2. Experimental Section

**Materials.** *N*-Isopropylacrylamide (NIPAm, purity 98%), *N*,*N*′-methylenebis(acrylamide) (BIS, 97%), styrene (99%), potassium peroxodisulfate (KPS, 95%), fumaric acid (FAc, 98%), cyclohexane (98%), 1-butanol, 1-pentanol, 1-octanol, and methyl methacrylate (MMA) were purchased from Wako Pure Chemical Industries, Ltd. and used as received. Decane and hexadecane were used as received from Tokyo Chemical Industry Co., Ltd. Nile Red (97.5%) was purchased from J&K Scientific Ltd. and also used as received. Fluorescein sodium salt was purchased from Sigma-Aldrich and used as purchased. For all experiments, water was distilled and then ion-exchanged (EYELA, SA-2100E1) before use.

**Microgel synthesis.** The parent microgels were synthesized by conventional precipitation polymerization. Initially, 440 mL of water, NIPAm (6.8747 g, 90 mol%), BIS (0.5204 g, 5 mol%), and FAc (0.3918 g, 5 mol%) were poured in a three-neck round bottom flask (1 L) equipped with a mechanical stirrer and a condenser. Next, the monomer solution was heated to 70 °C in a temperature-controlled oil bath and sparged with nitrogen for 30 min to purge the oxygen dissolved. Then, the KPS initiator (0.2433 g, 2 mM) dissolved in 10 mL of water was added to the monomer solution to start the polymerization. Subsequently, after 4 h, the monomer solution was cooled to room temperature and purified twice by centrifugation/redispersion with pure water. In this study, the microgels are denoted as **NF**, where **N** refers to pNIPAm and **F** to fumaric acid.

**Synthesis of Nanocomposite Microgels.** Hydrophobized nanocomposite microgels were synthesized by surfactant-free seeded emulsion polymerization (SEP) in the presence of **NF** microgels. Initially, a suitable amount of water (total volume: 200 mL) was poured in a three-neck

round bottom flask (300 mL) equipped with a mechanical stirrer and a condenser. Next, the water was heated to 70 °C in a temperature-controlled oil bath and sparged with nitrogen for 30 min to purge the oxygen dissolved. Then, a solution of NaOH (1 M) was added to maintain the pH value of the system under basic conditions (pH ≈ 10), before the purified **NF** microgel dispersion (final concentration: 0.17 wt%) and the KPS initiator (0.0540 g, 1 mM) were added dissolved in 5 mL of water. Finally, styrene (2.1028 g or 6.3084 g) or methyl methacrylate (4.0048 g) were injected to start the polymerization. The reaction was allowed to proceed for 24 h, and the resulting microgel dispersions were cooled to room temperature in an ice bath. The composite microgels were purified twice by centrifugation/redispersion with water. In all polymerization processes, secondary nanoparticles were not observed by FE-SEM imaging.

**Synthesis of Polystyrene Microspheres (PS).** Polystyrene microspheres (henceforth: **PS**) were prepared by soap-free emulsion polymerization. Initially, water (490 mL) was poured in a three-neck round bottom flask (1 L) equipped with a mechanical stirrer and a condenser. Next, the monomer solution was heated to 70 °C in a temperature-controlled oil bath and sparged with nitrogen for 30 min to purge the oxygen dissolved. Then, styrene (52.5700g, 1 M) and the KPS initiator (0.1622 g, 2 mM) dissolved in 10 mL water were added to start the polymerization. The polymerization was allowed to proceed for 24 h under a nitrogen atmosphere, and the resulting microgel dispersion was cooled to room temperature in an ice bath. The composite microgels were purified twice by centrifugation/redispersion with water.

**Synthesis of Core–Shell Microgels.** Core/hard–shell/gel microgels were synthesized by seeded precipitation polymerization [2] in the presence of polystyrene-based microspheres. At first, the core microspheres were prepared by soap-free emulsion polymerization: water (290 mL), NIPAm (3.3948 g, 10 mol%), and styrene (28.3978 g, 90 mol%) were poured in a three-neck round bottom flask (300 mL) equipped with a mechanical stirrer and a condenser. Next, the monomer solution was heated to 70 °C in a temperature-controlled oil bath and sparged with nitrogen for 30 min to purge the oxygen dissolved. After that, the KPS initiator (0.1622g, 2 mM) dissolved in 10 mL water was added to start the polymerization. The polymerization was allowed to proceed for 24 h, and the resulting microgel dispersion was cooled to room temperature in an ice bath. The polystyrene-based microspheres were purified twice by centrifugation/redispersion with water. In this manuscript, the polystyrene-based microspheres are denoted as **PSN**, where **S** refers to polystyrene and **N** to polyNIPAm.
Subsequently, the core–shell microgels were prepared by seeded precipitation polymerization. Initially, water (total volume: 30 mL) was poured in a three-neck round bottom flask equipped with a mechanical stirrer and a condenser. Next, a suitable amount of water was heated to 70 °C in a temperature-controlled oil bath and sparged with nitrogen for 30 min to purge the oxygen dissolved. After the addition of the concentrated **PSN** microsphere dispersion (final concentration: 1 wt%), the KPS initiator solution (1 mM, 0.0162 g) was injected. Finally, the monomer solution (5 mL) was injected to start the polymerization. The reaction was allowed to proceed for 4 h, and

the resulting microgel dispersion was cooled to room temperature. The composite microgels were purified twice by centrifugation/redispersion with water. In this manuscript, the composite microgels are denoted as **PSN-N(*X*)**, where **PSN** indicates the core microspheres, **N** refers to polyNIPAm, and ***X*** indicates the monomer concentration during the seeded precipitation polymerization.

**Preparation of Particle-stabilized Emulsions.** Particle-stabilized emulsions were prepared by mixing 1 mL of the particle dispersion at a suitable particle concentration (2–6 wt%) and 1 mL oil in an Ultra-Turrax T25 homogenizer. If not further specified, all emulsions were prepared with a T25 homogenizer operating at 5000 rpm for 60 s. The emulsions were first prepared without addition of a fluorescent dye. However, for optical microscopy imaging, the oil and water phases were stained with Nile red (~0.1 mM) and fluorescein sodium (~0.1 mM), respectively. In the present study, the pH value of the microgel dispersion was adjusted with NaOH (1 M).

**Characterization Methods.** The morphology of the samples was examined by scanning electron microscopy (FE-SEM, Hitachi Ltd., S-5000). For the sample preparation, a diluted particle dispersion (~0.05 wt%) was placed on a polystyrene substrate and dried at room temperature. Then, the dried sample was washed with pure water to remove the sodium salts. The sample substrates were sputtered with Pt/Pd prior to observation (15 mA, 6 Pa, 80 s).
The electrophoretic mobility (EPM) was evaluated on a Zetasizer NanoZS instrument (Malvern, Zetasizer software v. 4.20). For the sample preparation, the particle concentration was adjusted to ~0.005 wt% and the ionic strength to 1 mM using solutions of NaOH, HCl, and NaCl. The EPM data correspond to an average of 20 independent measurements from three independent measurements. For all measurements, the samples were equilibrated for 300 s at the set temperature before measurement.
The obtained emulsions were evaluated with an optical microscope (BX51, Olympus) equipped with a fluorescence system (ramp: U-RFL-T, excitation: 451-485 and 541-565 nm, emission: 500-523 and 584-675 nm) and a digital camera (ImageX Earth Type A-5.0M Ver.3.0.4, Kikuchi-Optical Co. Ltd.). For all microscopy measurements, the emulsions were sampled from the mixed solution with pipette and observed as soon as possible (within 30 min after the homogenization. Prior to the observation, the emulsions were diluted with water or the appropriate oils.

## 4.3. Results and discussion

### 4.3.1. Synthesis and characterization of nanocomposite microgels

As part of our ongoing research, the author initially synthesized a series of nanocomposite microgels by seeded emulsion polymerization (SEP) in the presence of microgels.[22-27] Given the stability of poly(*N*-isopropyl acrylamide-*co*-fumaric acid) (henceforth denoted as **NF**) microgels during SEP, which is due to the presence of the carboxyl groups on the surface, **NF** was selected as the core material for the SEP.[25,26,28] Thus, nanocomposite microgels were prepared by SEP with methyl methacrylate (MMA) monomers (**NF-M**) or polystyrene (**NF-S**).[25,26] Field emission scanning electron microscopy (FE-SEM) images (Figure 4-1a) show that all these nanocomposite microgels and their parent microgels are uniform in size, and that byproducts or independent hydrophobic particles were not generated during the SEP. Moreover, the surface of the nanocomposite microgels was not smooth, and the amount of nanoparticles immobilized in the **NF** microgels increased with increasing concentration of monomer added during the SEP (styrene: 1.05 g/system for **NF-S1**; 6.31 g/system for **NF-S2**; Figure 4-1a). Structural details of the microgels, including their size, the size of the nanoparticles, and their distribution, are summarized in **Table 4-1**. Furthermore, it was confirmed by electrophoresis experiments that all nanocomposite microgels exhibit a hydrogel layer on their surface. Furthermore, similar to the parent NF microgels, all nanocomposite microgels showed pH-dependent changes in their electrophoretic mobility (EPM), mainly due to the (de)protonation of the fumaric acid moieties located on the microgel surface (Figure 4-1b). Compared to pure **PS** microspheres, these hydrophobized nanocomposite microgels exhibited high colloidal stability during the centrifugal concentration, indicating that the hydrogel shell is present on the surface of hydrophobized nanocomposite microgels, which is consistent with our previous reports.[25,26]

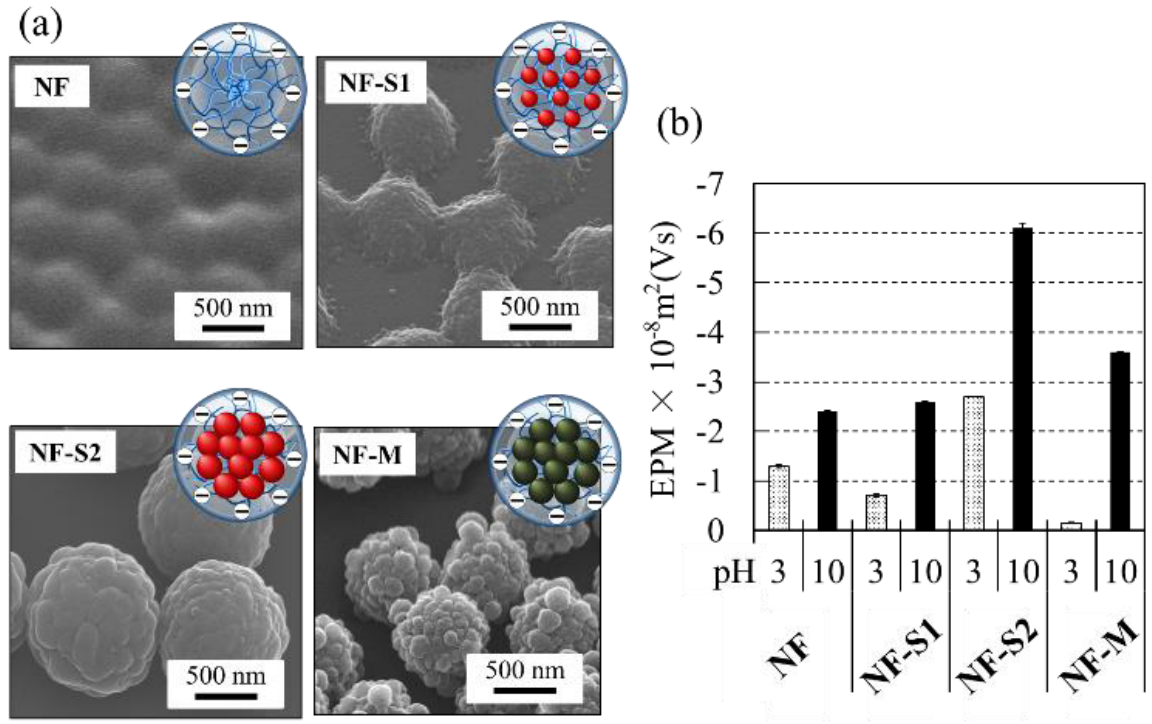


**Figure 4-1.** (a) FE-SEM images of the microgels and nanocomposite microgels. The parts shown in the scheme in red and green represent polystyrene and polymethacrylate, respectively. (b) Electrophoretic mobility (EPM) of the microgels and nanocomposite microgels under acidic (pH = 3) and basic conditions (pH = 10).

**Table 4-1**. Diameter of the (nanocomposite) microgels and small hydrophobic particles attached to the microgel surface

| Code | Microspheres | | Small hydrophobic particles | |
|---|---|---|---|---|
| | Diameter / nm | CV / % | Diameter / nm | CV / % |
| NF | 569 ± 44 | 7.7 | - | - |
| NF-S1 | 682 ± 40 | 5.9 | 37 ± 5.3 | 15 |
| NF-S2 | 986 ± 37 | 3.8 | 151 ± 51 | 34 |
| NF-M | 790 ± 35 | 4.4 | 120 ± 42 | 35 |

### 4.3.2. Preparation of Microgel Stabilized Emulsions with various oils

Then, the author prepared **MS-E**s using the **NF**-derived microgels and non-polar (cyclohexane and styrene) or polar oils (1-pentanol) at a fixed water/oil ratio (1:1, v/v) (Figure 4-2). The thus obtained emulsions were unequivocally covered with the microgels (Figure 4-3). The fluorescence microscopy images clearly show that the nature of the emulsions changes with the type of microgel employed as the emulsifier. For instance, different from the other microgels studied here, the **NF-S2** nanocomposite microgels produced a W/O emulsion with cyclohexane as the oil phase (Figure 4-1, left column). Moreover, in the case of styrene as the oil phase, both the **NF-S2** and **NF-M** nanocomposite microgels afforded W/O emulsions (Figure 4-2, middle column). In contrast, a W/O emulsion was only obtained with the **NF-M** nanocomposite microgels when 1-pentanol was used (Figure 4-2, right column). These results suggest that the solubility characteristics of polystyrene and poly(methyl methacrylate) are similar to those of oils in which W/O emulsions can be successfully prepared (Table 4-2). Thus, these results indicate that both the amount of nanoparticles formed inside the microgels and the type of hydrophobic polymer immobilized inside the microgels determine the type of emulsion obtained.

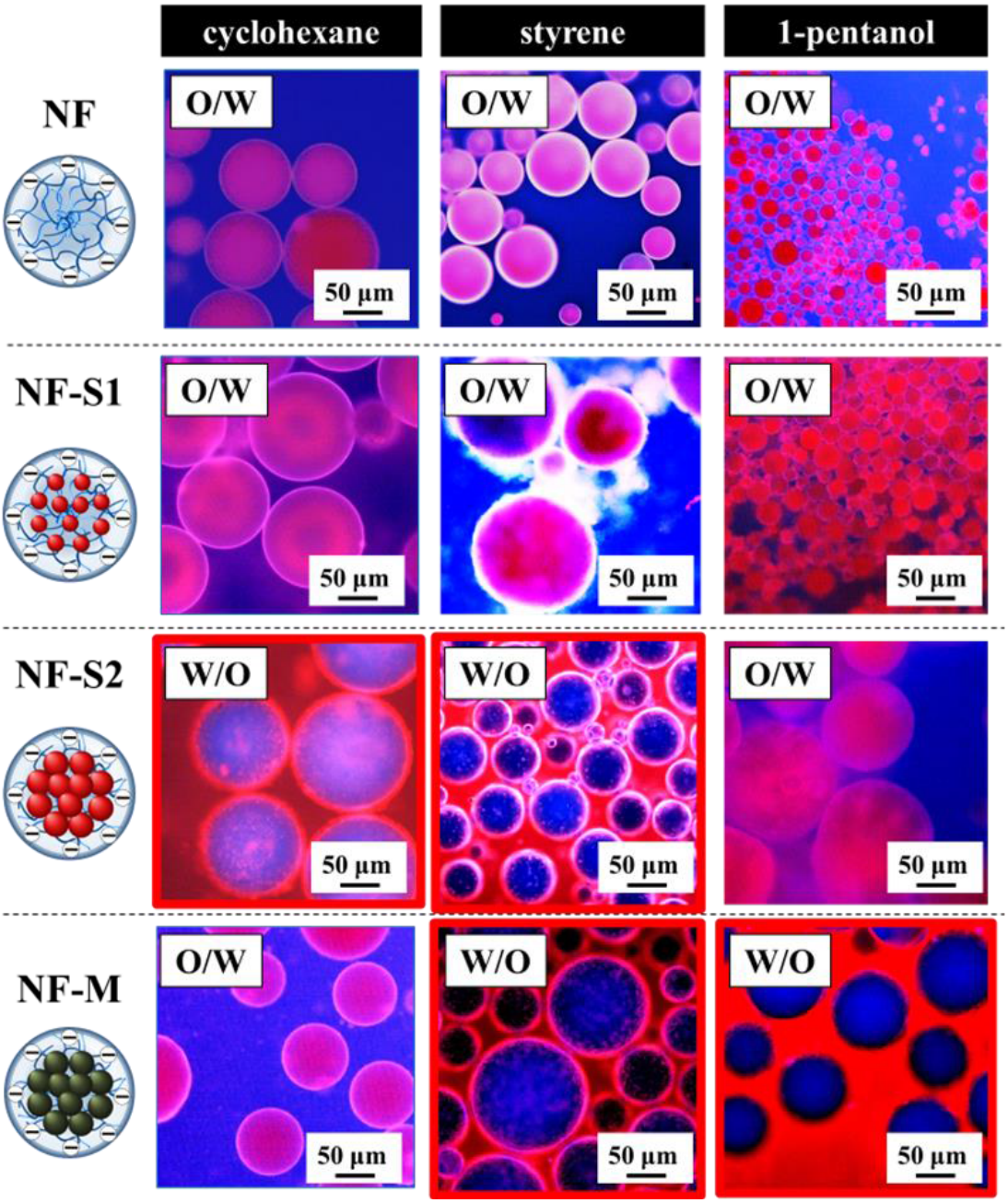


**Figure 4-2.** Fluorescence microscopy images of **MS-E**s prepared with cyclohexane (left column), styrene (middle column), and 1-pentanol (right column) for the different aqueous microgel dispersions.

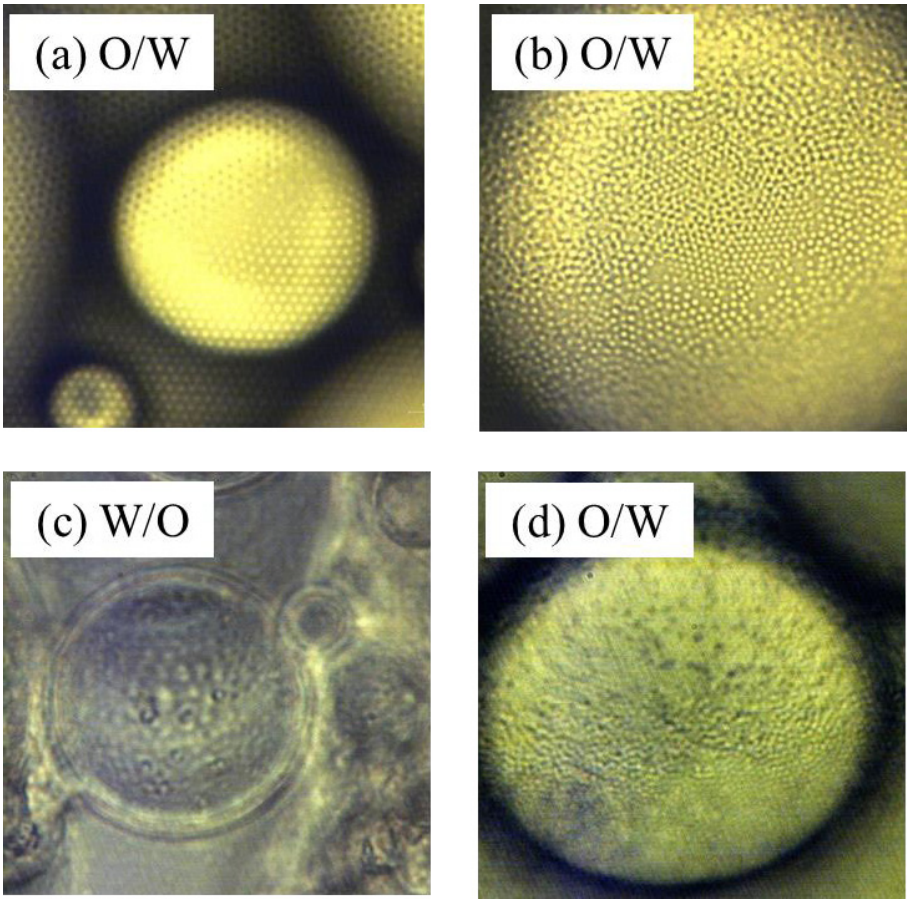


**Figure 4-3.** Fluorescence microscopy images of **MS-E**s prepared with (a) **NF** microgels (2 wt%), (b) **NF-S1** nanocomposite microgels (4 wt%), (c) **NF-S2** nanocomposite microgels (6 wt%), and (d) **NF-M** nanocomposite microgels (6 wt%). In this case, the emulsions were prepared by mixing 1 mL of cyclohexane and 1 mL of individual microgel dispersions under basic conditions (pH ≈ 10). The images confirm that all emulsions are covered by the corresponding microgels.

**Table 4-2**. Solubility parameters of oils and polymers used in this study

| Type | Solubility Parameter [ $MPa^{1/2}$] |
|---|---|
| n-Decane | 15.8 |
| Hexadecane | 16.4 |
| Cyclohexane | 16.8 |
| Styrene | 19.0 |
| Octanol | 20.9 |
| Pentanol | 21.7 |
| Butanol | 23.1 |
| polystyrene | 18.6 |
| poly (methy methacrylate) | 19.6 |

※ All solubility parameters were taken from a polymer handbook.[3]

### 4.3.3. The Effect of Volume Fraction of Oil on Emulsion Type

As for the particle wettability, it is known that the volume fraction of oil used during emulsification influences the resulting emulsion type.[29-32] In order to clarify the observed phase-inversion effect induced by the nanocomposite microgels, the effect of the oil mixing ratio during emulsification on the type of emulsion was investigated in detail using a wider variety of oils (Figure 4-4). The solubility parameter (SP) values of the oils and the hydrophobic polymers used in this study are summarized in Table 4-2. Indeed, the resulting emulsion type varied upon changing the water/oil ratio during emulsification. For instance, in the case of the parent **NF-S2** microgels, the type of emulsion changed from W/O to O/W with the increasing volume fraction of water when polar oils such as octanol were used (Figure 4-4c). Similarly, in the case of the **NF** or **NF-M** nanocomposite microgels, W/O emulsions were successfully obtained with polar oils upon changing the water volume ratio during emulsification (Figure 4-4a,c). Most importantly, these nanocomposite microgels allowed us to prepare W/O emulsions with a wide range of oils, including polar and non-polar oils (Figure 4-4b,c). The present results also suggest that the type of hydrophobic polymer immobilized within the microgels determines the type of oils from which W/O emulsions can be obtained. In a previous study, Zanini *et al.* have reported that the surface roughness of silica-based microspheres inhibits the phase inversion due to a pinning effect between the rough structure and oil/water interface.[33] In our present study, however, such a phase inversion,

i.e., microgel transport from the water to the oil phase, occurs in those cases where W/O emulsions are successfully formed, since the microgels studied here are all located in the aqueous phase prior to emulsification. Given that the rough surface of poly(methyl methacrylate) nanoparticles is covered with a hydrogel layer (*vide supra*), such a pinning effect[33] may not be effective in this study. In contrast, the nanoparticles in the microgels increase their hydrophobicity, which facilitates the formation of W/O emulsions.

Furthermore, it was confirmed that the obtained **MS-E**s with hydrophobized nanocomposite microgels exhibit remarkable properties originating from the microgels. Control experiments, in which polystyrene microspheres without **NF** microgel cores were used as the emulsifier, showed that stable emulsions were not obtained using cyclohexane and other non-polar oils (Figure 4-5), which is presumably due to electrostatic repulsion between the polystyrene microspheres and the oil/water interface.[34] Conversely, similar to **NF** microgels, **MS-E**s were formed after a short homogenization (~10 s; Figure 4-6) when **NF-S2** nanocomposite microgels were used as the emulsifier, even though a large amount of polystyrene was immobilized in the parent **NF** microgels. Furthermore, Buchcic *et al.* have demonstrated that a hydrogel layer (~100 nm) on the surface of polystyrene microspheres (~400 nm) (core/shell microgels) improves the interfacial activity of solid polystyrene microspheres.[15] At this point the author assume that such core/shell microgels might exhibit a similar behavior to our nanocomposite microgels since their structures are similar; polystyrene is covered with a hydrogel. However, different from the case of **NF-S2** nanocomposite microgels (Figure 4-1), W/O emulsions were not obtained when using polystyrene core–hydrogel shell microgels prepared following the report by Buchcic *et al.*,[15] regardless of the thickness of the hydrogel shell (Figure 4-7). Therefore, the surface roughness should be an important factor for achieving efficient contact between the hydrophobic nanoparticles and the water/oil interface. This result implies that the nanocomposite structure fabricated via SEP in the presence of microgels is crucial to obtain W/O emulsions with microgels in terms of the hydrophobicity and surface roughness,[35] although further studies are still necessary to clarify the mechanism in more detail.

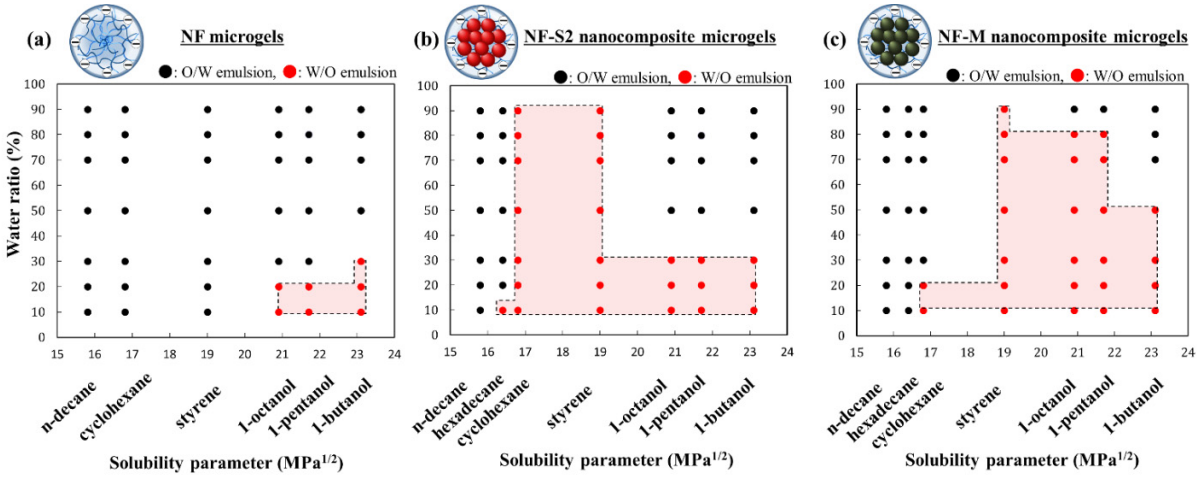


**Figure 4-4.** Phase diagram of the emulsion type (W/O or O/W) and water mixing ratio during emulsification using **NF** microgels as well as **NF-S2** and **NF-M** nanocomposite microgels as emulsifiers. All emulsions were prepared by mixing the (nanocomposite) microgel dispersion at a particle concentration (2 wt%) with the different oils for 1 min.

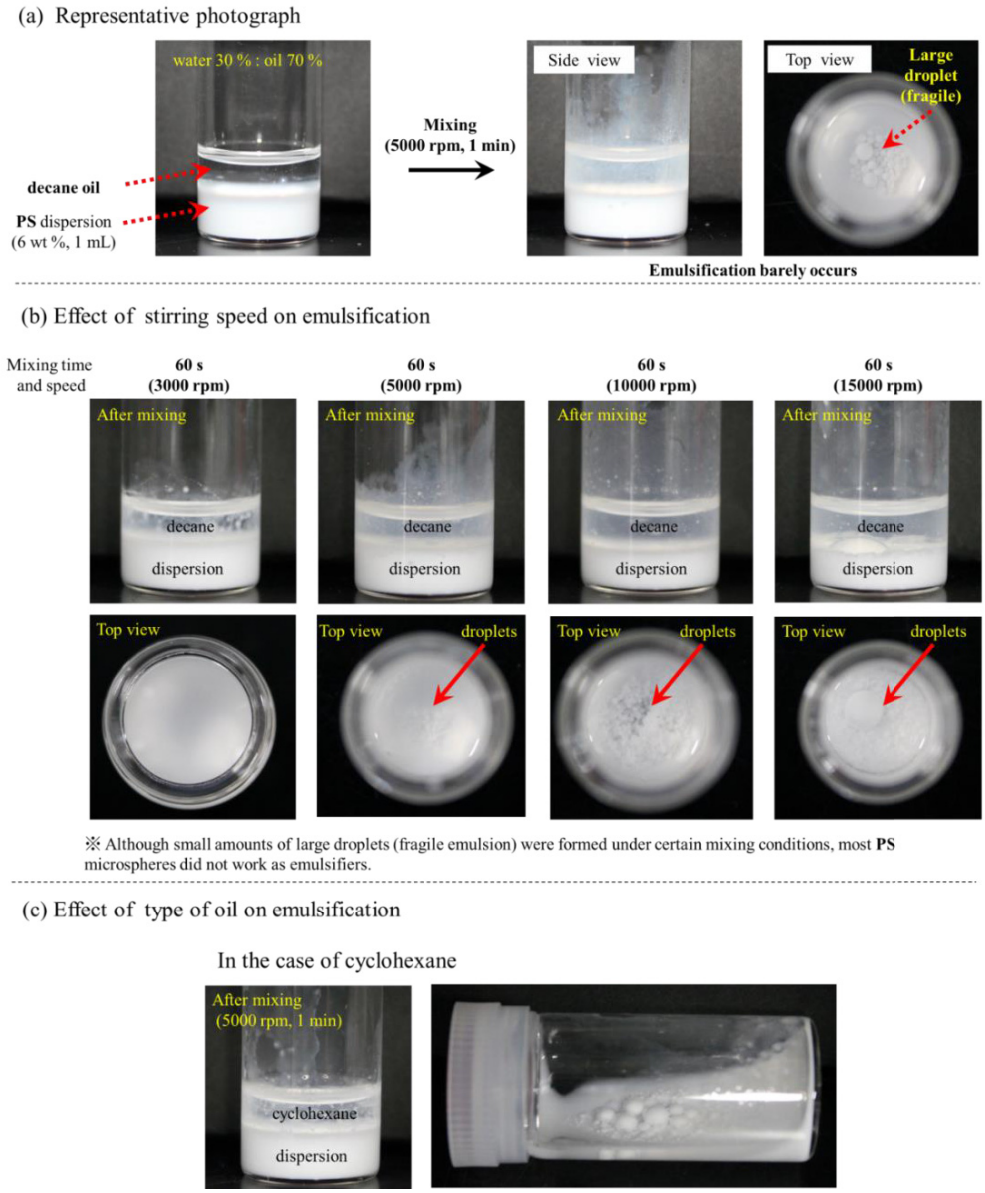


**Figure 4-5.** Photographic images of **MS-E**s prepared using **PS** microspheres. The effect of the stirring speed during the preparation of the emulsions on the emulsification behavior in the case of (a, b) *n*-decane and (c) cyclohexane as the oil phase is summarized above. All emulsions were prepared by mixing 0.6 mL of a **PS** dispersion (2 wt%) and 1.4 mL of the oil. Under these conditions, the preparation of particle-stabilized emulsions did not occur.

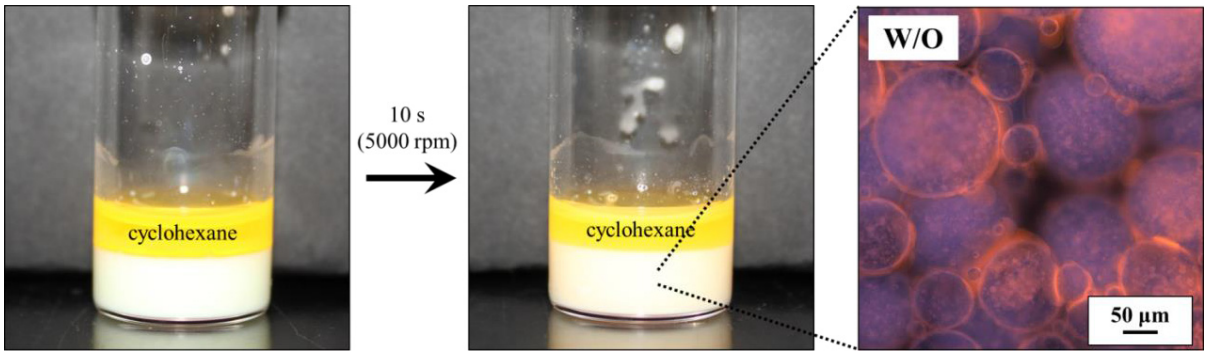


**Figure 4-6.** Photographic images of **MS-E**s prepared with **NF-S2** nanocomposite microgels before and after emulsification. The emulsions were prepared by a short homogenization (10 s, 5000 rpm).

| Code | Monomer conc. [mM] | Monomer [mol%] | | | *D*h (pH 3)[nm] | Shell Thickness |
|---|---|---|---|---|---|---|
| | | NIPAm | BIS | FAc | 25° C | [nm] |
| **PSN** | - | - | - | - | 380±4 | - |
| **PSN-N(10)** | 10 | 90 | 5 | 5 | 386 ± 4 | 3 |
| **PSN-N(30)** | 30 | 90 | 5 | 5 | 449 ± 1 | 35 |
| **PSN-N(50)** | 50 | 90 | 5 | 5 | 652±3 | 136 |

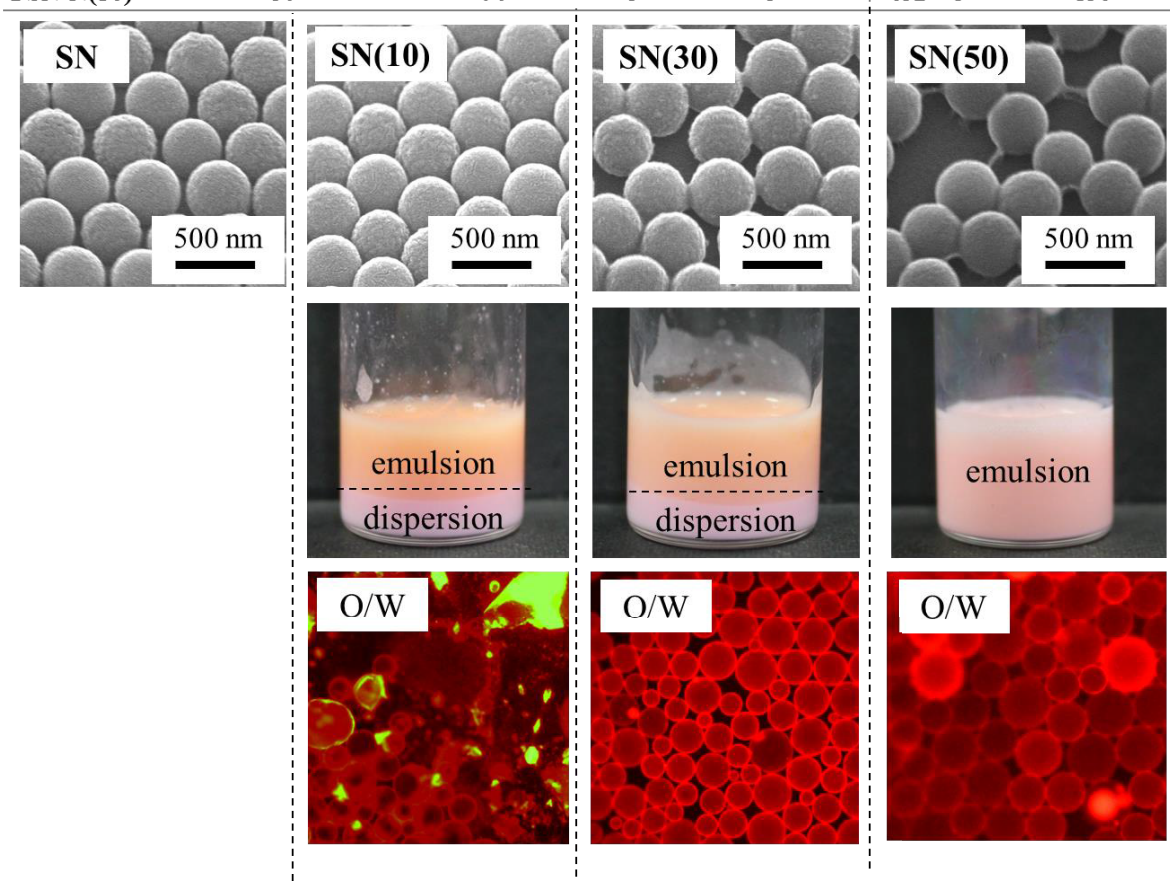


**Figure 4-7.** Photographic and fluorescence-microscopy images, as well as FE-SEM images of core–shell microgel-stabilized emulsions using **PSN-N(10)**, **PSN-N(30)**, and **PSN-N(50)** core–shell microgels. The emulsions were prepared with cyclohexane (red, stained with Nile red). A series of core–shell microgels were prepared by precipitation polymerization in the presence of **PSN** microspheres composed of 90 mol% styrene and 10 mol% NIPAm. The polymerization protocol is shown in the table in this figure. The emulsions were prepared under constant stirring (5000 rpm, 1 min) with different microgel dispersions at a fixed concentration.

## 4.4. Conclusions

In conclusion, the author has used hydrophobized nanocomposite microgels as emulsion stabilizers, which led to the first example of a W/O emulsions using non-polar oils. Moreover, the emulsion type (W/O or O/W) can be controlled by changing the amount of immobilized hydrophobic nanoparticles or the type of polymer formed inside the microgels. These results clearly indicate that hydrophobization of microgels by SEP is an effective approach to control the characteristics of **MS-E**s, such as are changing the softness[36] and charge distribution.[21,37] Since control over specific properties of nanocomposite microgels, including their softness, shape, chemical species, and surface charge, is now possible, such emulsions stabilized by nanocomposite microgels may lead to new applications in e.g. cosmetics and biomaterials.

## 4.5. References


1. Ramsden. W. Separation of solids in the surface-layers of solutions and 'suspensions'(observations on surface-membranes, bubbles, emulsions, and mechanical coagulation).-Preliminary account, *Proc. R. Soc. London* **1903**, *72*, 156-164.
2. Pickering, S. U. Cxcvi.-emulsions.*J. Chem. Soc. Trans*. **1907**, *91*, 2001-2021.
3. Iwasaki, Y.; Takahata Y.; Fujii, S. Self-setting particle-stabilized emulsion for hard-tissue engineering. *Coll. Surf., B*., **2015**, *126*, 394-400.;
4. Wu, J.; Ma, G. H. Recent studies of Pickering emulsions: particles make the difference. *Small*, **2016**, *12*, 4633-4648.;
5. Binks, B. P.; Olusanya, S. O. Pickering emulsions stabilized by coloured organic pigment particles. *Chem. Sci.*, **2017**, *8*, 708-723.
6. Binks, B. P. Colloidal particles at a range of fluid–fluid interfaces. *Langmuir* **2017**, *33*, 6947-6963.
7. Richtering, W. Responsive emulsions stabilized by stimuli-sensitive microgels: emulsions with special non-Pickering properties. *Langmuir* **2012**, *28*, 17218-17229.
8. Li, Z.; Ngai, T. Microgel particles at the fluid–fluid interfaces. *Nanoscale* **2013**, *5*, 1399-1410.
9. Schmitt, V.: Ravaine, V. Surface compaction versus stretching in Pickering emulsions stabilised by microgels. *Curr. Opin. Colloid Interface Sci.* **2013**, *18*, 532-541.
10. French, D. J.; Brown, A. T.; Schofield, A. B.; Fowler, J.; Taylor, P.; Clegg, P. S. The secret life of Pickering emulsions: particle exchange revealed using two colours of particle. *Sci. Rep.,* **2016**, *6*, 31401.
11. T. Ngai, Behrens, S. H.; Auweter, H. Novel emulsions stabilized by pH and temperature sensitive microgels. *Chem. Commun*. **2005**, *0*, 331-333.
12. Fujii, S.; Read, E. S.; Binks, B. P.; Armes, S. P. Stimulus‐Responsive Emulsifiers Based on Nanocomposite Microgel Particles. *Adv. Mater*. **2005**, *17*, 1014-1018.

13. Tsuji, S.; Kawaguchi, H. Thermosensitive Pickering emulsion stabilized by poly (N-isopropylacrylamide)-carrying particles. *Langmuir* **2008**, *24*, 3300-3305.
14. Destribats, M.; Lapeyre, V.; Sellier, E.; Leal-Calderon, F.; Schmitt, V.; Ravaine, V. Water-in-oil emulsions stabilized by water-dispersible poly (N-isopropylacrylamide) microgels. *Langmuir* **2011**, 27, 14096-14107.
15. Buchcic, C.; Tromp, R. H.; Meinders, M. B. J.; Stuart, M. A. C. Harnessing the advantages of hard and soft colloids by the use of core–shell particles as interfacial stabilizers. *Soft Matter* **2017**, *13*, 1326-1334.
16. Wiese, S.; Tsvetkova, Y.; Daleiden, N. J. E.; Spieß, A. C.; Richtering, W. Microgel stabilized emulsions: Breaking on demand. *Colloids Surf., A*, **2016**, *495*, 193-199.
17. Li, Z.; Ming, T.; Wang, J.; Ngai, T. High internal phase emulsions stabilized solely by microgel particles. *Angew. Chem. Int. Ed.* **2009**, *45*, 8642-8645.
18. Finkle, P.; Draper, H. D.; Hildebrand, J. H. The theory of emulsification1. *J. Am. Chem. Soc.* **1923**, *45*, 2780-2788.
19. Destribats, M.; Gineste, S.; Laurichesse, E.; Tanner, H.; Leal-Calderon, F.; Hėroguez, V.; Schmitt, V. Pickering emulsions: what are the main parameters determining the emulsion type and interfacial properties?. *Langmuir* **2014**, *30*, 9313-9326.
20. Pelton, R. Temperature-sensitive aqueous microgels. *Adv. Colloid Interface Sci.* **2000**, *85*, 1-33.
21. Geisel, K.; Isa, L.; Richtering, W. Unraveling the 3D localization and deformation of responsive microgels at oil/water interfaces: a step forward in understanding soft emulsion stabilizers. *Langmuir* **2012***, 28,* 15770-15776.
22. Suzuki, D.; Yamagata, T.; Murai, M. Multilayered Composite Microgels Synthesized by Surfactant-Free Seeded Polymerization. *Langmuir* **2013**, *29*, 10579-10585.
23. Suzuki, D.; Kobayashi, C. Raspberry-Shaped Composite Microgel Synthesis by Seeded Emulsion Polymerization with Hydrogel Particles. *Langmuir* **2014**, *30*, 7085-7092.
24. Kobayashi, C.; Watanabe, T.; Murata, K.; Kureha, T.; Suzuki, D. Localization of Polystyrene Particles on the Surface of Poly(*N*-isopropylacrylamide-*co*-methacrylic acid) Microgels Prepared by Seeded Emulsion Polymerization of Styrene, *Langmuir* **2016**, *32*, 1429-1439.
25. Watanabe, T.; Kobayashi, C.; Song, C.; Murata, K.; Kureha, T.; Suzuki, D. Impact of Spatial Distribution of Charged Groups in Core Poly(*N*-isopropyl acrylamide)-Based Microgels on the Resultant Composite Structures Prepared by Seeded Emulsion Polymerization of Styrene. *Langmuir* **2016**, *32*, 12760-12773.
26. Watanabe,T.; Song, C.; Murata, K.; Kureha, T. Suzuki, D. Seeded Emulsion Polymerization of Styrene in the Presence of Water-Swollen Hydrogel Microspheres. *Langmuir* **2018**, *34*, 8571-8580.
27. Suzuki, D.; Horigome, K.; Kureha, T.; Matsui, S.; Watanabe, T. Polymeric Hydrogel Microspheres: Design, Synthesis, Characterization, Assembly and Applications. *Polymer Journal* **2017**, *49*, 695-702.

28. Hoare, T.; Pelton, R. Characterizing charge and crosslinker distributions in polyelectrolyte microgels. *Curr. Opin. Colloid Interface Sci.* **2008**, *13*, 413-428.
29. Binks, B. P.; Lumsdon, S. O. Influence of particle wettability on the type and stability of surfactant-free emulsions. *Langmuir* **2000**, *16*, 8622-8631.
30. Binks, B. P.; Lumsdon, S. O. Catastrophic phase inversion of water-in-oil emulsions stabilized by hydrophobic silica. *Langmuir* **2000**, *16*, 2539-2547.
31. Liu, M.; Chen, X.; Yang, Z.; Xu, Z.; Hong, L.; Ngai, T. Tunable pickering emulsions with environmentally responsive hairy silica nanoparticles. *ACS Appl. Mater. Interfaces* **2016**, *8*, 32250-32258.
32. Ngai, T.; Auweter, H.; Behrens, S. H. Environmental responsiveness of microgel particles and particle-stabilized emulsions. *Macromolecules* **2006**, *39*, 8171-8177.
33. Zanini, M.; Marschelke, C.; Anachkov, S. E.; Marini, E.; Synytska, A.; Isa, L. Universal emulsion stabilization from the arrested adsorption of rough particles at liquid-liquid interfaces. *Nat. Commun.* **2017**, *8*, 15701.
34. Nguyen, A. V.; George, P.; Jameson, G. J. Demonstration of a minimum in the recovery of nanoparticles by flotation: Theory and experiment. *Chem. Eng. Sci*. **2006**, *61*, 2494-2509.
35. San-Miguel, A.; Behrens, S. H. Influence of nanoscale particle roughness on the stability of pickering emulsions. *Langmuir* **2012**, *28*, 12038-12043.
36. Destribats, M.; Lapeyre, V.; Wolfs, M.; Sellier, E.; Leal-Calderon, F.; Ravaine, V.; Schmitt, V. Soft microgels as Pickering emulsion stabilisers: role of particle deformability. *Soft Matter* **2011**, *7*, 7689-7698.
37. Schmidt, S.; Liu, T.; Rütten, S.; Phan, K. H.; Möller, M.; Richtering, W. Influence of microgel architecture and oil polarity on stabilization of emulsions by stimuli-sensitive core–shell poly (N-isopropylacrylamide-co-methacrylic acid) microgels: Mickering versus Pickering behavior?. *Langmuir* **2011**, *27*, 9801-9806.

## 5. Summary

In this thesis, the impact of various microgel properties on the morphology of nanocomposite structure was revealed by systematically emulsion polymerization with various kinds of microgels. First, the three types of pNIPAm-based microgels with different charged distribution were used as seed microgels for SEP of styrene in the presence of microgels, and revealed that hydrophobic polystyrene nanoparticles were formed inside of pNIPAm microgels except for polyelectrolytes. The poly(NIPAm-*co*-FAc) microgels whose carboxyl groups were localized on the surface of microgels have some fascinate properties on SEPs in the presence of microgels. For example, the carboxyl groups were enhanced the colloidal stability of resultant nanocomposite microgels in terms of not only electrophoretic repulsion but also steric repulsion because polyelectrolytes remained on the surface of parent microgels after SEP. Furthermore, considering the result that polystyrene nanoparticles were formed the center of seed microgels even though enough charged groups were existed on the surface of core microgels. Additionally, since these phenomena were observed regardless of the hydrated state of seed microgels, therefore, the author reached the important conclusion the spatial distribution state of polyelectrolytes inside of microgels is a key factor in the morphological control of the nanocomposite microgels.

This design concept for microgels that focuses on “hydrophobicity “and “roughness” was important on microgel applications such as emulsion stabilizer. The hydrophobic nanoparticles combining inside of pNIPAm microgels enhanced the wettability (or compatibility) of hydrogel particles to oil phase, leading the stable water in the oil emulsions stabilized by microgels. These results also indicated that not only hydrophobicity but also roughness is important for preparing water in oil emulsion with microgels. This result opens new doors for the design strategy of microgels as emulsion stabilizer and may lead to the development of fluid materials such as an emulsion fuels, high functionality catalysis, and food. The present study demonstrates not only the structural control of nanocomposite microgels prepared by SEPs in the presence of microgels but also future possibility toward the development of composite materials.

# List of Publications

1. Takumi Watanabe, Chiaki Kobayashi, Chihong Song, Kazuyoshi Murata, Takuma Kureha, Daisuke Suzuki*:
"Impact of Spatial Distribution of Charged Groups in Core Poly(*N*-isopropyl acrylamide)-Based Microgels on the Resultant Composite Structures Prepared by Seeded Emulsion Polymerization of Styrene" *Langmuir*, *32*, 12760-12773 (2016).

2. Takumi Watanabe, Chihong Song, Kazuyoshi Murata, Takuma Kureha, Daisuke Suzuki*:
"Seeded Emulsion Polymerization of Styrene in the Presence of Water-Swollen Hydrogel Microspheres" *Langmuir*, *34*, 8571-8580 (2018).

3. Takumi Watanabe, Masaya Takizawa, Hang Jiang, To Ngai*, Daisuke Suzuki*.
"Hydrophobized Nanocomposite Hydrogel Microspheres as Particulate Stabilizers for Water-in-Oil Emulsions" *Chemical Communications*, *55*, 5990-5993. (2019).

# Other Publications

1. Chiaki Kobayashi. Takumi Watanabe, Kazuyoshi Murata, Takuma Kureha, Daisuke Suzuki*:
"Localization of Polystyrene Particles on the Surface of Poly(*N*-isopropylacrylamide-*co*-methacrylic acid) Microgels Prepared by Seeded Emulsion Polymerization of Styrene"
*Langmuir*, *32*, 1429-1439 (2016).

2. Saori Minami, Takumi Watanabe, Daisuke Suzuki*, Kenji Urayama*:
"Rheological Properties of Suspensions of Thermo-responsive Poly(*N*-isopropylacrylamide) Microgels Undergoing Volume Phase Transition"
*Polymer Journal, 48*, 1079-1086 (2016).

3. Haruka Minato, Masaki Murai, Takumi Watanabe, Shusuke Matsui, Masaya Talkizawa, Takuma Kureha, Daisuke Suzuki*:
"The Deformation of Hydrogel Microspheres at the Air/Water Interface"
*Chemical Communications*, *54*, 932-935 (2018).

4. Saori Minami, Takumi Watanabe, Daisuke Suzuki*, Kenji Urayama*:
"Viscoelasticity of Dense Suspensions of Thermosensitive Microgel Mixtures Undergoing Colloidal Gelation" *Soft Matter*, *14*, 1596-1607 (2018).

5. Ayaki Nakaishi, Saori Minami, Shun Oura, Takumi Watanabe, Daisuke Suzuki*, Kenji Urayama*.
"Elastic and Flow Properties of Densely Packed Microgel Mixtures with Size- and Stiffness Disparitiess" *Macromolecules*, *51*, 9901-9914 (2018).

6. Shun Oura, Takumi Watanabe, Haruka Minato, Daisuke Suzuki*:
"Impact of Particle Softness on Segregation of Binary Colloidal Suspensions Flowing in a Microchannel"
*KOBUNSHI RONBUNSHU*, *76*, 226-233 (2019).

7. Kenshiro Honda, Yuka Sazuka, Kojiro Iizuka, Shusuke Matsui, Takayuki Uchihashi, Takuma Kureha, Mitsuhiro Shibayama, Takumi Watanabe, Daisuke Suzuki*:
"Hydrogel Microellipsoids that Form Robust String-like Assemblies at the Air/Water Interface"
*Angew. Chem. Int. Ed.*, *58*, 7294-7298 (2019).

# Oral Presentation

1. ○渡邊拓巳、小林千玲、鈴木大介:
「階層構造を有するゲル微粒子をシードに用いたシード乳化重合による複合微粒子の創製」
第 64 回高分子学会年次大会、札幌コンベンションセンター、札幌、5 月 28 日(2015)、
口頭 (発表番号 2F18)

2. ○渡邊拓巳、小林千玲、鈴木大介:
「不均一系重合を基盤とした階層型ナノコンポジットゲル微粒子の創製」
第 64 回高分子討論会、東北大学、宮城、9 月 17 日(2015)、口頭(3C09)

3. ○渡邊拓巳、小林千玲、鈴木大介:
「不均一系重合法による機能性ナノコンポジットゲル微粒子の創製」
第 27 回ゲル研究討論会、東京大学、東京、1 月 19 日(2016)、口頭(発表番号 21)

4. ○渡邊拓巳、小林千玲、鈴木大介:
「ゲル微粒子存在下におけるシード乳化重合により得られる異型複合ゲル微粒子構造とシード粒子構造との関係」
平成 28 年度繊維学会年次大会、タワーホール船堀(江戸川区総合区民ホール)、東京、
6 月 9 日(2016)、口頭(2G07)

5. ○渡邊拓巳、小林千玲、ソンチホン、村田和義、呉羽拓真、鈴木大介:
「ミクロハイドロゲルをテンプレートに用いた新規複合ゲル微粒子の創製」
第 65 回高分子討論会、神奈川大学、神奈川、9 月 14 日(2016)、口頭(1I08)

6. ○渡邊拓巳、小林千玲、ソンチホン、村田和義、呉羽拓真、鈴木大介:
「新規固体複合化ヒドロゲル微粒子のナノ構造制御と評価」
第 67 回コロイドおよび界面化学討論会、北海道教育大学旭川校、北海道、9 月 23 日(2016)、
口頭( 2H07)

7. ○渡邊拓巳、小林千玲、ソンチホン、村田和義、呉羽拓真、鈴木大介:
「固体状ナノ粒子の固定位置を制御した新規複合ゲル微粒子の創製」
第 19 回高分子ミクロスフェア討論会、千葉大学、千葉、 11 月 8 日(2016)、口頭(2-18A)

8. ○Takumi Watanabe, Chiaki Kobayashi, Song Chihong, Kazuyoshi Murata, Takuma Kureha, Daisuke Suzuki:
「Morphology control of raspberry-shaped composite microgels prepared by seeded emulsion polymerization」第 66 回高分子学会年次大会、幕張メッセ、千葉、5 月 30 日(2017)、口頭(2K24)

9. ○渡邊拓巳、ソンチホン、村田和義、呉羽拓真、鈴木大介:
「水で膨潤したヒドロゲル微粒子内部で生じる疎水モノマーの重合挙動」
第 68 回コロイドおよび界面化学討論会、神戸大学、兵庫、9 月 8 日(2017)、口頭( 3D29)

10. ○渡邊拓巳、呉羽拓真、ソンチホン、村田和義、鈴木大介:
「Surfactant-Free Seeded Emulsion Polymerization of Styrene in the Presence of Water-Swollen Microgels」
第 27 回日本 MRS 年次大会、横浜市開港記念会館、神奈川、12 月 5 日(2017)、口頭(I-O5-022)

11. ○渡邊拓巳、ソンチホン、村田和義、呉羽拓真、鈴木大介:
「高分子電解質ゲル微粒子を活用した複合ゲル微粒子の創製」
第 29 回高分子ゲル研究討論会、東京工業大学、東京、1 月 11 日(2018)、口頭(4)

12. ○渡邊拓巳、Jiang Hang、Ngai To、鈴木大介:
「ナノコンポジットゲル微粒子を乳化剤としたエマルション」
第 69 回コロイドおよび界面化学討論会、筑波大学、茨城、9 月 18 日(2018)、口頭(1E39)

13. ○渡邊拓巳、鈴木大介:
「ハイドロゲル 微粒子存在下 における乳化重合挙動」
第 69 回コロイドおよび界面化学討論会、筑波大学、茨城、9 月 19 日(2018)、口頭(2F05)

14. ○渡邊拓巳、鈴木大介:
「シード乳化重合によるナノコンポジットハイドロゲル微粒子の創製」
第 20 回高分子ミクロスフェア討論会、岡山大学、岡山、11 月 14 日(2018)、口頭(1-12A)

15. ○渡邊拓巳、Jiang Hang、Ngai To、鈴木大介:
「ナノコンポジットハイドロゲル微粒子を用いたエマルション」
第 20 回高分子ミクロスフェア討論会、岡山大学、岡山、11 月 14 日(2018)、口頭(1-13A)

16. ○ Takumi Watanabe, Song Chihong, Kazuyoshi Murata, Daisuke Suzuki:
“Emulsion polymerization in the presence of water-swollen microgels”
1st G’L’owing Polymer Symposium in KANTO、早稲田大学、東京、12 月 15 日(2018)、口頭 (F04)

17. ○渡邊拓巳、滝沢優哉、Jiang Hang、To Ngai、鈴木大介:
「新規固体複合化ゲル微粒子で安定化されたエマルション」
第 68 回高分子学会年次大会、大阪府立国際会議場、大阪、5 月 29 日(2019)、口頭(1J20)

18. ○渡邊拓巳、大浦舜、鈴木大介:
「水膨潤ゲル微粒子存在下で行う乳化重合」
第 68 回高分子学会年次大会、大阪府立国際会議場、大阪、5 月 30 日(2019)、口頭(2E19)

19. 渡邊拓巳、濱田隼汰、ソンチホン、村田和義、○鈴木大介:
「ゲル微粒子を反応場とした乳化重合による機能性微粒子の創製と応用」
第 68 回高分子討論会、福井大学、福井、9 月 25 日(2019)、口頭(1J11)

20. ○Takumi Watanabe, Song Chihong, Kazuyoshi Murata, Takuma Kureha, Daisuke Suzuki:
"Nanocomposite Microgels Formed by Seeded Emulsion Polymerization of Styrene in the Presence of Hydrogel Microspheres"
*The 6th Asian Symposium on Emulsion Polymerization and Functional Polymeric Microspheres* (Fukui, Japan) March 9th (2018) Oral (3-11A)

21.○Takumi Watanabe, Chihong Song, Kazuyoshi Murata, Takuma Kureha, Daisuke Suzuki:
"Nanocomposite Microgels formed by Seeded Emulsion Polymerization in the Presence of Radially Structured Polyelectrolyte Microgels"
*255th ACS National Meeting* (New Orleans, America) March 18th (2018) Oral (POLY 99)

# Awards

1. ○渡邊拓巳、小林千玲、鈴木大介:
「ポリスチレン複合ゲル微粒子の表面内部構造制御への試み」
第 153 回東海高分子研究会講演会(2015 年夏季合宿)、サンパーク犬山、愛知、9 月 4 日(2015)、
ポスター(発表番号 P35-M) ※東海高分子研究会学生研究奨励賞

2. ○Takumi Watanabe, Chiaki Kobayashi, Kazuyoshi Murata, Takuma Kureha and Daisuke Suzuki:
"Synthesis and Characterization of pNIPAm/PS raspberry shaped composite particles"
*The 5th Asian Symposium on Emulsion Polymerization and Functional Polymeric Microspheres*
(Suzhou, Chaina) November 26th (2015) Poster (P-10)
※The 5th ASEPFPM Student Poster Award

3. ○渡邊拓巳、小林千玲、鈴木大介:
「シード乳化重合によるラズベリー型複合ゲル微粒子の創製」
平成 28 年度繊維学会年次大会、タワーホール船堀(江戸川区総合区民ホール)、6 月 9 日(2016)、
ポスター(2P238) ※若手優秀ポスター賞

4. ○渡邊拓巳、小林千玲、鈴木大介:
「ヒドロゲル微粒子をシードに用いたスチレンのシード乳化重合におけるゲル微粒子内電荷分布の影響」
第 62 回高分子研究発表会(神戸)、兵庫県民会館、兵庫、7 月 15 日(2016)、ポスター(Pb-20)
※エクセレントポスター賞

5. ○渡邊拓巳、小林千玲、ソンチホン、村田和義、鈴木大介:
「難水溶性高分子複合化新奇ナノコンポジットゲル微粒子の創製」
第 65 回高分子討論会、神奈川大学、神奈川、9 月 14 日(2016)、ポスター(1Pd060)
※公益社団法人高分子学会優秀ポスター賞

6. ○渡邊拓巳、小林千玲、ソンチホン、村田和義、呉羽拓真、鈴木大介:
「新規固体複合化ヒドロゲル微粒子のナノ構造制御と評価」
第 67 回コロイドおよび界面化学討論会、北海道教育大学旭川校、北海道、9 月 23 日(2016)、口頭(2H07) ※若手口頭講演賞

7. ○渡邊拓巳、小林千玲、ソンチホン、村田和義、呉羽拓真、鈴木大介:
「固体状ナノ粒子の固定位置を制御した新規複合ゲル微粒子の創製」
第 19 回高分子ミクロスフェア討論会、千葉大学、千葉、 11 月 8 日(2016)、口頭(2-18A)
※学生最優秀発表賞

8. ○渡邊拓巳、呉羽拓真、ソンチホン、村田和義、鈴木大介:
「Surfactant-Free Seeded Emulsion Polymerization of Styrene in the Presence of Water-Swollen Microgels」
第 27 回日本 MRS 年次大会、横浜市開港記念会館、神奈川、12 月 5 日、口頭(H-O5-022)
※奨励賞 (口頭発表)

9. ○渡邊拓巳、ソンチホン、村田和義、呉羽拓真、鈴木大介:
「高分子電解質ゲル微粒子を活用した複合ゲル微粒子の創製」
第 29 回高分子ゲル研究討論会、東京工業大学、東京、1 月 12 日(2018)、口頭(4)
※RSC Soft Matter 講演賞

10. ○Takumi Watanabe, Chihong Song, Kazuyoshi Murata, Daisuke Suzuki:
"Amphiphilic Raspbery-shaped Composite Microgels"
*The 13th International Symposium on Polymer Phisics* (Xi'an, China) June 15th (2018) Poster (P6-11)
※Best Poster Award PP2018

11. ○渡邊拓巳、ソンチホン、村田和義、鈴木大介:
「疎水性高分子複合化ナノコンポジットゲル微粒子の創製とその構造制御」
第 8 回 CSJ 化学フェスタ 2018、タワーホール船堀、東京、10 月 23 日(2018)、ポスター(P1-088)
※優秀ポスター発表賞

12. ○渡邊拓巳、鈴木大介
「シード乳化重合によるナノコンポジットハイドロゲル微粒子の創製」
○渡邊拓巳、Jiang, Hang、To Ngai、鈴木大介
「ナノコンポジットハイドロゲル微粒子を用いたエマルション」
第 20 回高分子ミクロスフェア討論会、岡山大学、岡山、11 月 14 日(2018)、口頭(1-12A,1-13A)
※学生優秀発表賞

13. ○渡邊拓巳
「親疎水空間が分割されたミクロ反応場における疎水モノマーのシード乳化重合」
平成 27 年度応用化学課程卒業論文発表会、3 月（2015）
※日本化学会東海支部長賞

14. ○渡邊拓巳
「Morphology-controllable Synthesis of Composite Hydrogel Microspheres by Seeded Emulsion Polymerization in the Presence of Microgels」
平成 29 年度 理工学研究科化学材料専攻修士論文発表会、3 月(2017)
※日本化学会東海支部長賞

# 6. Acknowledgements

First, I am most grateful to my supervisor Prof. Dr. Daisuke Suzuki (Shinshu University) for a lot of mindful helps and supports. Prof. Suzuki always gave me insightful comments and suggestions to develop these researches relevant to this doctoral thesis.

I am very grateful to Prof. Dr. Kazuyoshi Murata (National Institute for Physical Science) and Dr. Song Chihong (National Institute for Physical Science) for useful discussions and assistance regarding cryo-tomography measurement.

I am very grateful to Prof. Dr. To Ngai (The Chinese University of Hong Kong) and Mr. Jiang Hang (The Chinese University of Hong Kong) for useful discussions regarding microgel-stabilized emulsions.

I greatly thank to Emeritus Prof. Dr. Haruma Kawaguchi (Keio Univ.), Prof. Dr. Kenji Urayama (Kyoto Institute of Technology Univ.), Prof. Mizuo Maeda (RIKEN), Prof. Kohri Michinari (Chiba Univ.), Prof. Masahiro Suzuki (Shinshu Univ.), Prof. Yasuhiro, Kohsaka (Shinshu Univ.), Prof. Dr. Koji Horigome, Dr. Takuma Kureha (Tokyo Univ.), Dr. Shusuke Matsui, Ms. Chiaki Kobayashi, and Ms. Saori Minami for useful discussions about gel and colloid science.

My study was financially supported by fellowship (18J11622) from the Japan Society for the Promotion of Science (JSPS), and a Sasakawa Scientific Research Grant from the Japan Science Society (29-339). I am thankful for all the supports.

I would like to thank the Suzuki lab members. The daily discussions with all of you have had a lot of positive effects on me. I sincerely best wishes for your future success.

Finally, I would also like to express my special gratitude to my family (Masao, Hiromi, Satoshi) for their moral support and warm encouragements.

Takumi Watanabe
渡邊拓巳